Study on the structure-property relationship of hyperbranched polyimide-silica hybrid membranes

Masako MIKI

Table of Contents

Chapter 1

Introduction

Nowadays, every part of our society depends on energy mass consumption of fossil fuel. However, the significant increase in energy consumption due to the economic development and world population growth in recent years causes the depletion of fossil fuel. In order to build a sustainable development society, it is necessary to develop the alternative energy source of fossil fuel, renewable energy, and low environmental impact process. For example, the utilization of biomass is one of the preferable solutions. Biomass is biological material derived from not only plant-based materials but also animal-derived materials. We can convert biomass energy to useful energy forms by "direct burning", "gasification" or "fermentation". Biogas obtained from the fermentation of biomass such as waste wood, sewage sludge, livestock excreta, and waste oil is a flammable gas which consists primarily of methane and carbon dioxide. High purity methane gas as energy can be produced by separating and refining biogas [1-3].

In addition, global warming has been a problem for a long time as an international issue. For years, scientists have been trying to figure out what causes global warming, and reached the conclusion that there were several greenhouse gases such as carbon dioxide, exhausted from industrial and human activities such as the burning of fossil fuels and deforestation. Nowadays, many studies about Carbon dioxide Capture and Storage (CCS) are being carried out widely [4-6]. CCS is a technique of capturing waste carbon dioxide from industrial and energy-related sources before it enters the atmosphere, transporting it to a storage site, and injecting it into the deep secure geological formations.

In recent years, a large number of researches about polymeric membranes for CO_2 separation have been performed because membrane separation is a key technology for both utilization of renewable energy and CCS (Figure 1-1) [7].

Gas separation membranes can be classified into inorganic membranes and polymeric membranes. Inorganic membranes are porous membranes having nano-ordered fine

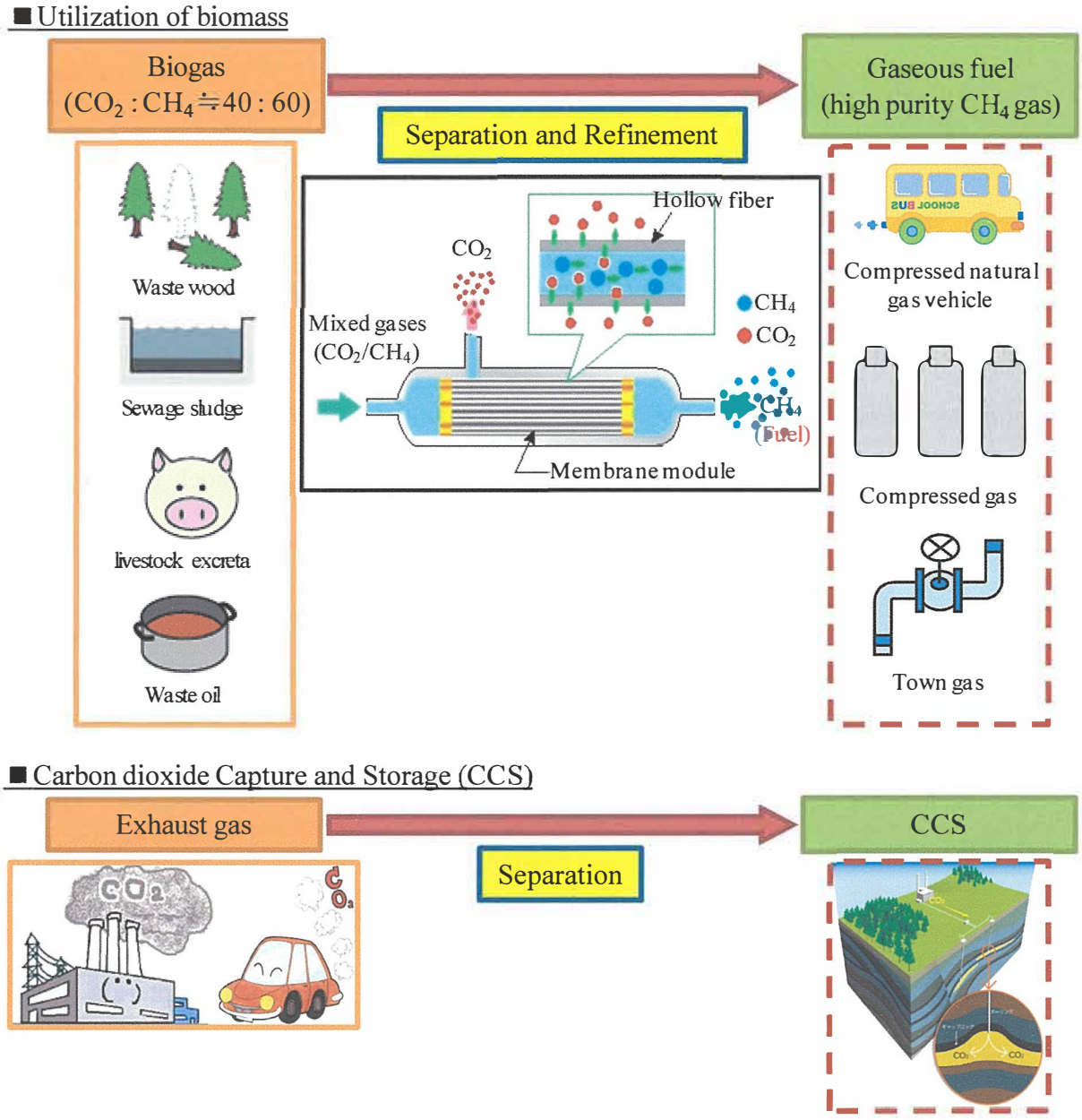

Figure 1-1 The conceptual diagram of utilization of biomass and CCS by using membrane separation

pores and exert the superior gas separation performance by molecular sieving function [8]. However, most gas separation membranes which have been put to practical use are polymeric membranes because of their low cost and good processability. Aromatic polyimides have been of particular interest in gas separation membranes because of their excellent mechanical and thermal properties, and high gas permeability and selectivity [9-12].

Polyimide is one of the most thermally stable engineering plastics, which was developed by DuPont for use in the aerospace and military applications in the early 1960's [13]. Today, polyimide is used in a wide range of industrial fields as electric and microelectronic materials as well as aerospace field because of their thermal stability, mechanical and electrical properties, chemical resistance and processability. Polyimides can be generally synthesized by a two-step polymerization process. In this method, firstly, polyamic acid as precursor is prepared by polycondensation reaction of a dianhydride and a diamine at ambient conditions in a dipolar aprotic solvent such as *N,N*-dimethylacetamide (*DMAc*) or *N*-methyl-2-pyrrolidone (*NMP*). And then, the prepared polyamic acid is cyclodehydrated to the corresponding polyimide by subsequent thermal or chemical imidization. A wide variety of polyimides suitable for the specific intended uses have been developed by choosing optimum monomers.

Hyperbranched polymers are highly branched three-dimensional dendritic polymers possessing unique properties (e.g., good solubility, reduced viscosity, higher fractional free volume, and multifunctionality) arising from multiple end groups. Hyperbranched polyimides (HBPIs) can be synthesized from either the self-polycondensation of AB_2-type monomers or the polycondensation reaction of A_2 + B_3 monomers, where A_2 represents a dianhydride monomer and B_3 represents a triamine monomer. In the case of an A_2 + B_3 type polycondensation reaction, a variety of HBPIs can be synthesized by

changing the monomer ratio and combining A_2 and B_3 monomers [14-16]. From this point of view, in recent years, a lot of researches on gas transport properties of HBPI membranes have been studied [17-20]. Fang et al. were the first to report the synthesis of HBPIs derived from a triamine, tris(4-aminophenyl)amine (*TAPA*), and commercially available dianhydrides. They have revealed that the HBPI membranes had a good gas separation performance compared with corresponding linear-type polyimides [17,18]. Suzuki et al. have also studied the gas transport properties of HBPI membranes prepared by polycondensation reaction of a triamine, 1,3,5-tris(4-aminophenoxy) benzene (*TAPOB*), and a dianhydride, 4,4'-hexafluoroisopropylidene diphthalic anhydride (*6FDA*), and found that these HBPI membranes exhibit high gas permeability and O_2/N_2 selectivity arising from its characteristic hyperbranched structure [21].

Organic-inorganic hybrid or composite materials have been extensively studied because the newly combined materials offer the advantages of both properties of an organic polymer (e.g., flexibility, dielectric, ductility, and processability) and an inorganic material (e.g., rigidity, thermal stability) [22,23]. In this thesis, the "hybrid materials" mean those that have strong (physicochemical) interaction between organic and inorganic components such as covalent bonding, and the "composite materials" mean those that show weak or no interactions between the two components. Synthesizing polyimide-silica hybrid or composite materials and investigating their physical and gas transport properties have also received much attention [24-27]. Suzuki et al. have studied the syntheses and gas transport properties of the HBPI-silica hybrid membranes prepared with commercially available dianhydride monomers and several kinds of triamine monomers. As an example, a schematic diagram for the preparation of 6FDA-TAPOB system HBPI-silica hybrid membrane is shown in Figure 1-2. They found that these membranes have shown characteristics quite different from the

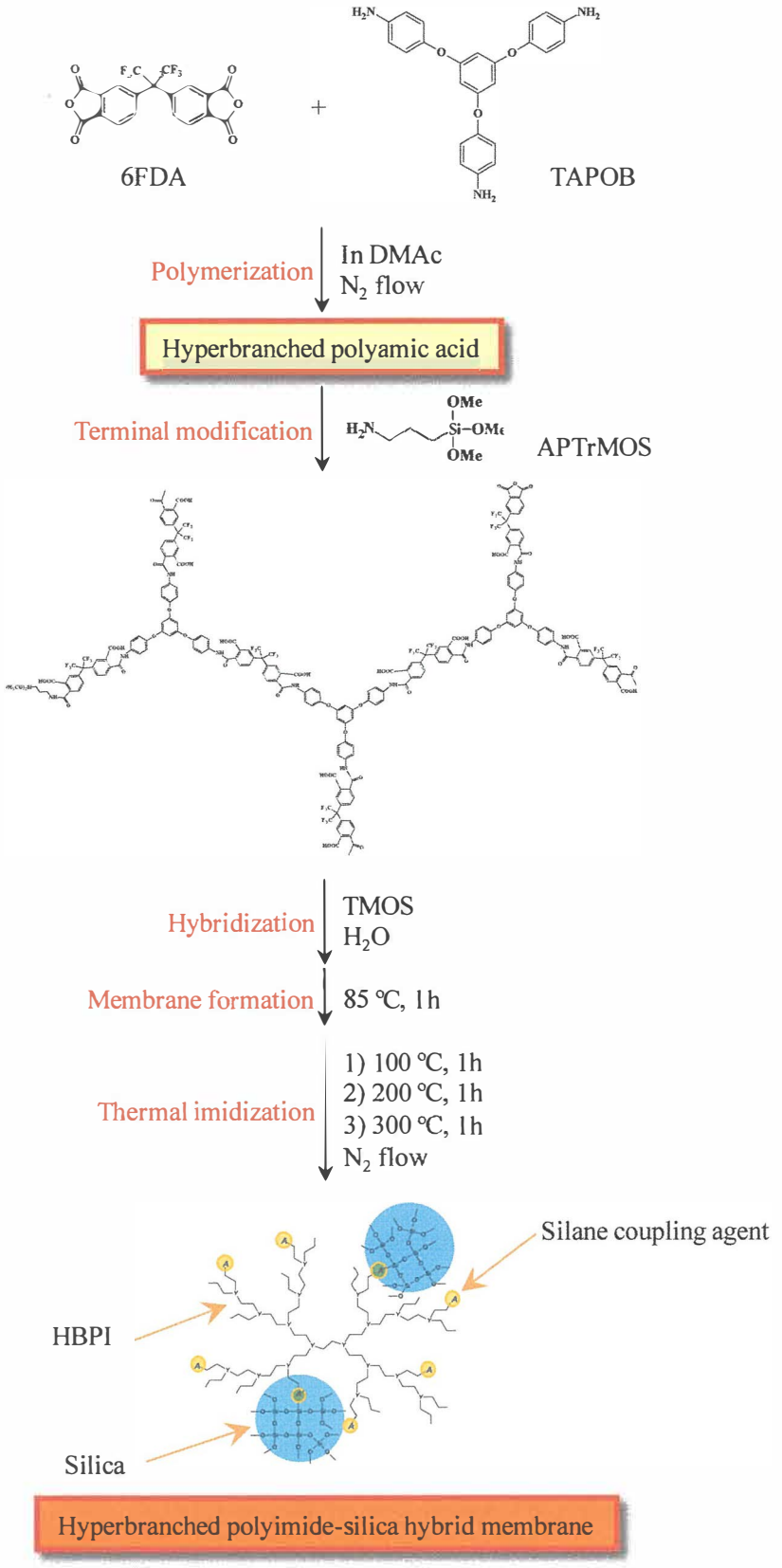

Figure 1-2 A schematic diagram for the preparation of 6FDA-TAPOB system HBPI-silica hybrid membrane.

conventional polymer membranes. Specifically, the gas permeability and the CO_2/CH_4 selectivity of the HBPI-silica hybrid membranes prepared by sol-gel reaction using tetramethoxysilane (*TMOS*) increased with increasing the silica content without any dependence on the HBPI molecular structure, suggesting the characteristic distribution and the interconnectivity of free volume holes created by the incorporation of silica [28-33].

However, at this stage, there are few systematically investigated works that respect to the structure-property relationship and gas transport mechanism of the HBPI-silica hybrid and composite membranes.

In this study, HBPI-silica hybrid and composite membranes with various structures were prepared and their physical and gas transport properties were investigated to clarify the structure-property relationship and gas transport mechanism.

This thesis consists of the following ten chapters.

Chapter 1: Introduction

Chapter 2: Synthesis and Gas Transport Properties of Hyperbranched Polyimide Membranes

Chapter 3: Effects of the Degree of Terminal Modification on Physical and Gas Transport Properties of Hyperbranched Polyimide-Silica Hybrid Membranes

Chapter 4: Effects of the Terminal Structure on Physical and Gas Transport Properties of Hyperbranched Polyimide-Silica Hybrid Membranes

Chapter 5: Physical and Gas Transport Properties of Asymmetric Hyperbranched Polyimide-Silica Hybrid Membranes

Chapter 6: Gas Transport Mechanism of Hyperbranched Polyimide-Silica Hybrid / Composite Membranes

Chapter 7: Study on Nanostructure-Gas Transport Property Relationship of

Hyperbranched Polyimide-Silica Hybrid Membranes

Chapter 8: Study on Physical and Gas Transport Properties of Polyimide-Silica Hybrid Membranes Treated with CO_2 Gas

Chapter 9: Conclusions

Chapter 10: Acknowledgement

The HBPI-silica hybrid and composite are composed of the HBPI matrix, silica domain, and interfacial region between HBPI matrix and silica. Therefore, it is necessary to investigate the influence of these three areas on the physical and gas transport properties of the HBPI-silica hybrid and composite membranes. The HBPI matrix structure-property relationship was investigated in chapter 2-5; the influence of silica domain was investigated in chapter 6. And the effect of interfacial region was determined in chapter 3 and 6. In addition, the nanostructure-gas transport property relationship and the influence of the molecular structure on the stability of gas transport property of HBPI-silica hybrid membranes treated with CO_2 gas were investigated in chapter 7 and 8, respectively.

References

[1] P. McKendry, Energy Production from Biomass (part 1): Overview of Biomass, Bioresource Technology, 83 (2002) 37–46.

[2] A. Demirbas, Progress and Recent Trends in Biofuels, Progr. Energ. Combust. Sci., 33 (2007) 1–18.

[3] P. Weiland, Biogas Production: Current State and Perspectives, Appl. Microbiol. Biotechnol., 85 (2010) 849–860.

[4] S.M. Benson, F.M. Orr Jr., Carbon Dioxide Capture and Storage, MRS Bulletin, 33 (2008) 303-305.

[5] R. S. Haszeldine, Carbon Capture and Storage: How Green Can Black Be?, Science, 325 (2009) 1647-1652.

[6] D.M. D'Alessandro, B. Smit, J.R. Long, Carbon Dioxide Capture: Prospects for New Materials, Angew. Chem. Int. Ed., 49 (2010) 6058 – 6082.

[7] Y. Yampolskii, B. Freeman (Eds.), Membrane Gas Separation, John Wiley & Sons Ltd, West Sussex, 2010.

[8] C. Cornelius, C. Hibshman, E. Marand, Hybrid Organic-Inorganic Membranes, Separ. Purif. Tech., 25 (2001) 181-193.

[9] T.H. Kim, W.J. Koros, G.R. Husk, K.C. O'Brien, Relationship between Gas Separation Properties and Chemical Structure in a Series of Aromatic Polyimides, J. Membr. Sci., 37 (1988) 45-62.

[10] S.A. Stern, Y. Mi, H. Yamamoto, Structure / Permeability Relationships of Polyimide Membranes. Applications to the Separation of Gas Mixtures, J. Polym. Sci. Part B: Polym. Phys., 27 (1989) 1887-1909.

[11] K. Okamoto, K. Tanaka, H. Kita, M. Ishida, M. Kakimoto, Y. Imai, Gas Permeability and Permselectivity of Polyimides Prepared from 4,4'-Diaminotriphenyl-amine, Polym. J., 24 (1992) 451-457.

[12] Y. Li, X. Wang, M. Ding, J. Xu, Effects of Molecular Structure on the Permeability and Permselectivity of Aromatic Polyimides, J. Appl. Polym. Sci., 61 (1996) 741-748.

[13] C.E. Sroog, A.L. Endrey, S.V. Abramo, C.E. Berr, W.M. Edwards, K.L. Olivier, Aromatic Polypyromellitimides from Aromatic Polyamic Acids, J. Polym. Sci. Part A: Polym. Chem., 3 (1965) 1373-1390.

[14] Y.H. Kim, Hyperbranched Polymers 10 Years After, J. Polym. Sci. Part A: Polym. Chem., 36 (1998) 1685-1698.

[15] C. Gao, D. Yan, Hyperbranched Polymers: from Synthesis to Applications, Prog. Polym. Sci., 29 (2004) 183-275.

[16] M. Jikei, M. Kakimoto, Dendritic Aromatic Polyamides and Polyimides, J. Polym. Sci. Part A: Polym. Chem., 42 (2004) 1293-1309.

[17] J. Fang, H. Kita, K. Okamoto, Hyperbranched Polyimides for Gas Separation Applications. 1. Synthesis and Characterization, Macromolecules, 33 (2000) 4639-4646.

[18] J. Fang, H. Kita, K. Okamoto, Gas Permeation Properties of Hyperbranched Polyimide membranes, J. Membr. Sci., 182 (2001) 245-256.

[19] H. Gao, D. Wang, W. Jiang, S.Guan, Z. Jiang, Gas Permeability of Fluorinated Hyperbranched Polyimide, J. Appl. Polym. Sci., 109 (2008) 2341–2346.

[20] J. Peter, A. Khalyavina, J. Kříž, M. Bleha, Synthesis and Gas Transport Properties of ODPA–TAP–ODA Hyperbranched Polyimides with Various Comonomer Ratios, Euro. Polym. J., 45 (2009) 1716–1727.

[21] T. Suzuki, Y. Yamada, Y. Tsujita, Gas Transport Properties of 6FDA-TAPOB Hyperbranched Polyimide Membrane, Polymer, 45 (2004) 7167-7171.

[22] G. Kickelbick (Eds.), Hybrid Materials, Wiley-VCH, Weinheim, 2007.

[23] H. Zou, S. Wu, J. Shen, Polymer/Silica Nanocomposites: Preparation, Characterization, Properties, and Applications, Chem. Rev., 108 (2008) 3893–3957.

[24] C.J. Cornelius, E. Marand, Hybrid Silica-Polyimide Composite Membranes Gas Transport Properties, J. Membr. Sci., 202 (2002) 97–118.

[25] G. Ragosta, P. Musto, Polyimide/Silica Hybrids via the Sol-Gel Route: High Performance Materials for the New Technological Challenges, eXPRESS Polym. Lett., 3 (2009) 413–428.

[26] A.I. Romero, M.L. Parentis, A.C. Habert, E.E. Gonzo, Synthesis of Polyetherimide/Silica Hybrid Membranes by the Sol–Gel Process: Influence of the

Reaction Conditions on the Membrane Properties, J. Mater. Sci., 46 (2011) 4701–4709.

[27] M.S. Boroglu, M.A. Gurkaynak, The Preparation of Novel Silica Modified Polyimide Membranes: Synthesis, Characterization, and Gas Separation Properties, Polym. Adv. Technol., 22 (2011) 545-553.

[28] T. Suzuki, Y. Yamada, Physical and Gas transport Properties of Novel Hyperbranched Polyimide – Silica Hybrid Membranes, Polym. Bull., 53 (2005) 139-146.

[29] T. Suzuki, Y. Yamada, Characterization of 6FDA-based Hyperbranched and Linear Polyimide-Silica Hybrid Membranes by Gas Permeation and 129Xe NMR Measurements, J. Polym. Sci. Part B: Polym. Phys., 44 (2006) 291-298.

[30] T. Suzuki, Y. Yamada, J. Sakai, Gas Transport Properties of ODPA-TAPOB Hyperbranched Polyimide-Silica Hybrid Membranes, High Perform. Polym., 18 (2006) 655-664.

[31] T. Suzuki, Y. Yamada, Effect of End Group Modification on Gas Transport Properties of 6FDA-TAPOB Hyperbranched Polyimide-Silica Hybrid Membranes, High Perform. Polym., 19 (2007) 553-564.

[32] T. Suzuki, Y. Yamada, K. Itahashi, 6FDA-TAPOB Hyperbranched Polyimide-Silica Hybrids for Gas Separation Membranes, J. Appl. Polym. Sci., 109 (2008) 813-819.

[33] T. Suzuki, Y. Yamada, Synthesis and Gas Transport Properties of Novel Hyperbranched Polyimide-Silica Hybrid Membranes, J. Appl. Polym. Sci., 127 (2013) 316-322.

Chapter 2

Synthesis and Gas Transport Properties of Hyperbranched Polyimide Membranes

1. Introduction

Gas permeabilities and gas selectivities of polymer membranes depend on their basic structure (chemical composition) and secondary structure (polymer chain arrangement) [1]. Thus a great number of studies on structure-gas transport property relationships have been done. For the linear type polyimide membranes, many studies also have been performed [2-5]. And from these previous researches, it was revealed that the more rigid the polyimide molecular backbone is, the larger the permeability or diffusion coefficient is.

The most widely practiced procedure in polyimide synthesis is the two-step polyamic acid process which involves the reaction of a dianhydride monomer and a diamine monomer. By using the two-step process, a variety of polyimides can be synthesized by changing the combination of monomers. This technique can be applied to the synthesis of the hyperbranched polyimides (HBPIs).

In chapter 2, a variety of HBPIs were synthesized and their physical and gas transport properties were investigated.

2. Experimental

2.1 Materials

1,3,5-Tris(4-aminophenoxy)benzene (*TAPOB*) was synthesized by the reduction of 1,3,5-tris(4-nitrophenoxy)benzene with palladium carbon and hydrazine in methanol [6].

In this study, four kinds of following dianhydride were used. Pyromellitic dianhydride (*PMDA*) and 3,3',4,4'-Biphenyltetracarboxylic dianhydride (*BPDA*) were purchased from Daicel Chemical Industries, Ltd (Osaka, Japan) and Sigma-Aldrich Co. LLC. (St. Louis, MO, USA), respectively. 4,4'-(Hexafluoroisopropylidene) diphthalic anhydride (*6FDA*) was kindly supplied by Daikin Industries (Osaka, Japan). 4,4'-Oxidiphthalic anhydride (*ODPA*) was purchased from Manac Inc. (Hiroshima, Japan). 3-Aminopropyltrimethoxysilane (*APTrMOS*) was purchased from Sigma-Aldrich Co. LLC. *N, N*-Dimethylacetamide (*DMAc*) used as a solvent was purchased from Nacalai Tesque (Kyoto, Japan). The chemical structures of monomers and silane coupling agent are shown in Figure 2-1.

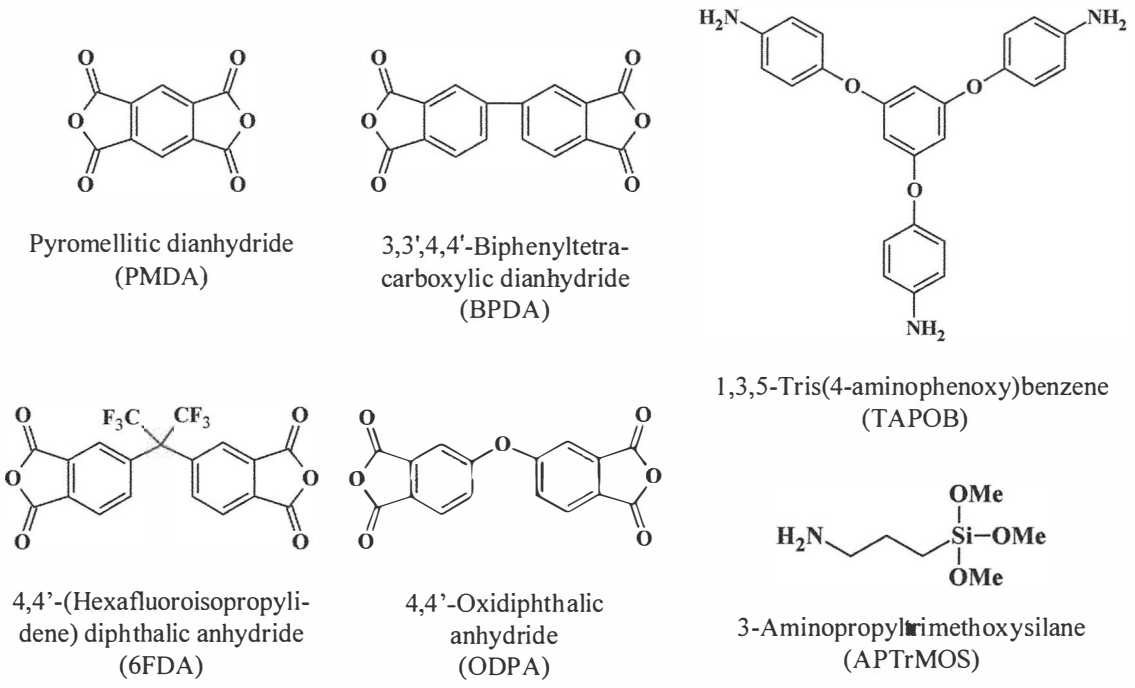

Figure 2-1 Chemical structures of monomers and silane coupling agent.

2.2 Polymerization

Three mmol of anhydride (6FDA, PMDA, ODPA or BPDA) was dissolved in 40 ml

of DMAc in a 100-ml three-neck flask under N_2 flow at room temperature. To this solution, 1.6 mmol of TAPOB in 20-40 ml of DMAc was then added dropwise through a syringe with stirring for 3 h to afford hyperbranched polyamic acids (HBPAAs). The solid contents of reaction solutions were controlled to *ca.* 3.5 wt%. Subsequently, 0.4 mmol of the silane coupling agent, APTrMOS, was added into the reaction mixture to modify the end groups of the HBPAAs with further stirring for 1 h.

2.3 Membrane formation

The HBPAA solutions were cast on PET films and dried at 85°C for 3 h. The prepared films were peeled off and subsequently imidized at 100°C for 1 h, 200°C for 1 h, and 300°C for 1 h in a heating oven under N_2 flow. A schematic diagram for the preparation of HBPI membranes is shown in Figure 2-2.

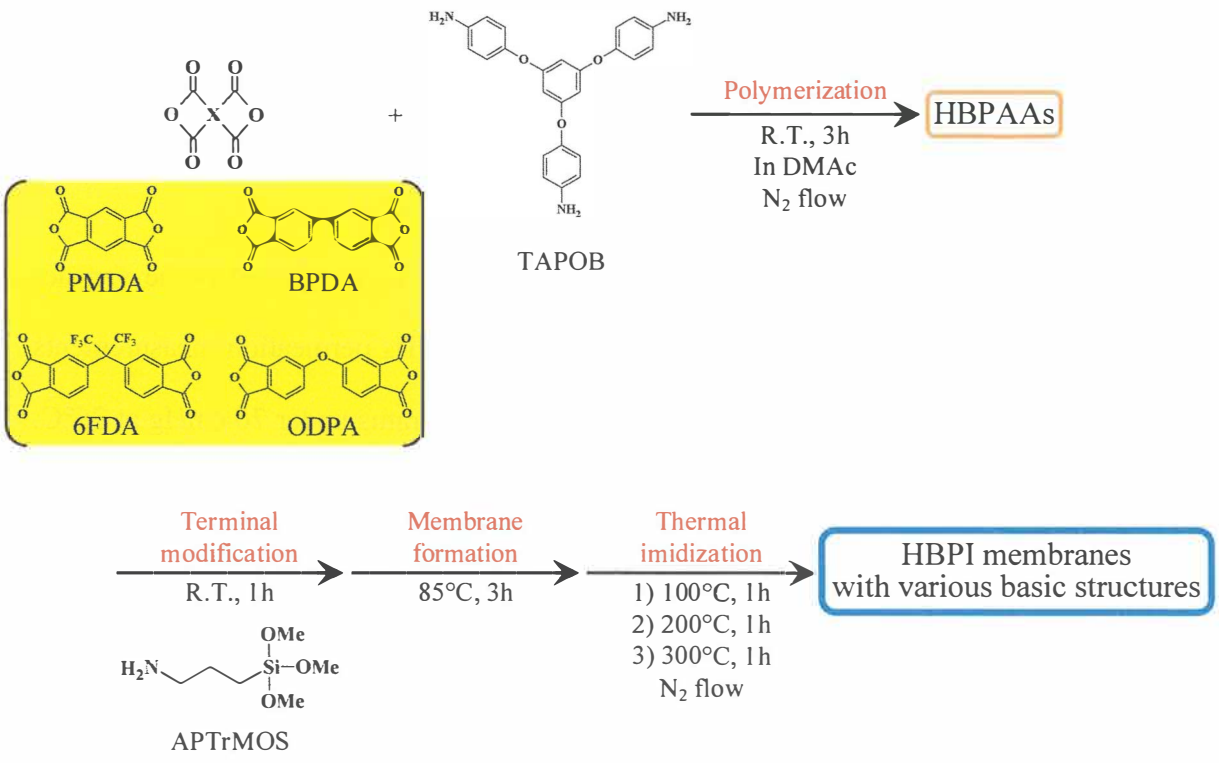

Figure 2-2 A schematic diagram for the preparation of HBPI membranes with various basic structures.

2.4 Measurements

Attenuated total reflection Fourier transform infrared (ATR FT-IR) spectra were recorded on a JASCO (Tokyo, Japan) FT/IR-4100 at a wavenumber range of 550–4000 cm^{-1} and a resolution of 1 cm^{-1}. Ultraviolet-visible (UV-vis) optical transmittances were measured with a JASCO V-530 UV/vis spectrometer at wavelengths of 200–800 nm. Thermogravimetric-differential thermal analysis (TG-DTA) experiments were performed with a Seiko Instruments (Chiba, Japan) TG/DTA5200 at a heating rate of 10°C/min under air flow. Thermal mechanical analysis (TMA) measurements were carried out using a Seiko Instruments TMA/SS6100 at a heating rate of 5°C/min under N_2 flow. The mechanical properties were measured at room temperature on a Tokyo Testing Machine Inc. (Aichi, Japan) Little Senstar LSC5/30 with a crosshead speed of 5 mm/min. The densities (ρs) of the HBPIs were measured by a floating method with bromoform and 2-propanol at 25°C. According to the group contribution method, the fractional free volume (FFV) of HBPIs can be estimated by the following equation [7]:

$$FFV = \frac{V_{sp} - 1.3V_w}{V_{sp}} \quad (1)$$

where V_{sp} (cm^3/mol) is the specific molar volume and V_w (cm^3/mol) is the van der Waals volume of the repeating unit. CO_2, O_2, N_2, and CH_4 permeation measurements were taken with a constant volume/variable pressure apparatus under 76 cmHg at 25°C. The permeability coefficient, P [cm^3(STP)cm/cm^2 s cmHg], was determined by the equation [8]:

$$P = \frac{22414}{A}\frac{L}{p}\frac{V}{RT}\frac{dp}{dt} \quad (2)$$

where A is the membrane area (cm^2), L is the membrane thickness (cm), p is the upstream pressure (cmHg), V is the downstream volume (cm^3), R is the universal gas

constant (6236.56 cm^3 cmHg/mol K), T is the absolute temperature (K), and dp/dt is the permeation rate (cmHg/s). The gas permeability coefficient can be explained on the basis of the solution-diffusion mechanism, which is represented by the equation [9,10]:

$$P = D \times S \quad (3)$$

where D (cm^2/s) is the diffusion coefficient and S [$cm^3(STP)/cm^3_{polym}$ cmHg] is the solubility coefficient. The diffusion coefficient was calculated by the time-lag method represented by the equation [11]:

$$D = \frac{L^2}{6\theta t} \quad (4)$$

where θt (s) is the time-lag.

3. Results and discussion

3.1 Polymer characterization

ATR FT-IR spectra of the prepared HBPI films are shown in Figure 2-3. The bands observed 1774-1784 cm^{-1} (C=O asymmetrical stretching), 1710-1721 cm^{-1} (C=O symmetrical stretching), 1368-1374 cm^{-1} (C-N stretching), and 720-743 cm^{-1} (C=O bending) are characteristic absorption bands of polyimides. In contrast, the characteristic absorption band of polyamic acid at 1680 cm^{-1} disappeared, indicating that the prepared films are well imidized [12,13]. Some strong absorption bands attributed to C–O and C–F stretching are observed in the region of 1100–1300 cm^{-1}. The bands observed at 1143cm^{-1} and 1273 cm^{-1} were attributed to the trifluoromethyl group in 6FDA-TAPOB and to the aromatic ether linkages in ODPA-TAPOB, respectively [14,15].

The appearances of the prepared films are shown in Figure 2-4. 6FDA-TAPOB and ODPA-TAPOB films are almost colorless in contrast to PMDA-TAPOB and BPDA-

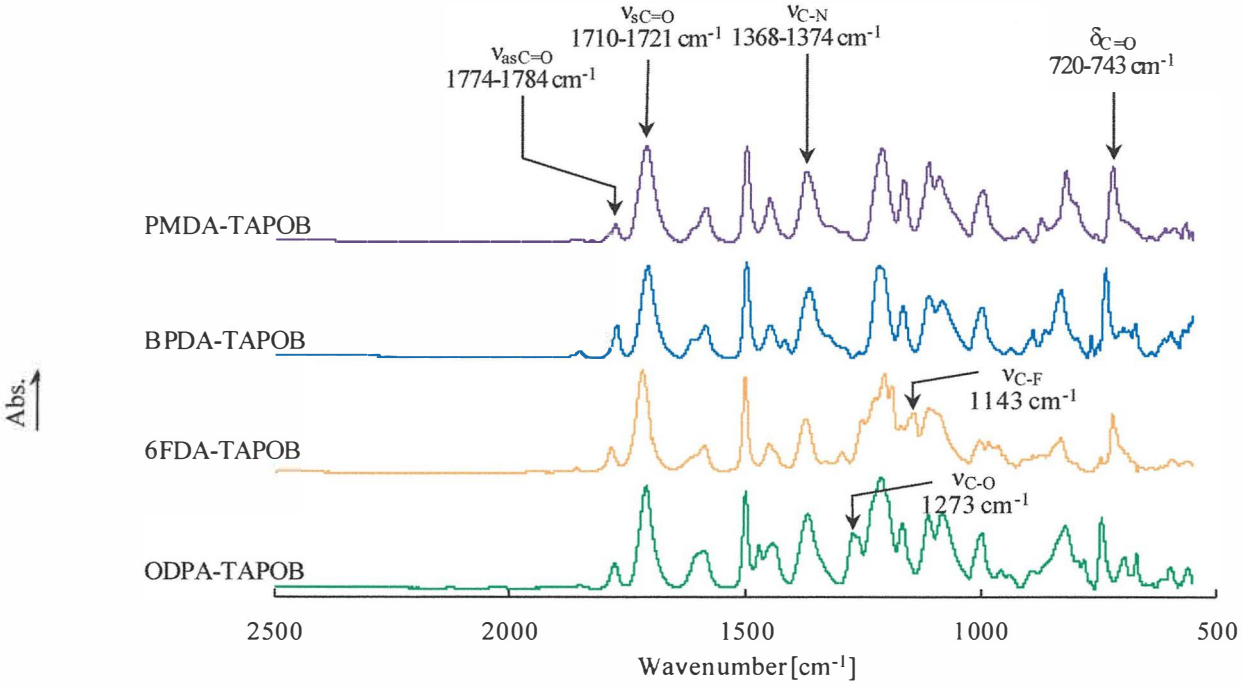

Figure 2-3 ATR FT-IR spectra of the HBPI films with various basic structures.

TAPOB films. More planar and rigid backbone of PMDA and BPDA-TAPOB molecules result in the strong intramolecular and intermolecular interactions that cause the charge transfer complex between alternating electron-donor (triamine) and electron-acceptor (dianhydride) moieties [16]. Nevertheless, the optical transmittances at 600nm of the prepared films were higher than 80% (Table 2-1).

Glass transition temperatures (T_gs) and 5% weight loss temperatures (T_d^5s) of HBPIs

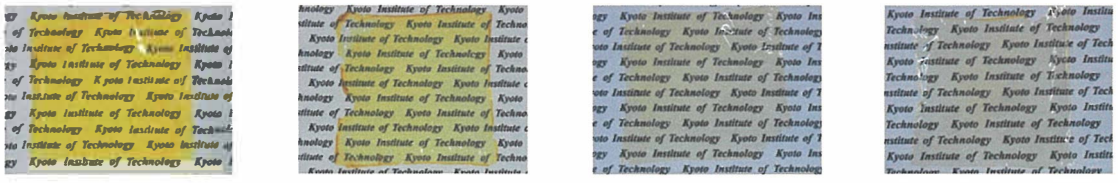

PMDA-TAPOB (thickness : *ca.* 22μm) | BPDA-TAPOB (thickness : *ca.* 20μm) | 6FDA-TAPOB (thickness : *ca.* 20μm) | ODPA-TAPOB (thickness : *ca.* 14μm)

Figure 2-4 The appearance of the HBPI films with various basic structures.

Table 2-1 Physical properties of the HBPIs.

	Transmittance at 600nm [%]	TG-DTA		TMA	Mechanical properties			ρ [g/cm^3]
		T_g [°C]	T_d^5 [°C]	CTE [a] [ppm/°C]	E [GPa]	σ [MPa]	ε [%]	
PMDA-TAPOB	85.2	326	478	35	2.9	88.9	5.3	1.399
BPDA-TAPOB	84.3	293	499	36	3.0	92.9	3.7	1.362
6FDA-TAPOB	88.9	282	457	54	2.4	74.3	3.7	1.433
ODPA-TAPOB	85.8	272	470	52	2.6	111.0	5.9	1.396

[a] CTE at 100-150°C

were investigated by TG-DTA and are summarized in Table 2-1. Generally, T_g depends on the rigidity of polymer chains. The HBPIs derived from PMDA or BPDA exhibited higher T_gs as a result of the rigid polymer backbone. On the other hand, the HBPIs derived from 6FDA or ODPA showed lower T_gs due to the bulky trifluoromethyl group in 6FDA-TAPOB and flexible ether linkage in ODPA-TAPOB. T_d^5 value of 6FDA-TAPOB was lower than those of other HBPIs. This may be related to the low thermal stability of the trifluoromethyl group in 6FDA.

Coefficients of thermal expansion (CTEs) from 100 to 150°C of the prepared HBPI films are listed in Table 2-1. CTEs of PMDA and BPDA-TAPOB HBPI films are lower than those of 6FDA and ODPA-TAPOB HBPI films. This result also related to the rigidity of HBPI molecular chains.

Young's moduli (E), tensile strength (σ), and elongation at break (ε) are listed in Table 2-1. The E values of PMDA and BPDA system HBPI films with rigid molecular chains were higher than those of 6FDA and ODPA system HBPI films. The σ and ε value of ODPA-TAPOB HBPI which contains flexible ether linkage was highest among the prepared films.

3.2 Gas transport properties

Gas permeability, diffusion, and solubility coefficients of the prepared HBPI membranes are summarized in Table 2-2 along with the FFV values calculated from the group contribution method, and diffusion coefficients were plotted against inverse FFV

Table 2-2 Gas transport properties of the HBPI membranes

	FFV	P×10^{10} [cm^3(STP)cm/cm^2 s cmHg]				D×10^8 [cm^2/s]				S×10^2 [cm^3(STP)/cm^3 polym cmHg]			
		CO_2	O_2	N_2	CH_4	CO_2	O_2	N_2	CH_4	CO_2	O_2	N_2	CH_4
PMDA-TAPOB	0.138	3.3	0.59	0.088	0.066	0.14	0.57	0.11	0.020	24	1.0	0.77	3.3
BPDA-TAPOB	0.125	0.56	0.12	0.012	0.0077	0.032	0.17	0.019	0.0020	18	0.69	0.63	3.9
6FDA-TAPOB	0.165	7.4	1.5	0.23	0.098	0.30	1.4	0.25	0.028	25	1.1	0.92	3.5
ODPA-TAPOB	0.129	0.63	0.13	0.013	0.0064	0.030	0.16	0.021	0.0019	21	0.81	0.60	3.3

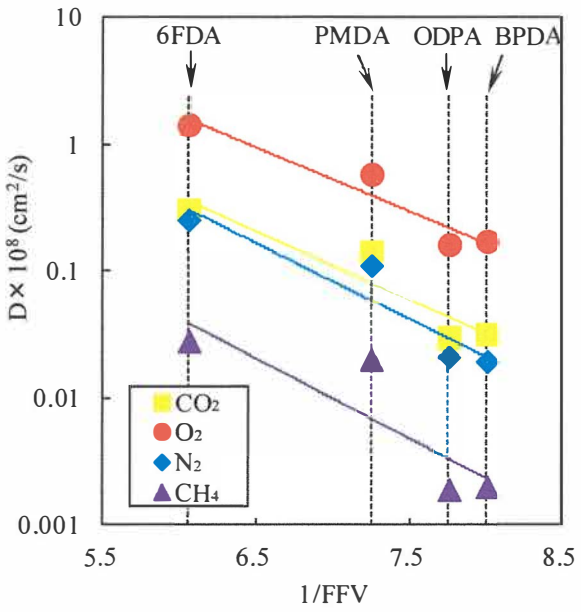

Figure 2-5 Relationship between 1/FFV and gas diffusivity coefficient (D) of the HBPI membranes.

in Figure 2-5.

It is well known that the gas diffusivities of polymers are strongly correlated to their FFVs [17,18]. In Figure 2-5, we can also see the distinct correlation between log D and inverse FFV. The FFVs rank in the following order: 6FDA-TAPOB > PMDA-TAPOB > ODPA-TAPOB > BPDA-TAPOB. This order agrees with the order of diffusion coefficient. The larger FFV of 6FDA system HBPI was caused because the bulky trifluoromethyl groups disrupt the polymer chain packing. On the other hand, the strong intermolecular interactions in PMDA and BPDA system HBPI and the flexible ether linkage in ODPA system HBPI lead to the compact chain packing (low FFV).

Table 2-3 O_2/N_2 and CO_2/CH_4 selectivities of the HBPI membranes at 76 cmHg and 25°C

	O_2/N_2 selectivity			CO_2/CH_4 selectivity		
	$\alpha(O_2/N_2)$	$\alpha^D(O_2/N_2)$	$\alpha^S(O_2/N_2)$	$\alpha(CO_2/CH_4)$	$\alpha^D(CO_2/CH_4)$	$\alpha^S(CO_2/CH_4)$
PMDA-TAPOB	6.7	5.9	1.3	50	6.9	7.3
BPDA-TAPOB	9.8	8.8	1.1	72	16	4.5
6FDA-TAPOB	6.8	5.8	1.2	75	11	7.0
ODPA-TAPOB	10	7.7	1.3	98	16	6.3

The ideal permselectivity for the combination of gases A and B [α(A/B)] is defined by the equation [19]:

$$\alpha(A/B)=\frac{P(A)}{P(B)}=\frac{D(A)}{D(B)}\times\frac{S(A)}{S(B)}=\alpha^D(A/B)\times\alpha^S(A/B) \qquad (5)$$

where $\alpha^D(A/B)$ is the diffusivity selectivity and $\alpha^S(A/B)$ is the solubility selectivity. The O_2/N_2 and CO_2/CH_4 selectivities of the HBPI membranes are listed in Table 2-3, and the O_2/N_2 and CO_2/CH_4 permselectivities are plotted against O_2 and CO_2 permeability coefficients, respectively (Figure 2-6 (a, b)). In Figure 2-6 a), it is recognized that the O_2/N_2 permselectivity of the prepared membranes changed along with the upper bound

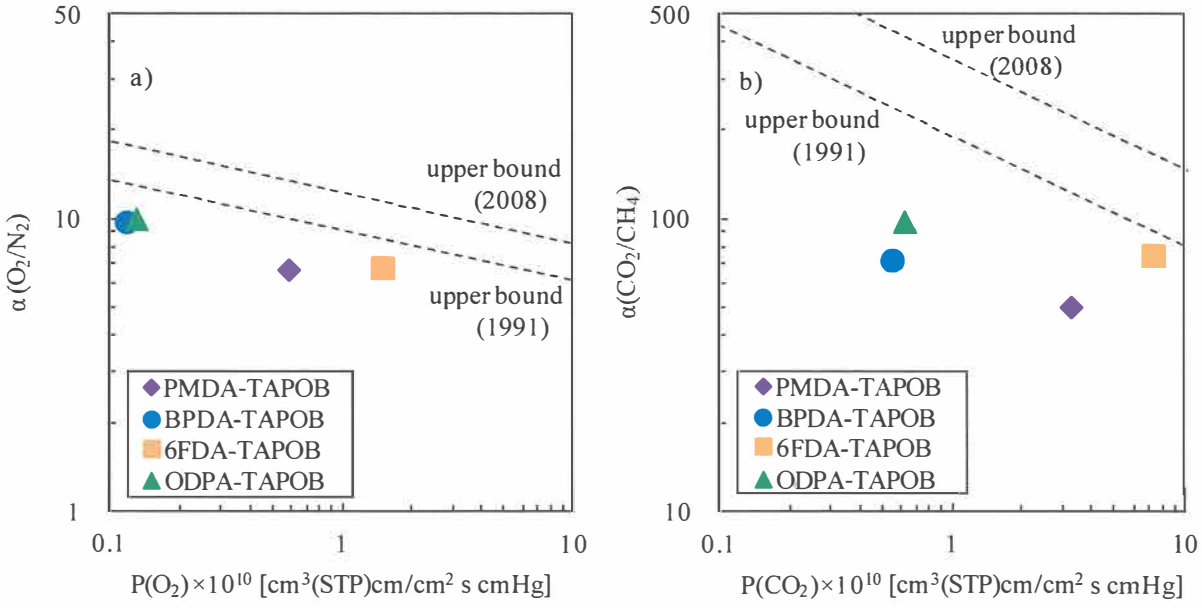

Figure 2-6 Ideal a) O_2/N_2 permselectivity [$\alpha(O_2/N_2)$] and b) CO_2/CH_4 permselectivity [$\alpha(CO_2/CH_4)$] of the HBPI membranes with various basic structures plotted against O_2 and CO_2 permeability coefficient, respectively.

trade-off lines demonstrated by Robeson [20,21]. This behavior is consistent with the general understanding that more permeable polymers are generally less selective, and *vice versa* [19]. On the other hand, compared to the other HBPI membrane, 6FDA-TAPOB membrane displayed around tenfold high CO_2 permeability and nearly equal CO_2/CH_4 permselectivity. For this result, it is considered that the free volume of 6FDA-TAPOB membrane is suitable for CO_2/CH_4 separation.

4. Conclusions

HBPIs with various molecular structures were prepared and their general and gas transport properties were investigated.

ATR FT-IR spectra revealed satisfactory imidization in all prepared HBPIs. 6FDA-TAPOB and ODPA-TAPOB films were almost colorless, whereas PMDA-TAPOB and BPDA-TAPOB films were colored to yellow. From the TG-DTA and TMA measurements and tensile test, it was suggested that the 6FDA-TAPOB molecular chain which contains bulky trifluoromethyl group and ODPA-TAPOB molecular chain which contains flexible ether linkage are more flexible than PMDA-TAPOB and BPDA-TAPOB. 6FDA-TAPOB HBPI membranes demonstrated the highest gas permeability and relatively high CO_2/CH_4 permselectivity due to the high FFV and the free volume suitable for CO_2/CH_4 separation.

References

[1] J. Schauer, P. Sysel, V. Maroušek, Z. Pientka, J. Pokorný, M. Bleha, Pervaporation and Gas Separation Membranes Made from Polyimide/ Polydimethylsiloxane Block Copolymer, J. Appl. Polym. Sci., 61 (1996) 1333-1337.

[2] S. Miyata, S. Sato, K. Nagai, T. Nakagawa, K. Kudo, Relationship Between Gas

Transport Properties and Fractional Free Volume Determined from Dielectric Constant in Polyimide Films Containing the Hexafluoroisopropylidene Group, J. Appl. Polym. Sci., 107 (2008) 3933–3944.

[3] A. Shimazu, T. Miyazaki, M. Maeda, K. Ikeda, Relationships between the Chemical Structures and the Solubility, Diffusivity, and Permselectivity of Propylene and Propane in 6FDA-Based Polyimides, J. Polym. Sci. Part B: Polym. Phys., 38 (2000) 2525–2536.

[4] Y. Li, X. Wang, M. Ding, J. Xu, Effects of Molecular Structure on the Permeability and Permselectivity of Aromatic Polyimides, J. Appl. Polym. Sci., 61 (1996) 741-748.

[5] Y. Hirayama, T. Yoshinaga, Y. Kusuki, K. Ninomiya, T.Sakakibara, T. Tamari, Relation of Gas Permeability with Structure of Aromatic Polyimides I, J. Membr. Sci., 111 (1996) 169-182.

[6] T. Takeichi, J. K. Stille, Star and Liner Imide Oligomers Containing Reactive End Caps: Preparation and Thermal Properties, Macromolecules, 19 (1986) 2093-2102.

[7] D.W. V Krevelen (Eds.), Properties of Polymers, Elsevier, Amsterdam, 1990, 71-107 (Chapter 4).

[8] R.S. Prabhakar, B.D. Freeman, I. Roman, Gas and Vapor Sorption and Permeation in Poly(2,2,4-trifluoro-5-trifluoromethoxy-1,3-dioxole-co-tetrafluoro-ethylene), Macromolecules, 37 (2004) 7688-7697.

[9] N. Muruganandam, W.J. Koros, D.R. Paul, Gas Sorption and Transport in Substituted Polycarbonates, J. Polym. Sci. Part B: Polym. Phys., 25 (1987) 1999-2026.

[10] A. Morisato, H.C. Shen, S.S. Sankar, B.D.Freeman, I. Pinnau, C.G. Casillas, Polymer Characterization and Gas Permeability of Poly(1-trimethylsilyl-1-propyne) [PTMST], Poly(1-phenyl-1-propyne) [PPP], and PTMSP/PPP Blends, J. Polym. Sci.

Part B: Polym. Phys., 34 (1996) 2209-2222.

[11] D.H. Weinkauf, H.D. Kim, D.R. Paul, Gas Transport Properties of Liquid Crystalline Poly(p-phenyleneterephthalamide), Macromolecules, 25 (1992) 788-796.

[12] H. Chen, J. Yin, Synthesis and Characterization of Hyperbranched Polyimides with Good Organosolubility and Thermal Properties Based on New Triamine and Conventional Dianhydrides, J. Polym. Sci. Part A: Polym. Chem, 40 (2002) 3804-3814.

[13] J. Fang, H. Kita, K. Okamoto, Hyperbranched Polyimides for Gas Separation Applications. 1. Synthesis and Characterization, Macromolecules, 33 (2000) 4639-4646.

[14] C.P. Yang, H.C. Chiang, Organosoluble and Light-Colored Fluorinated Polyimides Based on 9,9-Bis[4-(4-amino-2-trifluoromethylphenoxy)phenyl]fluorene and Aromatic Dianhydrides, Colloid. Polym. Sci., 282 (2004) 1347–1358.

[15] E. Hamciuc, C. Hamciuc, M. Olariu, Thermal and Electrical Behavior of Polyimide/Silica Hybrid Thin Films, Polym. Eng. Sci., 50 (2010) 520-529.

[16] S. Ando, T. Matsuura, S. Sasaki, Coloration of Aromatic Polyimides and Electronic Properties of Their Source Materials, Polym. J., 29 (1997) 69-76.

[17] J.Y. Park, D.R. Paul, Correlation and Prediction of Gas Permeability in Glassy Polymer Membrane Materials via a Modified Free Volume based Group Contribution Method, J. Membr. Sci., 125 (1997) 23-39.

[18] A. Thran, G. Kroll, F. Faupel, Correlation between Fractional Free Volume and Diffusivity of Gas Molecules in Glassy Polymers, J. Polym. Sci. Part B: Polym. Phys., 37 (1999) 3344-3358.

[19] B.D. Freeman, Basis of Permeability/Selectivity Tradeoff Relations in Polymeric Gas Separation Membranes, Macromolecules, 32 (1992) 375-380.

[20] L.M. Robeson, Correlation of Separation Factor versus Permeability for Polymeric Membranes, J. Membr. Sci., 62 (1991) 165-185.

[21] L.M. Robeson, The Upper Bound Revisited, J. Membr. Sci., 320 (2008) 390-400.

Chapter 3

Effects of the Degree of Terminal Modification on Physical and Gas Transport Properties of Hyperbranched Polyimide-Silica Hybrid Membranes

1. Introduction

The most remarkable characteristic of dendritic polymers is that they have a large number of molecular terminal groups that can be modified to create different types of multifunctional polymers [1,2]. In synthesizing the hyperbranched polyimide (HBPI) - silica hybrids, a part of molecular terminals of the HBPIs are modified with a silane coupling agent to enhance the compatibility between the HBPI and silica, and thereby to improve the dispersibility of the silica element. Some of the alkoxysilyl groups introduced into the molecular terminals may have cross-linked with each other. However, at this stage, there are no data pertinent to the physical and gas transport properties of the HBPI-silica hybrid membranes with different degrees of terminal modification.

The objective of chapter 3 is to prepare and characterize the HBPI-silica hybrid membranes with different degrees of terminal modification, which is expected that an increased degree of modification leads to improved characteristics and gas transport properties of the HBPI-silica hybrids.

2. Experimental

2.1 Materials

1,3,5-Tris(4-aminophenoxy)benzene (*TAPOB*) was synthesized by the reduction of

1,3,5-tris(4-nitrophenoxy)benzene with palladium carbon and hydrazine in methanol [3]. 4,4'-(Hexafluoroisopropylidene) diphthalic anhydride (*6FDA*) was kindly supplied by Daikin Industries (Osaka, Japan). 3-Aminopropyltrimethoxysilane (*APTrMOS*) was purchased from Sigma-Aldrich Co. LLC. (St. Louis, MO, USA) and tetramethoxysilane (*TMOS*) was purchased from AZmax, Co., Ltd (Tokyo, Japan). *N, N*-Dimethylacetamide (*DMAc*) used as a solvent was purchased from Nacalai Tesque (Kyoto, Japan). The chemical structures of monomers, silane coupling agent, and silicon alkoxide are shown in Figure 3-1.

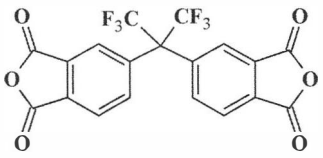

4,4'-(Hexafluoroisopropylidene) diphthalic anhydride (6FDA)

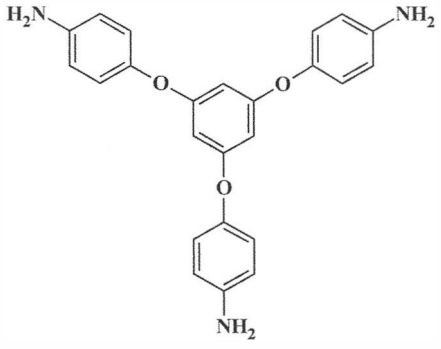

1,3,5-Tris(4-aminophenoxy)benzene (TAPOB)

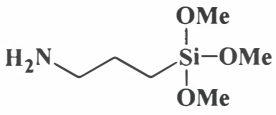

3-Aminopropyltrimethoxysilane (APTrMOS)

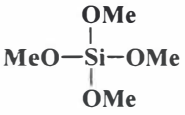

Tetramethoxysilane (TMOS)

Figure 3-1 Chemical structures of monomers, silane coupling agent, and silicon alkoxide.

2.2 Polymerization

Three mmol of 6FDA was dissolved in 40 ml of DMAc in a 100-ml three-neck flask under N_2 flow at room temperature. 1.6 mmol of TAPOB in 20 ml of DMAc was then added dropwise through a syringe with stirring. After stirring for 3 h, the reaction

mixture was diluted to *ca.* 2.0 wt% solid content to avoid gelation. Subsequently, an arbitrary quantity of the silane coupling agent, APTrMOS, was added into the reaction mixture to modify the end groups of the hyperbranched polyamic acids (HBPAAs) with different ratios. After stirring for 1 h, 6FDA-TAPOB HBPAAs with different degree of terminal modification were obtained.

2.3 Membrane formation

The 6FDA-TAPOB HBPI-silica hybrid membranes were prepared to react HBPAAs with silicon alkoxide, TMOS, by sol–gel reaction, and then followed by thermal imidization. Appropriate amounts of TMOS, deionized water (TMOS : deionized water = 1 : 6 as a molar ratio), and a drop of 1*N*-HCl were added into the DMAc solution of the HBPAAs. The mixed solutions were stirred for 24 h and then cast on PET films and dried at 85°C for 3 h. The prepared films were peeled off and subsequently imidized and hybridized at 100°C for 1 h, 200°C for 1 h, and 300°C for 1 h in a heating oven under N_2 flow. The average thickness of the HBPI-silica hybrid films was about 30 μm.

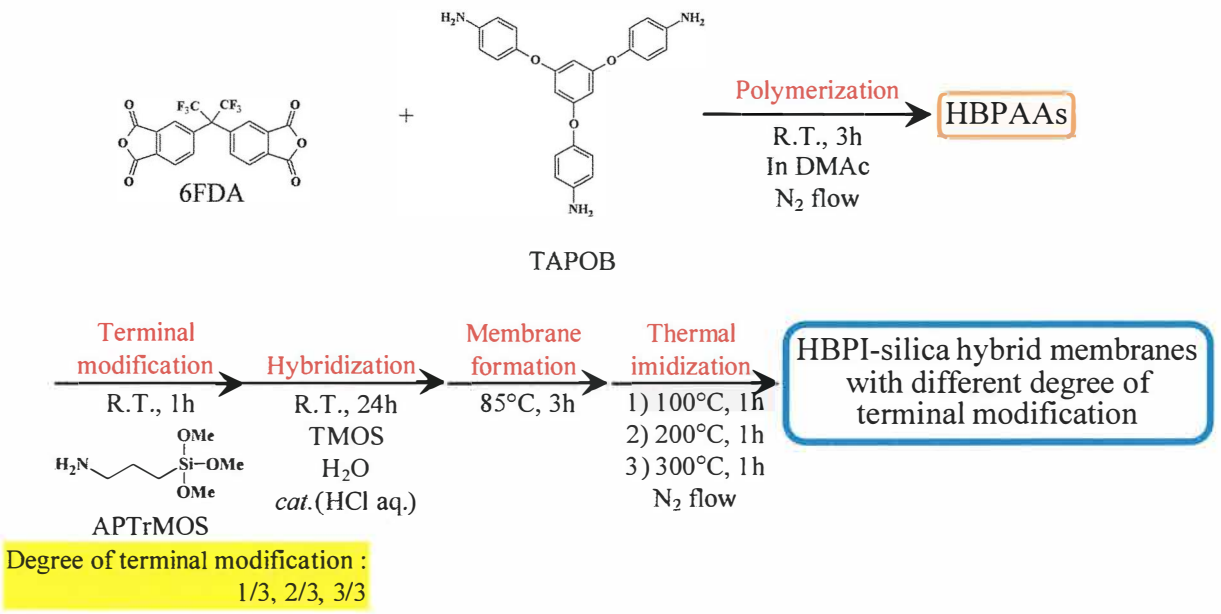

Figure 3-2 A schematic diagram for the preparation of HBPI-silica hybrid membranes with different degree of terminal modification.

A schematic diagram for the preparation of HBPI-silica hybrid membranes with different degree of terminal modification is shown in Figure 3-2.

2.4 Measurements

Inherent viscosity of HBPAAs was measured in a DMAc solution of 0.5 g/dl concentration at 25°C with an Ubbelohde viscometer. Attenuated total reflection Fourier transform infrared (ATR FT-IR) spectra were recorded on a JASCO (Tokyo, Japan) FT/IR-4100 at a wavenumber range of 550–4000 cm^{-1} and a resolution of 1 cm^{-1}. Ultraviolet-visible (UV-vis) optical transmittances were measured with a JASCO V-530 UV/vis spectrometer at wavelengths of 200–800 nm. Thermogravimetric-differential thermal analysis (TG-DTA) experiments were performed with a Seiko Instruments (Chiba, Japan) TG/DTA5200 at a heating rate of 10°C/min under air flow. Dynamic mechanical analysis (DMA) measurements were performed with a Seiko Instruments DMA6100 at a heating rate of 5°C/min under N_2 flow; the load frequency was 1 Hz. Thermal mechanical analysis (TMA) measurements were carried out using a Seiko Instruments TMA/SS6100 at a heating rate of 5°C/min under N_2 flow. Density of the pure HBPIs was measured by the floating method with bromoform and 2-propanol at 25°C. According to the group contribution method, the fractional free volume (FFV) of a polymer can be estimated by the following equation [4]:

$$FFV = \frac{V_{sp} - 1.3V_w}{V_{sp}} \qquad (1)$$

where V_{sp} (cm^3/mol) is the specific molar volume and V_w (cm^3/mol) is the van der Waals volume of the repeating unit. CO_2, O_2, N_2, and CH_4 permeation measurements were taken with a constant volume/variable pressure apparatus under 76 cmHg at 25°C. The permeability coefficient, P [cm^3(STP)cm/cm^2 s cmHg], was determined by the equation [5]:

$$P = \frac{22414}{A}\frac{L}{p}\frac{V}{RT}\frac{dp}{dt} \quad (2)$$

where A is the membrane area (cm^2), L is the membrane thickness (cm), p is the upstream pressure (cmHg), V is the downstream volume (cm^3), R is the universal gas constant (6236.56 cm^3 cmHg/mol K), T is the absolute temperature (K), and dp/dt is the permeation rate (cmHg/s). The gas permeability coefficient can be explained on the basis of the solution-diffusion mechanism, which is represented by the equation [6,7]:

$$P = D \times S \quad (3)$$

where D (cm^2/s) is the diffusion coefficient and S [cm^3(STP)/cm^3_{polym} cmHg] is the solubility coefficient. The diffusion coefficient was calculated by the time-lag method represented by the equation [8]:

$$D = \frac{L^2}{6\theta t} \quad (4)$$

where θt (s) is the time-lag.

3. Results and discussion

3.1 Polymer synthesis

Two types of HBPIs can be prepared by a different addition order and molar ratio of each monomer in the synthesis of HBPI by an $A_2 + B_3$ type polycondensation reaction [9]. In this study, the triamine solution was added into the dianhydride solution with a triamine and dianhydride monomer molar ratio of 1:2, thus obtaining the dianhydride terminated HBPIs. The influence of terminal groups on gas transport property is investigated in chapter 4. To prepare three kinds of HBPAA with different terminal modification rates, an arbitrary quantity of silane coupling agent, APTrMOS, was added into the reaction mixture. In a 6FDA-TAPOB system, a three-dimensional intermolecular cross-linking reaction can easily occur because of the high reactivity of

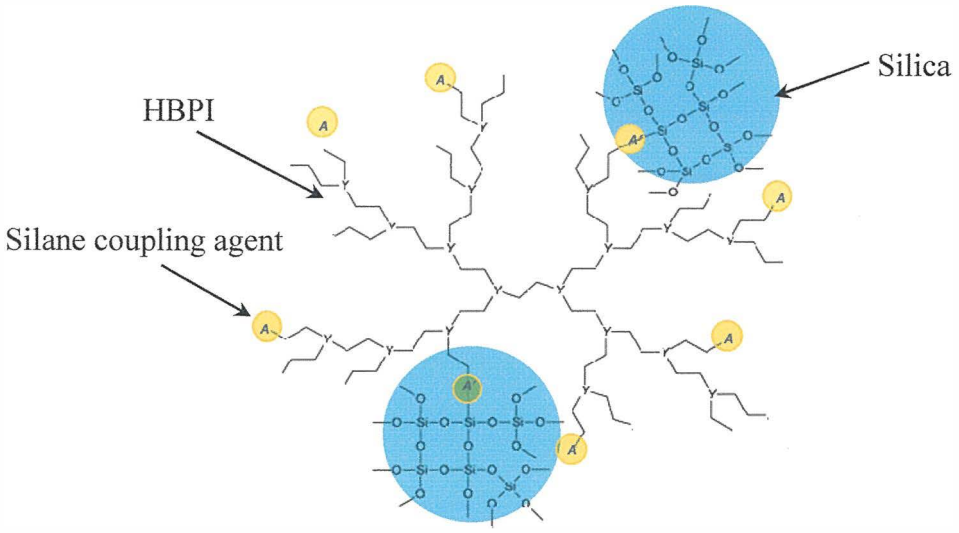

Figure 3-3 A schematic representation of the HBPI-silica hybrid.

6FDA monomers and the equivalent reactivity of the three amino groups of TAPOB. However, a series of HBPAAs were successfully prepared without gelation by controlling the reaction condition, mainly the monomer concentrations in this study. HBPI-silica hybrid films were prepared by sol-gel reaction using HBPAA, TMOS, water, and hydrochloric acid as a catalyst, followed by thermal imidization. A schematic representation of the HBPI-silica hybrid is shown in Figure 3-3.

Table 3-1 Physical properties of the HBPI-silica hybrid films.

	η_{inh}[a] [dl/g]	ρ [g/cm^3]	Transmittance at 600nm [%]
6FDA-TAPOB-APTrMOS(0/3)	0.33	1.439	88.3
6FDA-TAPOB-APTrMOS(1/3)	0.34	1.429	89.7
10wt%SiO_2	-	-	92.9
20wt%SiO_2	-	-	92.0
30wt%SiO_2	-	-	93.0
6FDA-TAPOB-APTrMOS(2/3)	0.36	1.420	92.0
10wt%SiO_2	-	-	92.8
20wt%SiO_2	-	-	91.2
30wt%SiO_2	-	-	94.4
6FDA-TAPOB-APTrMOS(3/3)	0.40	1.411	91.8
10wt%SiO_2	-	-	91.6
20wt%SiO_2	-	-	91.9
30wt%SiO_2	-	-	93.5

[a] η_{inh} value on corresponding HBPAA

The inherent viscosities (η_{inh}s) of HBPAAs are shown in Table 3-1 and plotted against the degree of modification in Figure 3-4. The η_{inh} value increased with increasing the degree of modification, suggesting the increase of molecular weight by

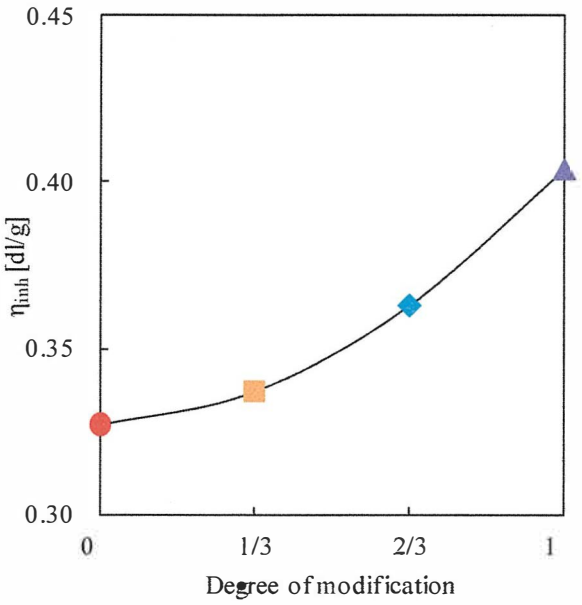

Figure 3-4 Relationship between the degree of modification and the inherent viscosity (η_{inh}) of HBPAA solutions.

the formation of cross-linking through the coupling agent.

3.2 Polymer characterization

The HBPI densities (ρ_s), listed in Table 3-1, decreased with increasing the degree of modification. This indicates that the HBPI molecular chains with a higher degree of modification are difficult to pack because of the cross-linking through the coupling agent.

ATR FT-IR spectra of the HBPI films with different degrees of terminal modification and the HBPI-silica hybrid films (degree of modification: 3/3) are shown in Figure 3-5 (a, b). The bands observed around 1784 cm^{-1} (C=O asymmetrical stretching), 1720 cm^{-1} (C=O symmetrical stretching), 1374 cm^{-1} (C-N stretching), and 720 cm^{-1} (C=O bending)

are characteristic absorption bands of polyimides [9,10]. In contrast, no characteristic bands of polyamic acids around 1680 cm^{-1} were found. These results indicate that the prepared films are well imidized. The band around 1857 cm^{-1} attributed to the terminal anhydride groups decreased with increasing the degree of modification, indicating that the coupling agents reacted with the terminal anhydride groups quantitatively. For the HBPI-silica hybrid membranes, the bands observed around 1100 cm^{-1}, assigned to Si-O-Si stretching, increased with increased silica content, indicating sufficient formation of the three-dimensional Si-O-Si network (Figure 3-5 b)) [11]. The broad absorption bands around 3480 cm^{-1} are likely attributed to silanol groups remaining in the silica domain.

The optical transmittances of the HBPI-silica hybrid films are shown in Table 3-1. These films had good transparency, indicating a favorable dispersion of silica nanoparticles. This high homogeneity results not only from the covalent bonds between

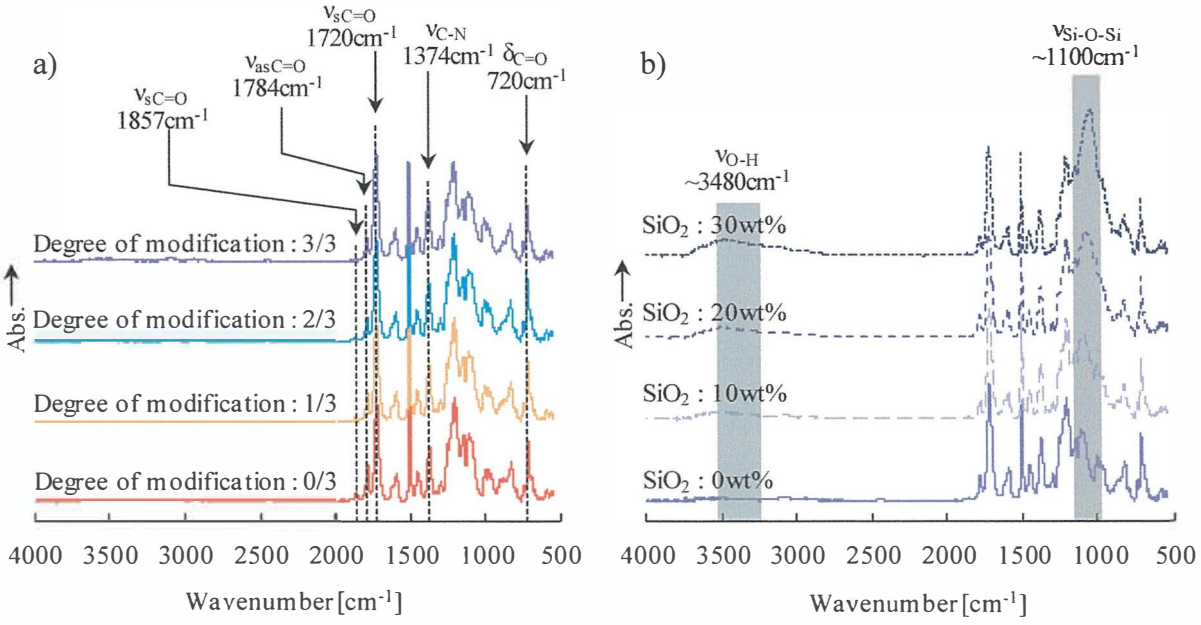

Figure 3-5 ATR-FTIR spectra of the a) HBPI and b) HBPI-silica hybrid films (degree of modification = 3/3).

Table 3-2 Thermal properties of the HBPI-silica hybrid films.

	TG-DTA		DMA	TMA	
	T_d^5 [°C]	Residue [a] [%]	Tg [°C]	CTE [b] (<Tg) [ppm/°C]	CTE [c] (>Tg) [ppm/°C]
6FDA-TAPOB-APTrMOS(0/3)	484	0	279	51	4345
6FDA-TAPOB-APTrMOS(1/3)	469	0	293	52	1679
10wt%SiO_2	488	10	316	49	730
20wt%SiO_2	499	20	330	39	292
30wt%SiO_2	508	32	341	31	123
6FDA-TAPOB-APTrMOS(2/3)	462	0	312	55	1352
10wt%SiO_2	494	11	346	48	503
20wt%SiO_2	502	22	356	36	148
30wt%SiO_2	510	32	371	31	71
6FDA-TAPOB-APTrMOS(3/3)	460	1	331	58	984
10wt%SiO_2	482	9	361	52	334
20wt%SiO_2	500	21	376	45	132
30wt%SiO_2	509	30	390	36	67

[a] Determined from the residual at 800°C
[b] CTE at 100-150°C
[c] CTE at the temperature that the dimensional change marks the maximum

the HBPI and the silica domain formed by APTrMOS but also from the characteristic hyperbranched structure of the molecular chains [12].

Thermal properties of the HBPI-silica hybrid films were investigated by TG-DTA,

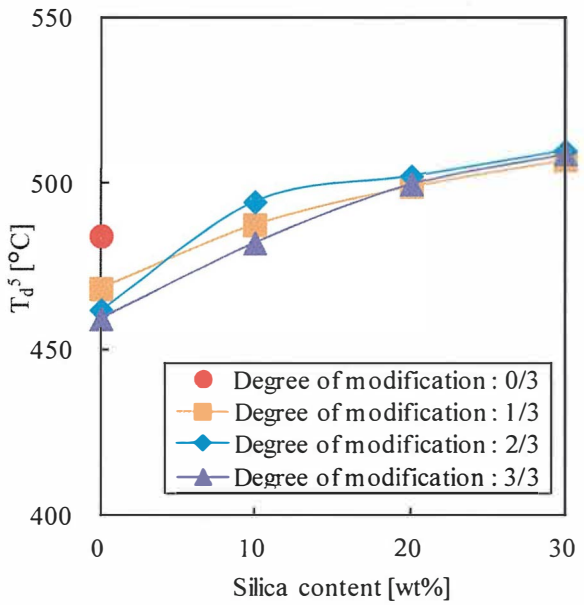

Figure 3-6 5% weight loss temperatures (T_d^5s) of the HBPI-silica hybrids with different degree of terminal modification.

DMA, and TMA measurements. 5% weight loss temperatures (T_d^5s) of the HBPI-silica hybrids were investigated by TG-DTA and are summarized in Table 3-2 along with the silica content determined from the residues at 800°C. The residues showed that all hybrids contained an appropriate amount of silica, as expected. In Figure 3-6, T_d^5 values of the HBPI-silica hybrids are plotted against the silica content. The T_d^5s of the pristine HBPIs without silica decreased with increasing the degree of modification. This is probably because C-N bonds formed by the addition of APTrMOS are less thermally stable. The T_d^5s of the HBPI-silica hybrids increased with increasing silica content. This increased thermal stability of the HBPI-silica hybrids results from the formation of cross-linking mediated by the silica domain, the introduction of inorganic characteristics, and the radical trapping effect of silica.

The storage moduli (E's) and tan δ of the HBPI films with different degrees of terminal modification are shown in Figure 3-7 a). In the rubbery region, E's of the HBPI films increased with increasing the degree of modification. This result indicates that, in

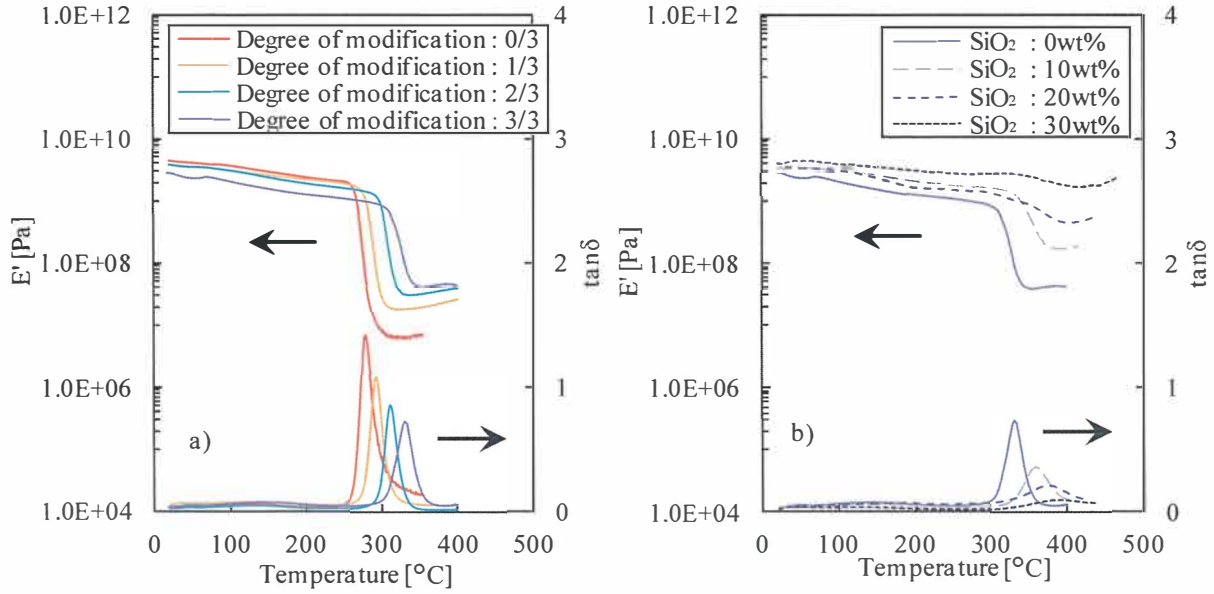

Figure 3-7 Strage moduli (E's) and tan δ of the a) HBPI films with different degree of modification and b) HBPI-silica hybrid films (degree of modification = 3/3).

rubbery region, the mobility of the HBPI molecular chains decreases due to the increased degree of cross-linking through the coupling agent. In contrast, in the glassy region, the E's decreased with increasing the degree of modification. This is because, in the glassy region, the HBPI molecular chains with a higher degree of modification are difficult to pack because of the cross-linking through the coupling agent, leading to an enlargement of the free volume holes [13]. E's of the HBPI-silica hybrid films increased with increasing the silica content in both regions (Figure 3-7 b)). This increase is caused by the increasing of inorganic behavior and the decreasing of mobility of HBPI molecular chains by hybridization with silica.

Glass transition temperatures (T_gs) of the HBPI-silica hybrid films determined from the peak of tan δ are summarized in Table 3-2 and plotted against the silica content in Figure 3-8. When the degree of modification and the silica content were increased, T_gs shifted to a higher temperature along with a decrease of peak intensity and a broadening of the half-width of tan δ. This result indicates that T_gs increased with the increase of

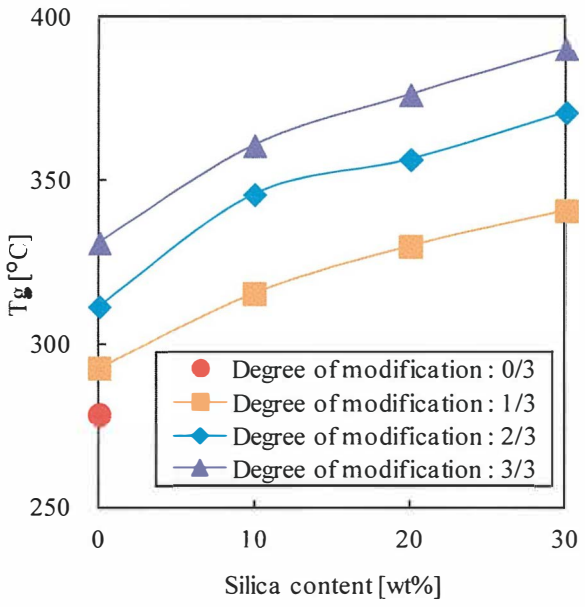

Figure 3-8 Glass transition temperatures (T_gs) of the HBPI-silica hybrid films derived from the peak of tan δ.

inorganic behavior and the decrease of mobility of the HBPI molecular chains caused by cross-linking through the coupling agent and/or silica domains.

Coefficients of thermal expansion (CTEs) of the HBPI films with different degrees of terminal modification are listed in Table 3-2 and plotted against the degree of modification in Figure 3-9. CTEs in the glassy region increased with increasing the degree of modification. This result indicates that the free volume holes of the HBPIs increase in the glassy region due to the increase of the degree of cross-linking through the coupling agent. In contrast, CTEs in the rubbery region decreased with increasing the degree of modification. This result indicates that the mobility of the HBPI molecular chains decreases in the rubbery region due to the increase of the degree of cross-linking through the coupling agent [13]. For the HBPI-silica hybrid films, in both regions, CTEs decreased with increasing the silica content. This is also caused by the enhancement of the thermal mechanical stability of the HBPI matrix by the formation of a robust three-dimensional Si-O-Si network and the decreased mobility of the HBPI molecular chains

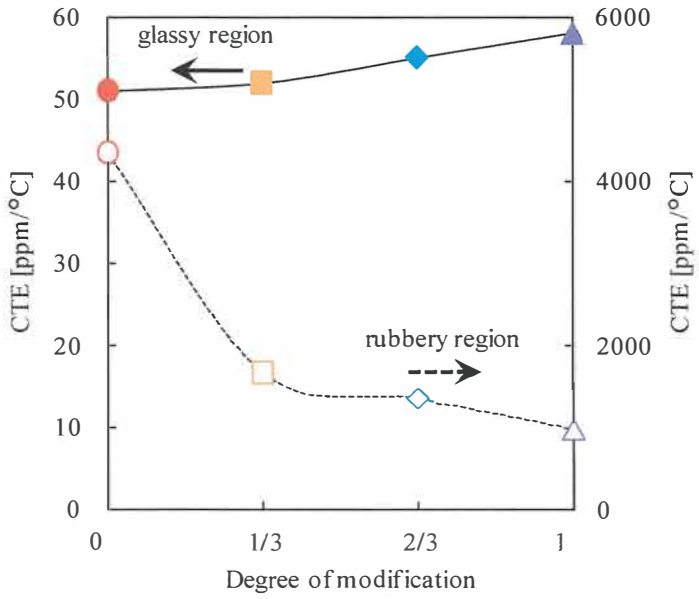

Figure 3-9 Coefficients of thermal expansion (CTEs) of the HBPI films plotted against the degree of terminal modification.

by hybridization with silica. The results obtained from DMA and TMA measurement are satisfactorily correlated.

3.3 Gas transport properties

Gas permeability, diffusion, and solubility coefficients of the HBPI-silica hybrid membranes with different degrees of terminal modification are summarized in Table 3-3, along with the FFV values calculated from the group contribution method. Gas permeability coefficients and FFV values of pristine HBPI membranes without silica increased with increasing the degree of terminal modification. This is due to the increased rigidity of the HBPI molecules due to the formation of cross-linking through the coupling agent. The increase of FFV with increasing the degree of modification supports the above discussion about the decrease of E' and the increase of CTE in the glassy region.

Gas permeability coefficients of the HBPI-silica hybrid membranes increased with

Table 3-3 Gas transport properties of the HBPI-silica hybrid membranes at 76cmHg and 25°C

	FFV	$P\times10^{10}$ [cm^3(STP)cm/cm^2 s cmHg]				$D\times10^{8}$ [cm^2/s]				$S\times10^{2}$ [cm^3(STP)/cm^3 polym cmHg]			
		CO_2	O_2	N_2	CH_4	CO_2	O_2	N_2	CH_4	CO_2	O_2	N_2	CH_4
6FDA-TAPOB -APTrMOS(0/3)	0.163	4.2	0.94	0.12	0.050	0.20	0.86	0.18	0.015	21	1.1	0.68	3.3
6FDA-TAPOB -APTrMOS(1/3)	0.164	7.9	1.6	0.24	0.11	0.35	1.4	0.28	0.030	22	1.1	0.86	3.5
10wt%SiO_2	-	9.0	1.8	0.26	0.13	0.36	1.4	0.27	0.039	25	1.3	0.95	3.3
20wt%SiO_2	-	11	2.0	0.30	0.13	0.36	1.4	0.25	0.028	30	1.5	1.2	4.8
30wt%SiO_2	-	14	2.4	0.36	0.17	0.39	1.4	0.27	0.052	36	1.7	1.3	3.3
6FDA-TAPOB -APTrMOS(2/3)	0.164	11	2.1	0.32	0.17	0.43	1.6	0.33	0.051	25	1.3	0.99	3.4
10wt%SiO_2	-	14	2.6	0.40	0.18	0.45	1.6	0.31	0.038	31	1.7	1.3	4.8
20wt%SiO_2	-	14	2.5	0.38	0.20	0.42	1.5	0.27	0.042	34	1.7	1.4	4.9
30wt%SiO_2	-	19	3.2	0.47	0.23	0.52	1.8	0.31	0.060	37	1.8	1.5	3.7
6FDA-TAPOB -APTrMOS(3/3)	0.165	14	2.7	0.42	0.24	0.51	1.9	0.34	0.058	27	1.4	1.2	4.0
10wt%SiO_2	-	17	3.0	0.47	0.26	0.54	1.9	0.37	0.063	31	1.6	1.3	4.1
20wt%SiO_2	-	19	3.2	0.52	0.23	0.53	1.9	0.36	0.047	36	1.7	1.4	5.0
30wt%SiO_2	-	22	3.6	0.55	0.25	0.59	2.1	0.38	0.050	38	1.7	1.5	5.1

increasing the silica content due to the contribution of the diffusion coefficient as well as the solubility coefficient. These results suggest the additional formation of free volume holes and a Langmuir sorption site effective for gas transport properties by hybridization with silica [14-16]. Similar gas transport properties have been reported in several other studies. Park et al. studied the gas permeation properties of siloxane containing polyimide-porous silica hybrid membranes and suggested that gas transport could occur through the porous silica network or in the interfacial region between the narrow silica networks and the organic matrix [17]. With regard to the increase of the diffusion coefficient, Merkel et al. studied a superglassy polymer-fumed silica nanocomposite and found that the relatively high free volume around the periphery of silica particles, where the rigid polymer chains are unable to pack efficiently, causes the gas molecules to diffuse more rapidly compared to their movement in the bulk polymer [18]. Boroglu et al. also reported that the permeability coefficient of the polyimide-siloxane hybrid polymer membranes increased with increasing the siloxane content and suggested that the increased gas permeability results from the disturbed polymer chain packing and thus the increased free volume [19]. The increased solubilities suggest that the Langmuir sorption site is additionally formed by the incorporation of silica domains. Takahashi et al. reported that the poly(ether imide)-silica nanocomposite membranes have shown the increase in relative solubility when SiO_2 content is increased, which is contrary to Maxwell's theory, and suggested that these results may reflect the presence of voids in addition to sorption in the matrix polymer and possibly some contribution of adsorption to the filler or at the filler-matrix interface [20]. Garcia et al. also reported that sorption in the carbon particles or at the interface of a particle-polymer increased the apparent solubility for the poly(ether imide)-carbon composite membranes [21].

3.4 O_2/N_2 and CO_2/CH_4 selectivities

The ideal permselectivity for the combination of gases A and B [α(A/B)] is defined by the equation [22]:

$$\alpha(A/B)=\frac{P(A)}{P(B)}=\frac{D(A)}{D(B)}\times\frac{S(A)}{S(B)}=\alpha^{D}(A/B)\times\alpha^{S}(A/B) \quad (5)$$

where $\alpha^{D}(A/B)$ is the diffusivity selectivity and $\alpha^{S}(A/B)$ is the solubility selectivity. The O_2/N_2 and CO_2/CH_4 selectivities of the HBPI-silica hybrid membranes are listed in Table 3-4, and the O_2/N_2 and CO_2/CH_4 permselectivities are plotted against the O_2 and CO_2 permeability coefficients, respectively in Figures 3-10 (a, b). In Figure 3-10 (a, b), the open symbols represent the data of the pristine HBPI, and the darkness of filled symbols increase with increasing the silica content.

In general, there is a trade-off relationship between permeability and permselectivity in both glassy and rubbery polymers: the gas permselectivity decreases with increasing the permeability, or *vice versa* [22]. In Figure 3-10 a), we can see that the O_2/N_2 permselectivity of the HBPI and the HBPI-silica hybrid membranes slightly decreases

Table 3-4 Ideal O_2/N_2 and CO_2/CH_4 selectivities of the HBPI-silica hybrid membranes with different degree of terminal modification at 76 cmHg and 25°C

	O_2/N_2 selectivity			CO_2/CH_4 selectivity		
	$\alpha(O_2/N_2)$	$\alpha^{D}(O_2/N_2)$	$\alpha^{S}(O_2/N_2)$	$\alpha(CO_2/CH_4)$	$\alpha^{D}(CO_2/CH_4)$	$\alpha^{S}(CO_2/CH_4)$
6FDA-TAPOB-APTrMOS(0/3)	7.8	4.9	1.6	84	13	6.2
6FDA-TAPOB-APTrMOS(1/3)	6.5	5.1	1.3	73	12	6.3
10wt%SiO_2	6.8	5.2	1.4	68	9.2	7.6
20wt%SiO_2	6.7	5.5	1.3	81	13	6.3
30wt%SiO_2	6.8	5.3	1.3	83	7.5	11
6FDA-TAPOB-APTrMOS(2/3)	6.6	5.0	1.3	62	8.5	7.4
10wt%SiO_2	6.5	5.1	1.3	76	12	6.5
20wt%SiO_2	6.5	5.5	1.2	70	10	6.9
30wt%SiO_2	6.8	5.8	1.2	85	8.6	10
6FDA-TAPOB-APTrMOS(3/3)	6.3	5.6	1.2	60	8.8	6.8
10wt%SiO_2	6.4	5.0	1.2	65	8.5	7.6
20wt%SiO_2	6.1	5.2	1.2	81	11	7.2
30wt%SiO_2	6.5	5.5	1.1	88	12	7.5

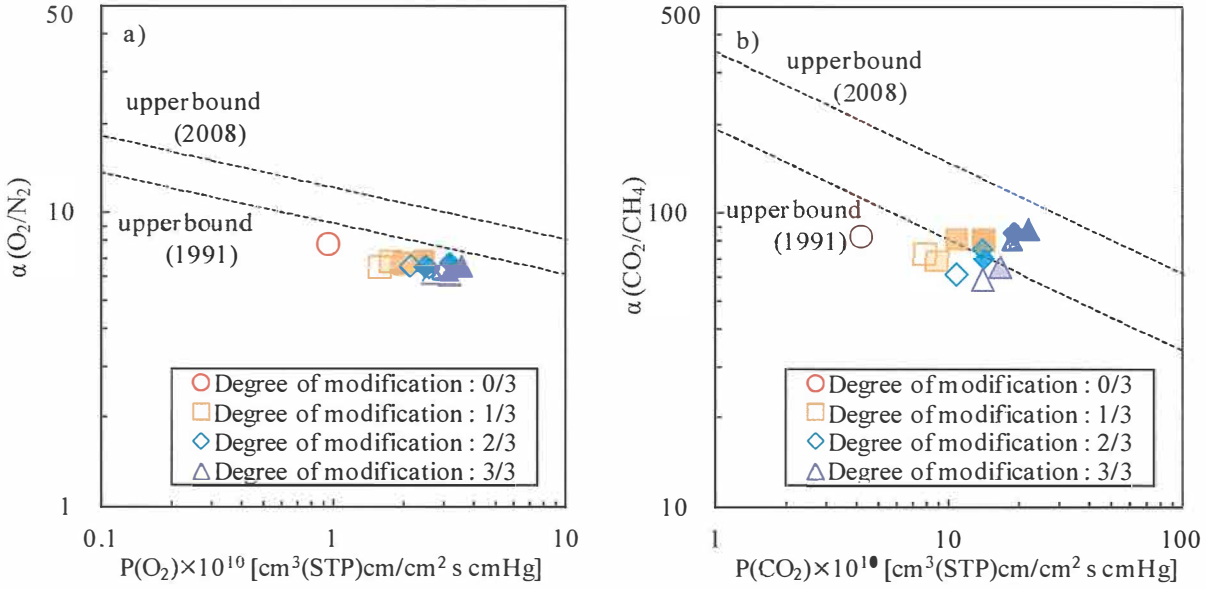

Figure 3-10 Ideal a) O_2/N_2 permselectivity [$\alpha(O_2/N_2)$] and b) CO_2/CH_4 permselectivity [$\alpha(CO_2/CH_4)$] of the HPBI-silica hybrid membranes with different degree of terminal modification plotted against O_2 and CO_2 permeability coefficient, respectively.

with increasing the O_2 permeability along with the upper bound trade-off line for O_2/N_2 separation demonstrated by Robeson [23,24]. That is, free volume holes formed by terminal modification and/or hybridization with silica are not sufficiently effective for the separation of O_2 and N_2 that have similar kinetic diameters and shapes. However, the HBPI-silica hybrid membranes show relatively high $\alpha(O_2/N_2)$ values.

In contrast, both CO_2 permeability and CO_2/CH_4 permselectivity of the HBPI-silica hybrid membranes increased with increasing the silica content, with a significant rise in permselectivity for the HBPI-silica hybrid membranes with a higher degree of modification (Figure 3-10 b)). These results suggest that 1) permeability is increased by the additional formation of free volume holes due to the cross-linking mediated by terminal modification and/or the incorporation of silica and the formation of an interfacial region by the hybridization with silica, and 2) CO_2/CH_4 permselectivity is increased by characteristic distribution and interconnectivity of free volume holes

effective for CO_2/CH_4 separation. An even greater effectiveness of the incorporation of silica domains can be obtained by homogeneous dispersion of silica nanoparticles arising from the characteristic hyperbranched structure. In addition, it is considered that the nano pore inside the porous silica domains formed by the sol-gel reaction in HBPI-silica hybrids is suitable for CO_2/CH_4 separation.

4. Conclusions

6FDA-TAPOB HBPI-silica hybrid membranes with different degree of terminal modification were prepared by sol-gel reaction and their physical and gas transport properties were investigated. The inherent viscosity of HBPAA increased with increasing the degree of modification, suggesting the formation of cross-linking through coupling agents. ATR FT-IR spectra revealed satisfactory imidization and sufficient formation of a three-dimensional Si-O-Si network in all prepared films. TG-DTA measurements showed that the T_d^5s of HBPIs decreased with increasing the degree of modification because of the low thermal stability of C-N bonds formed by the addition of a silane coupling agent. The DMA and TMA measurements suggested that the mobility of the HBPI molecular chains decreased in the rubbery region and that the free volume holes of the HBPI increased in the glassy region due to the increase of the degree of cross-linking through the coupling agent. The CO_2, O_2, N_2, and CH_4 gas permeability coefficients of the HBPI-silica hybrid membranes increased with increasing the degree of modification and silica content, probably due to the additional formation of free volume holes caused by the cross-linking mediated by terminal modification and/or the incorporation of silica domains and the formation of an interfacial region caused by the hybridization with silica. The CO_2/CH_4 permselectivity of the HBPI-silica hybrid membranes also increased with increasing the silica content,

suggesting a characteristic distribution and interconnectivity of free volume holes created by the incorporation of silica.

References

[1] Y.H. Kim, Hyperbranched Polymers 10 Years After, J. Polym. Sci. Part A: Polym. Chem., 36 (1998) 1685-1698.

[2] C. Gao, D. Yan, Hyperbranched Polymers: from Synthesis to Applications, Prog. Polym. Sci., 29 (2004) 183-275.

[3] T. Takeichi, J. K. Stille, Star and Liner Imide Oligomers Containing Reactive End Caps: Preparation and Thermal Properties, Macromolecules, 19 (1986) 2093-2102.

[4] D.W. V Krevelen (Eds.), Properties of Polymers, Elsevier, Amsterdam, 1990, 71-107 (Chapter 4).

[5] R.S. Prabhakar, B.D. Freeman, I. Roman, Gas and Vapor Sorption and Permeation in Poly(2,2,4-trifluoro-5-trifluoromethoxy-1,3-dioxole-co-tetrafluoro-ethylene), Macromolecules, 37 (2004) 7688-7697.

[6] N. Muruganandam, W.J. Koros, D.R. Paul, Gas Sorption and Transport in Substituted Polycarbonates, J. Polym. Sci. Part B: Polym. Phys., 25 (1987) 1999-2026.

[7] A. Morisato, H.C. Shen, S.S. Sankar, B.D.Freeman, I. Pinnau, C.G. Casillas, Polymer Characterization and Gas Permeability of Poly(1-trimethylsilyl-1-propyne) [PTMST], Poly(1-phenyl-1-propyne) [PPP], and PTMSP/PPP Blends, J. Polym. Sci. Part B: Polym. Phys., 34 (1996) 2209-2222.

[8] D.H. Weinkauf, H.D. Kim, D.R. Paul, Gas Transport Properties of Liquid Crystalline Poly(p-phenyleneterephthalamide), Macromolecules, 25 (1992) 788-796.

[9] J. Fang, H. Kita, K. Okamoto, Gas Permeation Properties of Hyperbranched Polyimide Membranes, J. Membr. Sci., 182 (2001) 245-256.

[10] H. Chen, J. Yin, Synthesis and Characterization of Hyperbranched Polyimides with Good Organosolubility and Thermal Properties Based on New Triamine and Conventional Dianhydrides, J. Polym. Sci. Part A: Polym. Chem., 40 (2002) 3804-3814.

[11] C. Hibshman, C.J. Cornelius, E.J. Marand, The Gas Separation Effects of Annealing Polyimide–Organosilicate Hybrid Membranes, J. Membr. Sci., 211 (2003) 25-40.

[12] N. Tomokiyo, Y. Yamada, T. Suzuki, J. Oku, Preparation and Characterization of Hyperbranched Polyimide - Colloidal Silica Hybrids, Polym. Prep. Japan, 55 (2006) 5175-5176.

[13] M. Ogata, N. Kinjo, T. Kawata, Effect of Crosslinking on Physical Properties of Phenol-Formaldehde Novolac Cured Epoxy Resins, J. Appl. Polym. Sci., 48 (1993) 583-601.

[14] T. Suzuki, Y. Yamada, Y. Tsujita, Gas Transport Properties of 6FDA-TAPOB Hyperbranched Polyimide Membrane, Polymer, 45 (2004) 7167-7171.

[15] T. Suzuki, Y. Yamada, Physical and Gas Transport Properties of Novel Hyperbranched Polyimide – Silica Hybrid Membranes, Polym. Bull., 53 (2005) 139-146.

[16] T. Suzuki, Y. Yamada, K. Itahashi, 6FDA-TAPOB Hyperbranched Polyimide-Silica Hybrids for Gas Separation Membranes, J. Appl. Polym. Sci., 109 (2008) 813-819.

[17] H. B. Park, J.K. Kim, S.Y. Nam, Y.M. Lee, Imide-Siloxane Block Copolymer/Silica Hybrid Membranes: Preparation, Characterization and Gas Separation Properties, J. Membr. Sci., 220 (2003) 59-73.

[18] A.L. Andrady, T.C. Merkel, L.G. Toy, Effect of Particle Size on Gas Permeability of Filled Superglassy Polymers, Macromolecules, 37 (2004) 4329-4331.

[19] M.S. Boroglu, M.A. Gurkaynak, The Preparation of Novel Silica Modified Polyimide Membranes: Synthesis, Characterization, and Gas Separation Properties, Polym. Adv. Technol., 22 (2011) 545-553.

[20] S. Takahashi, D.R. Paul, Gas Permeation in Poly(ether imide) Nanocomposite Membranes Based on Surface-Treated Silica. Part 2: With Chemical Coupling to Matrix, Polymer, 47 (2006) 7535-7547.

[21] M.G. García, J. Marchese, N.A. Ochoa, Effect of the Particle Size and Particle Agglomeration on Composite Membrane Performance, J. Appl. Polym. Sci., 118 (2010) 2417-2424.

[22] B.D. Freeman, Basis of Permeability/Selectivity Tradeoff Relations in Polymeric Gas Separation Membranes, Macromolecules, 32 (1992) 375-380.

[23] L.M. Robeson, Correlation of Separation Factor versus Permeability for Polymeric Membranes, J. Membr. Sci., 62 (1991) 165-185.

[24] L.M. Robeson, The Upper Bound Revisited, J. Membr. Sci., 320 (2008) 390-400.

Chapter 4

Effects of the Terminal Structure on Physical and Gas Transport Properties of Hyperbranched Polyimide-Silica Hybrid Membranes

1. Introduction

Hyperbranched polyimides (HBPIs) can be synthesized from either the self-polycondensation of AB_2-type monomers or the polycondensation reaction of $A_2 + B_3$ monomers, where A_2 represents a dianhydride monomer and B_3 represents a triamine monomer. In the case of an $A_2 + B_3$ type polycondensation reaction, a variety of HBPIs can be synthesized by changing the monomer ratio and combining A_2 and B_3 monomers [1-3]. Besides, dianhydride-terminated (DA-) and amine-terminated (AM-) HBPIs can be prepared by a different addition order and molar ratio of each monomer in the synthesis of hyperbranched polyamic acid as a precursor [4]. A schematic image representation of DA- and AM-HBPI is shown in Figure 4-1. These two kinds of HBPIs have the

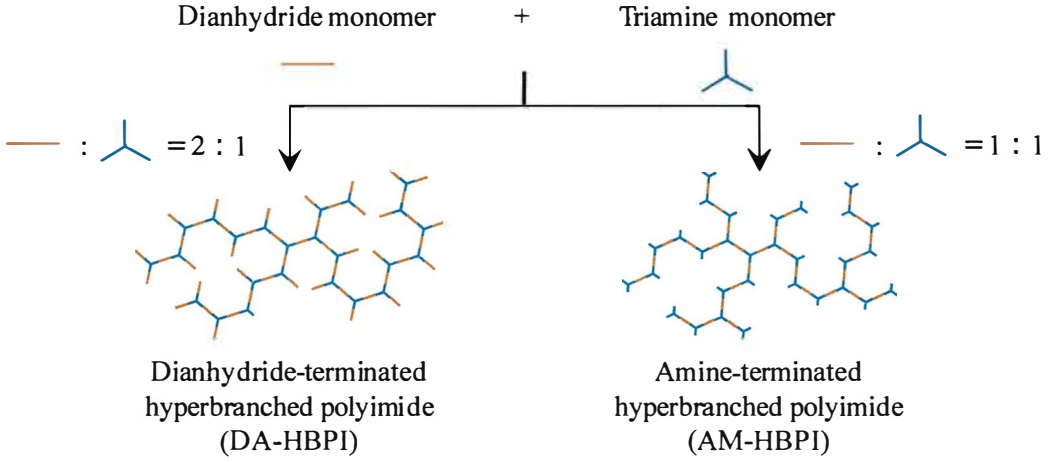

Figure 4-1 A schematic image representation of the DA- and AM-HBPI.

following characteristics; 1) a different terminal structure and 2) a different ratio of branching unit.

In this chapter, the DA- and AM-HBPI-silica hybrid membranes were prepared and their physical and gas transport properties were investigated.

2. Experimental

2.1 Materials

1,3,5-Tris(4-aminophenoxy)benzene (*TAPOB*) was synthesized by the reduction of 1,3,5-tris(4-nitrophenoxy)benzene with palladium carbon and hydrazine in methanol [5]. 4,4'-(Hexafluoroisopropylidene) diphthalic anhydride (*6FDA*) was kindly supplied by Daikin Industries (Osaka, Japan). 3-Aminopropyltrimethoxysilane (*APTrMOS*) and 3-(triethoxysilyl) propyl succinic anhydride (*TEOSPSA*) were purchased from Sigma-Aldrich Co. LLC. (St. Louis, MO, USA) and Gelest Inc. (Morrisville, PA, USA), respectively. Tetramethoxysilane (*TMOS*) was purchased from AZmax, Co., Ltd (Tokyo, Japan). *N, N*-Dimethylacetamide (*DMAc*) used as a solvent was purchased from Nacalai Tesque (Kyoto, Japan). The chemical structures of the monomers, silane coupling agents, and silicon alkoxide are shown in Figure 4-2.

2.2 Polymerization

2.2.1 Dianhydride-terminated hyperbranched polyamic acids (DA-HBPAAs)

Three mmol of 6FDA was dissolved in 40 ml of DMAc in a 100-ml three-neck flask under N_2 flow at room temperature. 1.6 mmol of TAPOB in 20 ml of DMAc was then added dropwise through a syringe with stirring. The solid content of the reaction mixtures was controlled to *ca.* 3.5 wt%. After stirring for 3 h, 0.4 mmol of APTrMOS as a coupling agent was added into the reaction mixture with further stirring for 1 h to afford DA-HBPAA.

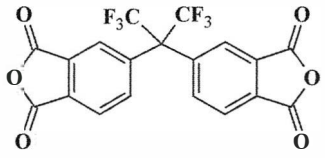

4,4'-(Hexafluoroisopropyli-dene) diphthalic anhydride

(6FDA)

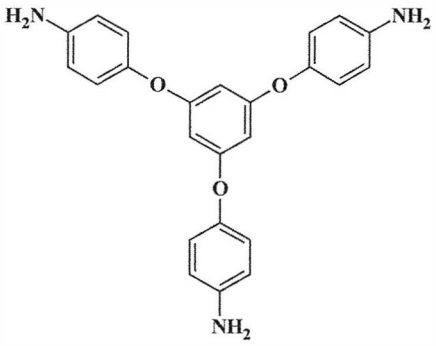

1,3,5-Tris(4-aminophenoxy)benzene

(TAPOB)

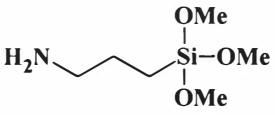

3-Aminopropyltrimethoxysilane

(APTrMOS)

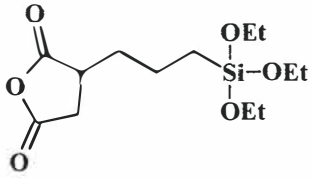

3-(Triethoxysilyl) propyl succinic anhydride

(TEOSPSA)

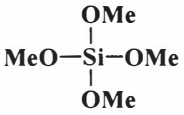

Tetramethoxysilane

(TMOS)

Figure 4-2 Chemical structures of monomers, silane coupling agents, and silicon alkoxide.

2.2.2 Amine-terminated hyperbranched polyamic acids (AM-HBPAAs)

Three mmol of TAPOB was dissolved in 34 ml of DMAc in a 100-ml three-neck flask under N_2 flow at room temperature. 3.0 mmol of 6FDA in 40 ml of DMAc was then added dropwise through a syringe with stirring. The solid content of the reaction mixtures was controlled to *ca.* 3.5 wt%. After stirring for 3 h, 1.0 mmol of TEOSPSA as a coupling agent was added into the reaction mixture with further stirring for 1 h to afford AM-HBPAA.

2.3 Membrane formation

The DA- and AM-HBPI-silica hybrid membranes were prepared to react HBPAAs with silicon alkoxide, TMOS, via sol–gel reaction, and then followed by thermal imidization. Appropriate amounts of TMOS and deionized water (TMOS : deionized water = 1 : 6 as a molar ratio) were added into the DMAc solution of the HBPAAs. The

mixed solutions were stirred for 24 h and then cast on PET films and dried at 85°C for 3 h. These prepared films were peeled off and subsequently imidized and hybridized at 100°C for 1 h, 200°C for 1 h, and 300°C for 1 h in a heating oven under N_2 flow. The average thickness of the DA- and AM-HBPI-silica hybrid films was about 30 μm. A schematic diagram for the preparation of DA- and AM-HBPI-silica hybrid membranes is shown in Figure 4-3.

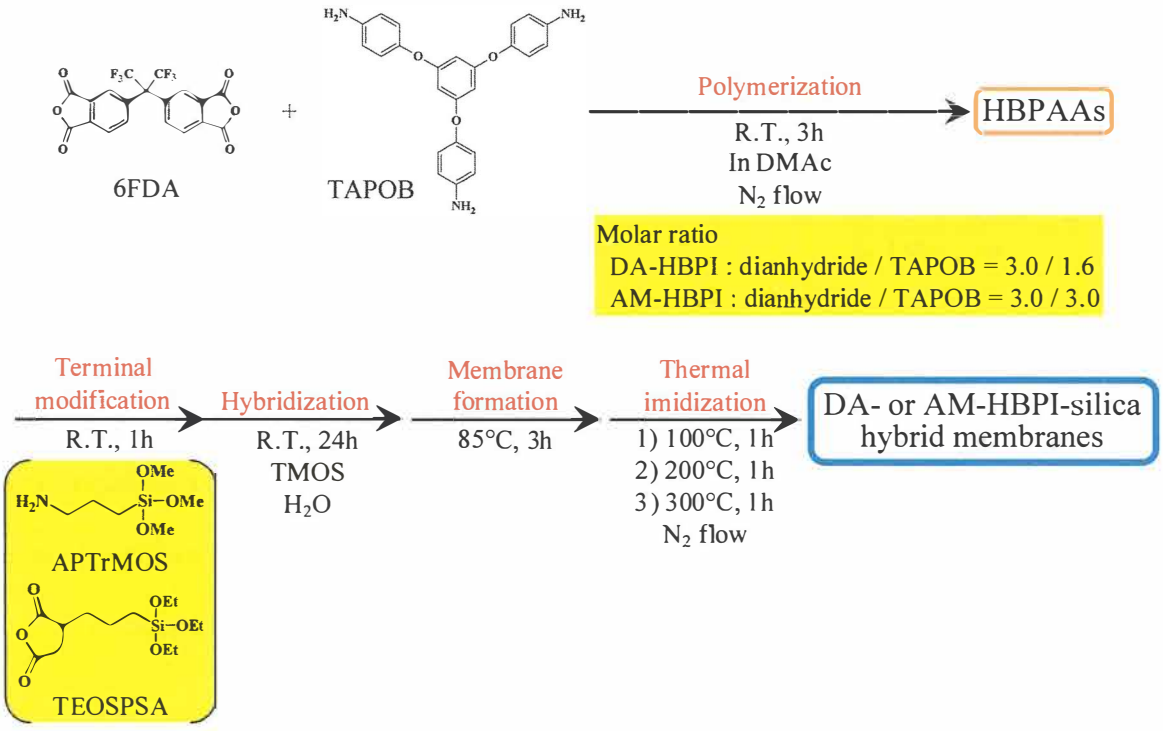

Figure 4-3 A schematic diagram for the preparation of DA- and AM-HBPI-silica hybrid membranes.

2.4 Measurements

Attenuated total reflection Fourier transform infrared (ATR FT-IR) spectra were recorded on a JASCO (Tokyo, Japan) FT/IR-4100 at a wavenumber range of 550--4000 cm^{-1} and a resolution of 1 cm^{-1}. Ultraviolet-visible (UV–vis) optical transmittances were

measured with a JASCO V-530 UV/vis spectrometer at wavelengths of 200–800 nm. Thermogravimetric-differential thermal analysis (TG-DTA) experiments were performed with a Seiko Instruments (Chiba, Japan) TG/DTA5200 at a heating rate of 10°C/min under air flow. Dynamic mechanical analysis (DMA) measurements were performed with a Seiko Instruments DMA6100 at a heating rate of 5°C/min under N_2 flow; the load frequency was 1 Hz. Thermal mechanical analysis (TMA) measurements were carried out using a Seiko Instruments TMA/SS6100 at a heating rate of 5°C/min under N_2 flow. CO_2, O_2, N_2, and CH_4 permeation measurements were taken with a constant volume/variable pressure apparatus under 76 cmHg at 25°C. The permeability coefficient, P [cm^3(STP)cm/cm^2 s cmHg], was determined by the equation [6]:

$$P = \frac{22414}{A}\frac{L}{p}\frac{V}{RT}\frac{dp}{dt} \qquad (1)$$

where A is the membrane area (cm^2), L is the membrane thickness (cm), p is the upstream pressure (cmHg), V is the downstream volume (cm^3), R is the universal gas constant (6236.56 cm^3 cmHg/mol K), T is the absolute temperature (K), and dp/dt is the permeation rate (cmHg/s). The gas permeability coefficient can be explained on the basis of the solution-diffusion mechanism, which is represented by the equation [7,8] :

$$P = D \times S \qquad (2)$$

where D (cm^2/s) is the diffusion coefficient and S [cm^3(STP)/cm^3_{polym} cmHg] is the solubility coefficient. The diffusion coefficient was calculated by the time-lag method represented by the equation [9] :

$$D = \frac{L^2}{6\theta t} \qquad (3)$$

where θt (s) is the time-lag.

3. Results and discussion

3.1 Polymer synthesis

DA- and AM-HBPAAs can be prepared by a different addition order and molar ratio of each monomer in the synthesis of HBPAAs [4]. For the synthesis of the DA-HBPAA, the TAPOB solution was added into the 6FDA solution with a TAPOB and 6FDA monomer molar ratio of 1 : 2, and subsequently, a silane coupling agent, APTrMOS, was added into the reaction mixture to prepare DA-HBPAA of which 1/3 of the molecular terminal was modified. By contrast, for the synthesis of AM-HBPAA, the 6FDA solution was added into the TAPOB solution with a TAPOB and 6FDA monomer molar ratio of 1 : 1, and subsequently, a silane coupling agent, TEOSPSA, was added into the reaction mixture to prepare AM-HBPAA of which molecular terminal was modified as same degree as DA-HBPAA. In the 6FDA-TAPOB system, a three-dimensional intermolecular cross-linking reaction can easily occur because of the high reactivity of 6FDA monomers and the equivalent reactivity of the three amino groups of TAPOB. However, a series of HBPAAs were successfully prepared without gelation by controlling the reaction condition, mainly the monomer concentrations in this study. The DA- and AM-HBPI-silica hybrid membranes were prepared via sol-gel reaction using HBPAA, TMOS and water, followed by thermal imidization.

3.2 Polymer characterization

ATR FT-IR spectra of the DA- and AM-HBPI-silica hybrid films are shown in Figure 4-4. The bands observed around 1784 cm^{-1} (C=O asymmetrical stretching), 1720 cm^{-1} (C=O symmetrical stretching), 1373 cm^{-1} (C-N stretching), and 720 cm^{-1} (C=O bending) are characteristic absorption bands of polyimides [10,11]. In contrast, no characteristic bands of polyamic acids around 1680 cm^{-1} were found. These results indicate that the prepared films are well imidized. The band around 1857 cm^{-1} for the DA-HBPI film is

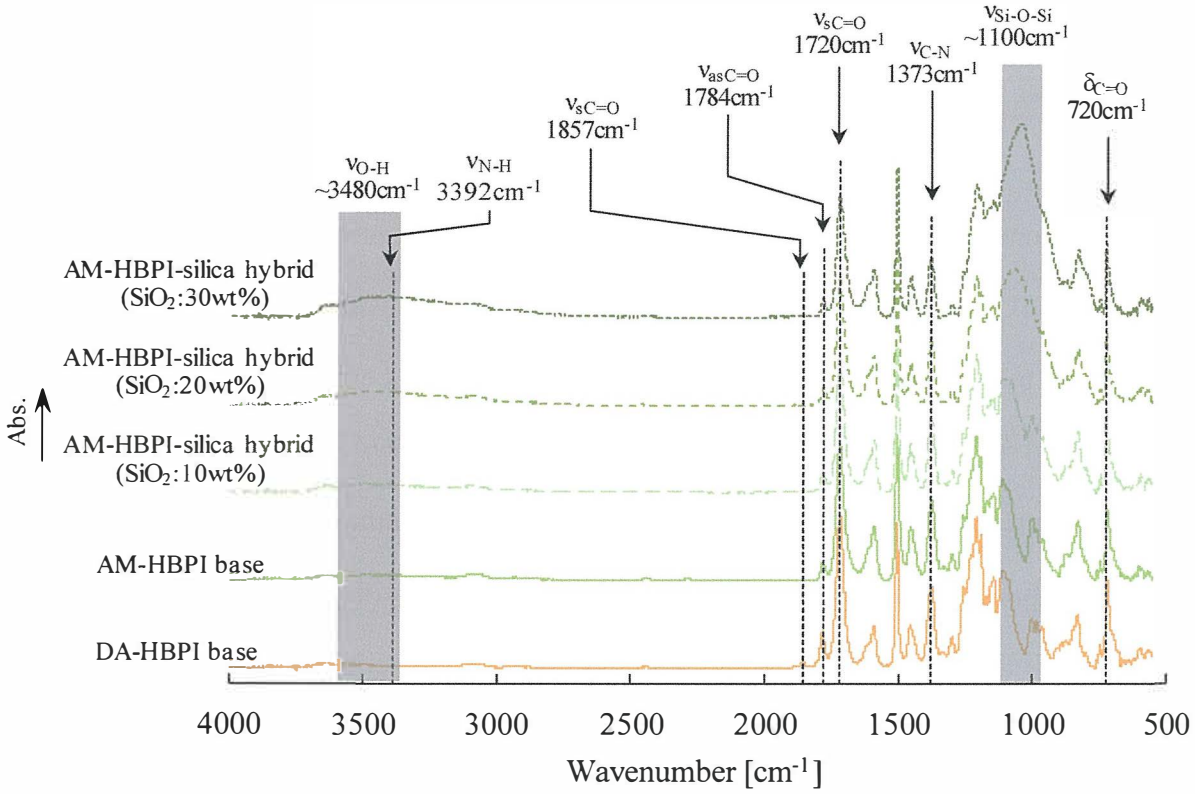

Figure 4-4 ATR FT-IR spectra of the DA-HBPI and AM-HBPI-silica hybrid films.

attributed to the stretching of C=O of the terminal anhydride groups [4,11]. The characteristic bands around 3392cm^{-1} attributed to the stretching of N-H of the terminal amino groups in the AM-HBPI films overlapped with the peak of O-H groups, and could not be observed. For the HBPI-silica hybrid films, it can be observed that the broad and strong absorption bands around 1100 cm^{-1} assigned to Si-O-Si stretching are enhanced with increasing SiO_2 content, indicating sufficient formation of the three-dimensional Si-O-Si network [12]. The broad absorption bands around 3480 cm^{-1} are likely attributed to silanol groups remaining in the silica domain.

The appearance of the DA- and AM-HBPI silica hybrid films are shown in Figure 4-5. The AM-HBPI films are colored to dark brown. For this reason, it is supposed that a part of terminal amino groups of the AM-HBPIs are denatured by heating during thermal imidization. However the optical transmittances of the DA- and AM-HBPI-

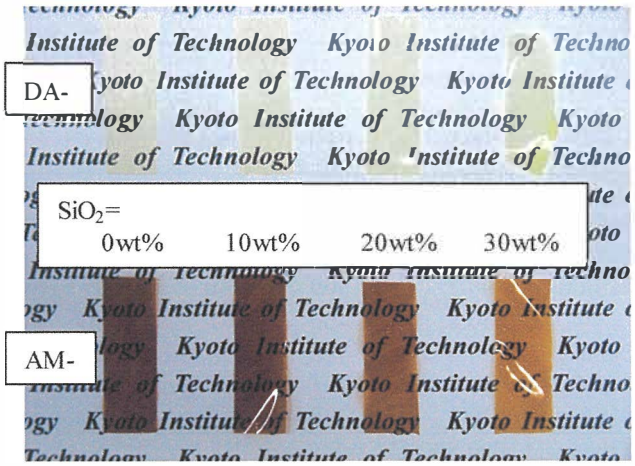

Figure 4-5 Appearance of the DA- and AM-HBPI-silica hybrid films.

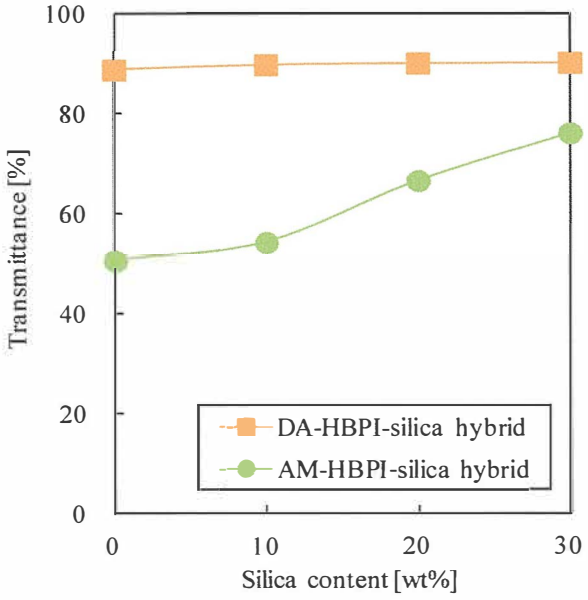

Figure 4-6 Optical transmittances of the DA- and AM-HBPI-silica hybrid films at 600nm.

silica hybrid films increased with increasing silica content (Table 4-1 and Figure 4-6), which might be attributed to decreased imide group density in a unit volume and favorable dispersion of silica. Also, this result shows the favorable dispersion of silica. The fine and homogeneous dispersion of silica is brought not only by coupling agents which offer covalent bonds between organic and inorganic components but also by the

Table 4-1 Physical properties of the DA- and AM-HBPI-silica hybrid films.

	Transmittance at 600nm [%]	TG-DTA		DMA	TMA	
		T_d^5 [°C]	Residue [a] [%]	Tg [°C]	CTE [b] (<Tg) [ppm/°C]	CTE [c] (>Tg) [ppm/°C]
DA-HBPI	88.9	457	0	304	54	2020
silica hybrid 10wt%SiO_2	89.9	490	10	320	47	311
silica hybrid 20wt%SiO_2	90.2	496	20	337	38	228
silica hybrid 30wt%SiO_2	90.3	509	30	351	31	170
AM-HBPI	50.8	466	0	366	53	155
silica hybrid 10wt%SiO_2	54.4	477	7	379	47	124
silica hybrid 20wt%SiO_2	66.8	481	20	378	41	86
silica hybrid 30wt%SiO_2	76.3	495	33	N.D. [d]	31	45

[a] Determined from the residual at 800°C
[b] CTE at 100-150°C
[c] CTE at the temperature that the dimensional change marks the maximum
[d] Not detected

characteristic hyperbranched structures of molecular chains [13].

Thermal properties of the DA- and AM-HBPI-silica hybrids were investigated by TG-DTA, DMA, and TMA measurements. 5% weight loss temperatures (T_d^5s) of the HBPI-silica hybrids were investigated by TG-DTA and are summarized in Table 4-1 along with the silica content determined from the residues at 800°C. The residues

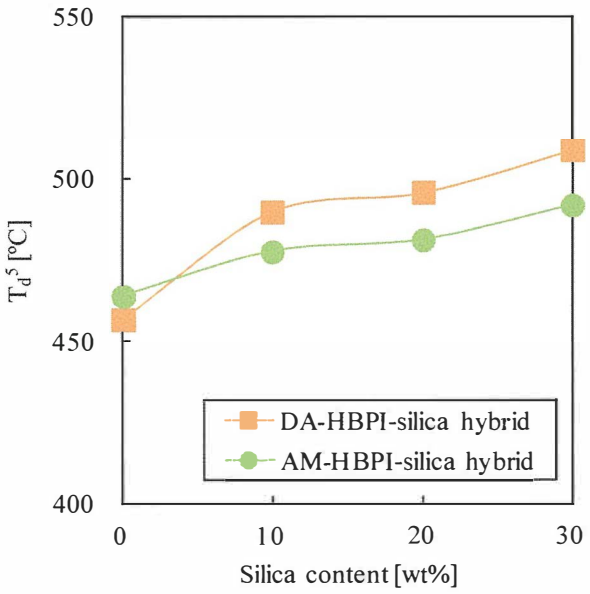

Figure 4-7 5% weight loss temperatures (T_d^5s) of the DA- and AM-HBPI-silica hybrids.

showed that all hybrids contained an appropriate amount of silica, as expected. In Figure 4-7, T_d^5 values of the DA- and AM-HBPI-silica hybrids are plotted against silica content. The T_d^5 value of the pristine DA-HBPI without silica is lower than the corresponding DA-HPBI. This is likely related to higher content of 6FDA component in DA-HBPI than in AM-HBPI. In contrast, the T_d^5 values of the DA-HBPI-silica hybrids increased more remarkably than the AM-HBPI-silica hybrids with increasing silica content. This is because the following reasons; the AM-HBPI is more rigid than the DA-HBPI because there are many branching units in the AM-HBPI molecular chains. Therefore, sol-gel reaction is hard to progress and many silanol groups remain in the AM-HBPI-silica hybrids. The dehydration from these silanol groups causes the decrease of T_d^5s.

The storage moduli (E's) and tan δ of the DA- and AM-HBPI-silica hybrid films are shown in Figure 4-8 (a, b). In the glassy region, no remarkable difference between DA system and AM system hybrids was observed. In contrast, in rubbery region, the E's of

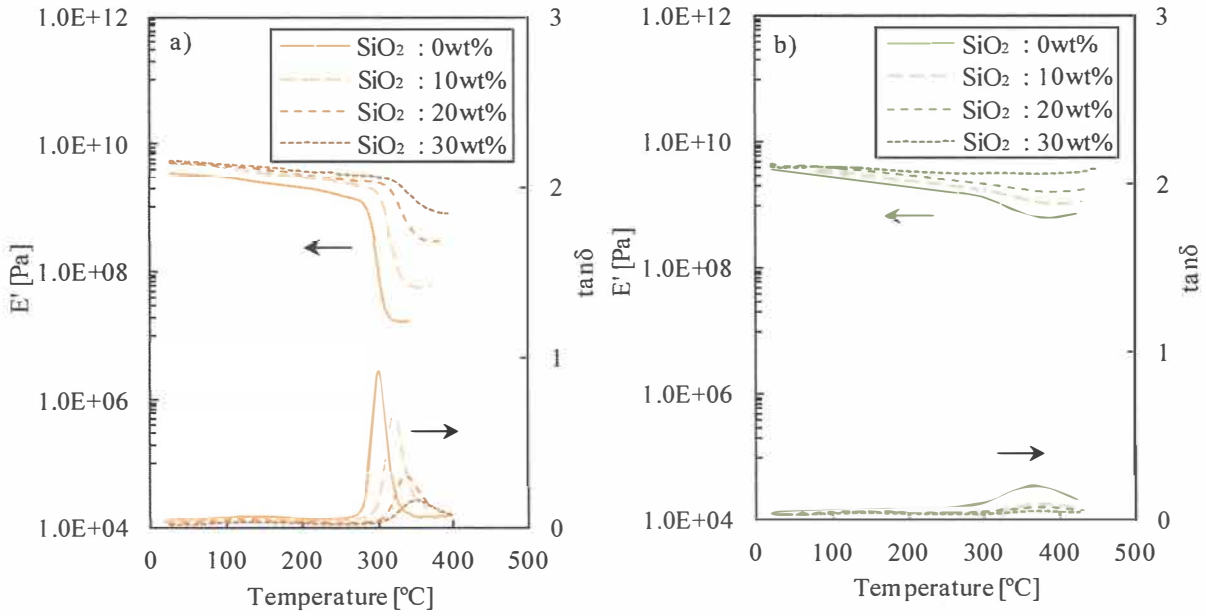

Figure 4-8 Storage moduli (E's) and tan δ of the a) DA- and b) AM-HBPI-silica hybrid films.

the AM-HBPI-silica hybrid films were clearly higher than that of corresponding DA-HBPI-silica hybrid films. This result indicates that in the rubbery region, the mobility of the AM-HBPI-silica hybrid molecular chains is much lower than that of DA-HBPI-silica hybrids because AM-HBPIs contain more branching units than DA-HBPIs and terminal amino groups of AM-HBPIs form the hydrogen bonding each other. E's of the DA- and AM-HBPI-silica hybrid films increased with increasing the silica content in both regions. This increase is caused by increasing the inorganic behavior and decreasing the mobility of HBPI molecular chains by hybridization with silica.

Glass transition temperatures (T_gs) of the DA- and AM-HBPI-silica hybrid films determined from the peak top of tan δ are summarized in Table 4-1 and plotted against the silica content in Figure 4-9. With increasing the silica content, T_gs shifted to a higher temperature along with a decrease of peak intensity and a broadening of the half-width of tan δ. This result indicates that T_gs increased with the increase of inorganic behavior and the decrease of mobility of the HBPI molecular chains caused by cross-

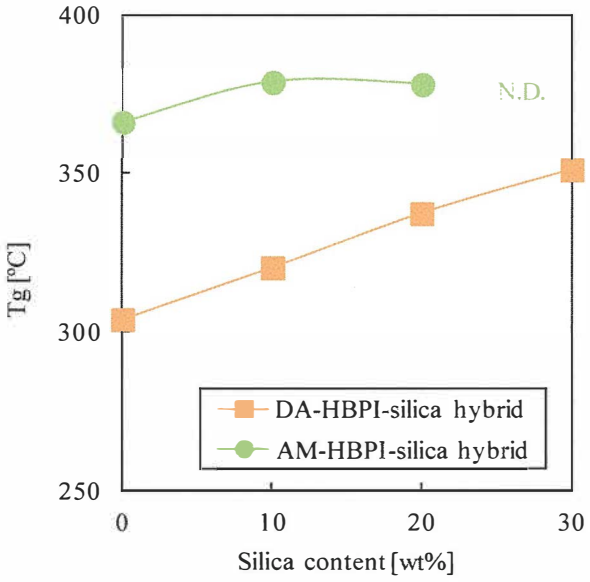

Figure 4-9 Glass transition temperatures (T_gs) of the DA- and AM-HBPI-silica hybrids.

linking through silica domains.

Coefficients of thermal expansion (CTEs) of the DA- and AM-HBPI-silica hybrid films are listed in Table 4-1 and plotted against the silica content in Figure 4-10. In the glassy region, CTEs of the pristine AM-HBPI film was approximately same as that of the pristine DA-HBPI film. By contrast, CTEs of the pristine AM-HBPI film in the rubbery region was much lower than corresponding DA-HBPI film. Same as a result of DMA measurements, this result is also caused by the rigidity of the AM-HBPI molecular chains. With increasing silica content, CTEs of the DA- and AM-HBPI-silica hybrid films decreased in both glassy region and rubbery region. This is caused by the enhancement of the thermal mechanical stability of the HBPI matrix by the formation of a robust three-dimensional Si-O-Si network and the decreased mobility of the HBPI molecular chains by hybridization with silica.

3.3 Gas transport properties

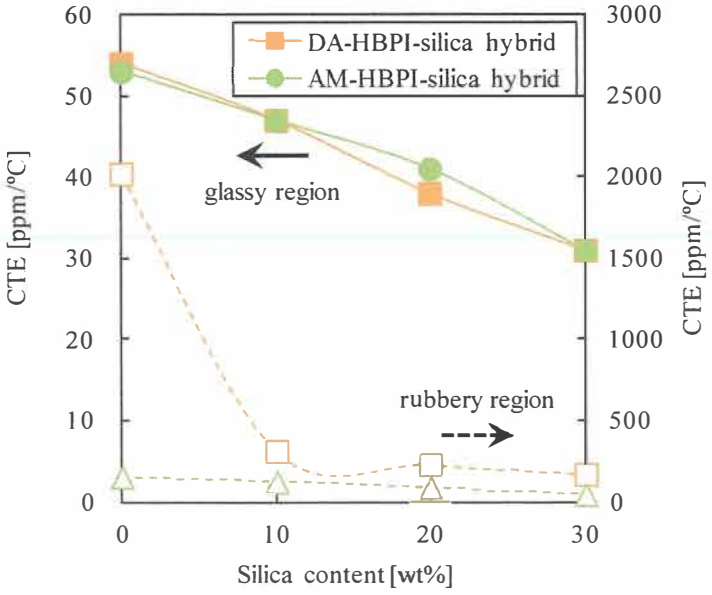

Figure 4-10 Coefficients of thermal expansion (CTEs) of the DA- and AM-HBPI-silica hybrid films.

Gas permeability, diffusion, and solubility coefficients of the DA- and AM-HBPI-silica hybrid membranes are summarized in Table 4-2. Gas permeability coefficient of the pristine AM-HBPI membrane without silica was higher than that of pristine DA-HBPI membrane. This was probably resulting from the rigidity of the molecular chain of the AM-HBPI. Gas permeability coefficients of the DA- and AM-HBPI-silica hybrid membranes increased with increasing the silica content. Similar gas transport properties have been reported in several other studies. For the imide-siloxane block copolymer/silica hybrid membranes prepared via sol-gel reaction, Park et al. also reported that the addition of the organosiloxane in polyimide improved the gas permeabilities of the hybrid membranes, and suggested that the gas transport could occur through the porous silica network or in the interfacial region between the narrow silica networks and the organic matrix [14].

Gas permeability coefficients of the DA-HBPI-silica hybrid membranes increased with increasing the silica content due to the contribution of the diffusion coefficient as well as the solubility coefficient. On the other hand, for the AM-HBPI-silica hybrid membranes, the effect of hybridization to gas permeability coefficient was very small, in particular, the diffusion coefficient did not increase even when the silica content

Table 4-2 Gas transport properties of the DA- and AM-HBPI-silica hybrid membranes.

	$P\times10^{10}$ [cm^3(STP)cm / cm^2 s cmHg]				$D\times10^{8}$ [cm^2 / s]				$S\times10^{2}$ [cm^3(STP) / cm^3 $_{polym}$ cmHg]			
	CO_2	O_2	N_2	CH_4	CO_2	O_2	N_2	CH_4	CO_2	O_2	N_2	CH_4
DA-HBPI	7.4	1.5	0.23	0.098	0.3	1.4	0.25	0.028	25	1.1	0.92	3.5
silica hybrid 10wt%SiO_2	10	2.0	0.31	0.13	0.35	1.5	0.29	0.026	30	1.4	1.1	5.0
silica hybrid 20wt%SiO_2	13	2.1	0.32	0.16	0.37	1.3	0.25	0.030	35	1.7	1.3	5.2
silica hybrid 30wt%SiO_2	23	3.0	0.46	0.24	0.57	1.7	0.29	0.040	41	1.8	1.6	6.0
AM-HBPI	13	2.3	0.35	0.22	0.41	1.5	0.26	0.048	30	1.5	1.3	4.5
silica hybrid 10wt%SiO_2	15	2.4	0.37	0.23	0.47	1.7	0.32	0.055	31	1.4	1.2	4.1
silica hybrid 20wt%SiO_2	16	2.5	0.38	0.22	0.41	1.4	0.27	0.048	38	1.8	1.4	4.6
silica hybrid 30wt%SiO_2	19	2.9	0.43	0.21	0.46	1.5	0.24	0.054	42	1.9	1.8	3.9

increased. The increasing of the permeability coefficient due to the hybridization with silica was caused by 1) the additional formation of free volume holes, 2) the increased rigidity of the polymer chains resulting from the formation of cross-linking mediated by the silica domain, and 3) the formation of a Langmuir sorption site effective for the gas transport properties [15-17]. In the AM-HBPI-silica hybrid membranes, it is thought that an effect of the hybridization was hard to be taken because unreacted silanol groups remain in the silica domain due to the rigidity of the polymer chains, which inhibit the progress of the sol-gel reaction. With regard to the increase of the diffusion coefficient, Boroglu et al. reported that the permeability coefficient of the polyimide-siloxane hybrid membranes increased with increasing the siloxane content. And they suggested that the increased gas permeability resulted from the large enhancements of mean size and total amount of free volume holes attributed to the loose Si–O–Si networks and the cross-linked structure of the hybrid membranes [18]. The increased solubilities suggest that the Langmuir sorption site is additionally formed by the incorporation of silica domains. Garcia et al. also reported that sorption in the carbon particles or at the interface of a particle-polymer increased the apparent solubility for the poly(ether imide)-carbon composite membranes [19].

3.4 O_2/N_2 and CO_2/CH_4 selectivities

The ideal permselectivity for the combination of gases A and B [α(A/B)] is defined by the equation[20] :

$$\alpha(A/B)=\frac{P(A)}{P(B)}=\frac{D(A)}{D(B)}\times\frac{S(A)}{S(B)}=\alpha^{D}(A/B)\times\alpha^{S}(A/B) \qquad (4)$$

where $\alpha^{D}(A/B)$ is the diffusivity selectivity and $\alpha^{S}(A/B)$ is the solubility selectivity. The O_2/N_2 and CO_2/CH_4 selectivities of the HBPI-silica hybrid membranes are listed in

Table 4-3 O_2/N_2 and CO_2/CH_4 selectivities of the DA- and AM-HBPI-silica hybrid membranes.

	O_2/N_2 selectivity			CO_2/CH_4 selectivity		
	$\alpha(O_2/N_2)$	$\alpha^D(O_2/N_2)$	$\alpha^S(O_2/N_2)$	$\alpha(CO_2/CH_4)$	$\alpha^D(CO_2/CH_4)$	$\alpha^S(CO_2/CH_4)$
DA-HBPI	6.8	5.8	1.2	75	11	7.0
silica hybrid 10wt%SiO_2	6.6	5.2	1.3	79	13	5.9
silica hybrid 20wt%SiO_2	6.7	5.3	1.3	82	12	6.8
silica hybrid 30wt%SiO_2	6.6	5.8	1.1	95	14	6.7
AM-HBPI	6.6	5.8	1.2	59	8.5	6.7
silica hybrid 10wt%SiO_2	6.5	5.3	1.2	65	8.6	7.6
silica hybrid 20wt%SiO_2	6.6	5.2	1.3	73	8.5	8.3
silica hybrid 30wt%SiO_2	6.7	6.3	1.1	90	8.5	11

Table 4-3, and O_2/N_2 and CO_2/CH_4 permselectivities are plotted against the O_2 and CO_2 permeability coefficients, respectively in Figure 4-11 (a, b). In Figure 4-11 (a, b), the open symbols represent the data of the pristine HBPI, and the darkness of filled symbols increase with increasing silica content.

In general, there is a trade-off relationship between permeability and permselectivity in both glassy and rubbery polymers: the gas permselectivity decreases with increasing the permeability, or *vice versa*[20]. In this study, the O_2/N_2 permselectivity slightly decreased with increasing O_2 permeability (Figure 4-11 a)). That is, free volume holes

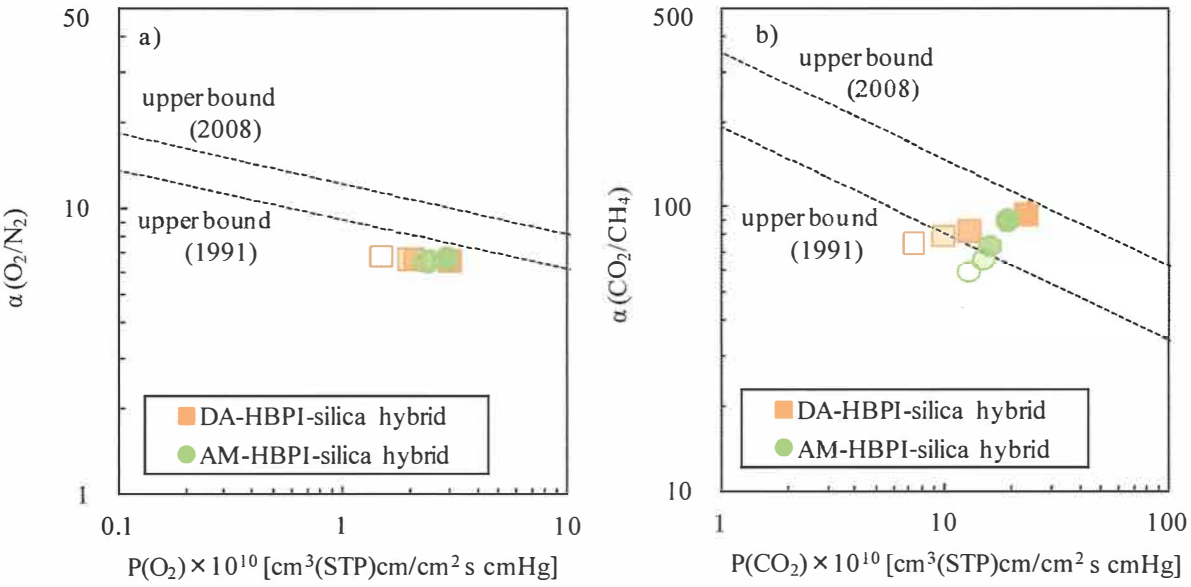

Figure 4-11 Ideal a) O_2/N_2 permselectivity [$\alpha(O_2/N_2)$] and b) CO_2/CH_4 permselectivity [$\alpha(CO_2/CH_4)$]of the DA- and AM-HPBI-silica hybrid membranes plotted against O_2 and CO_2 permeability coefficient, respectively.

formed by hybridization with silica are not sufficiently effective to separate O_2 and N_2 that have similar kinetic diameters and shapes. In contrast, in Figure 4-11 b), it is recognized that both CO_2 permeability and CO_2/CH_4 permselectivity of the HBPI-silica hybrid membranes increased with increasing the silica content and tended close up to the upper bound for CO_2/CH_4 separation[21,22], with a significant increase in permselectivity for the AM-HBPI-silica hybrid membranes. These results suggest that CO_2/CH_4 permselectivity is increased by characteristic distribution and interconnectivity of free volume holes effective for CO_2/CH_4 separation, and furthermore, the high affinity of silanol groups remaining in the AM-HBPI-silica hybrid membranes to CO_2 gas.

4. Conclusions

The DA- and AM-HBPI-silica hybrid membranes were prepared via sol-gel reaction and their physical and gas transport properties were investigated. ATR FT-IR spectra revealed satisfactory imidization and sufficient formation of a three-dimensional Si-O-Si network in all prepared films. Even though the silica content increased, the 5% weight loss temperatures of the AM-HBPI-silica hybrids did not increase so conspicuously as DA-HBPI-silica hybrids. This was probably because there were more silanol groups left in the AM-HBPI-silica hybrids than the DA-HBPI-silica hybrids. From the DMA and TMA measurements, it was suggested that thermomechanical property and dimensional stability of the AM-HBPI-silica hybrid films were higher than those of DA-HBPI-silica hybrid films because of the rigidity of the AM-HBPI molecular chains which contain terminal amino groups and more branching units than DA-HBPI. The CO_2, O_2, N_2, and CH_4 gas permeability coefficient of the pristine AM-HBPI membrane without silica was higher than that of pristine DA-HBPI membrane

due to the rigidity of the molecular chain of the AM-HBPI. The gas permeability and CO_2/CH_4 permselectivity of the DA- and AM-HBPI-silica hybrid membranes increased with increasing silica content. Especially, CO_2/CH_4 permselectivity of the AM-HBPI-silica hybrid membranes remarkably increased with increasing silica content. This behavior was probably due to the characteristic distribution and interconnectivity of free volume holes created by the incorporation of silica and the high affinity of hydroxyl groups remaining in the silica domain to CO_2.

References

[1] Y.H. Kim, Hyperbranched Polymers 10 Years After, J. Polym. Sci. Part A: Polym. Chem., 36 (1998) 1685-1698.

[2] C. Gao, D. Yan, Hyperbranched Polymers: from Synthesis to Applications, Prog. Polym. Sci., 29 (2004) 183-275.

[3] T. Takeichi, J. K. Stille, Star and Liner Imide Oligomers Containing Reactive End Caps: Preparation and Thermal Properties, Macromolecules, 19 (1986) 2093-2102.

[4] J. Fang, H. Kita, K. Okamoto, Hyperbranched Polyimides for Gas Separation Applications. 1. Synthesis and Characterization, Macromolecules, 33 (2000) 4639-4646.

[5] T. Takeichi, J. K. Stille, Star and Liner Imide Oligomers Containing Reactive End Caps: Preparation and Thermal Properties, Macromolecules, 19 (1986) 2093-2102.

[6] R.S. Prabhakar, B.D. Freeman, I. Roman, Gas and Vapor Sorption and Permeation in Poly(2,2,4-trifluoro-5-trifluoromethoxy-1,3-dioxole-co-tetrafluoro-ethylene), Macromolecules, 37 (2004) 7688-7697.

[7] N. Muruganandam, W.J. Koros, D.R. Paul, Gas Sorption and Transport in Substituted Polycarbonates, J. Polym. Sci. Part B: Polym. Phys., 25 (1987) 1999-2026.

[8] A. Morisato, H.C. Shen, S.S. Sankar, B.D.Freeman, I. Pinnau, C.G. Casillas,

Polymer Characterization and Gas Permeability of Poly(1-trimethylsilyl-1-propyne) [PTMST], Poly(1-phenyl-1-propyne) [PPP], and PTMSP/PPP Blends, J. Polym. Sci. Part B: Polym. Phys., 34 (1996) 2209-2222.

[9] D.H. Weinkauf, H.D. Kim, D.R. Paul, Gas Transport Properties of Liquid Crystalline Poly(p-phenyleneterephthalamide), Macromolecules, 25 (1992) 788-796.

[10] J. Fang, H. Kita, K. Okamoto, Gas Permeation Properties of Hyperbranched Polyimide membranes, J. Membr. Sci., 182 (2001) 245-256.

[11] H. Chen, J. Yin, Synthesis and Characterization of Hyperbranched Polyimides with Good Organosolubility and Thermal Properties Based on New Triamine and Conventional Dianhydrides, J. Polym. Sci. Part A: Polym. Chem., 40 (2002) 3804-3814.

[12] C. Hibshman, C.J. Cornelius, E.J. Marand, The Gas Separation Effects of Annealing Polyimide–Organosilicate Hybrid Membranes, J. Membr. Sci., 211 (2003) 25-40.

[13] N. Tomokiyo, Y. Yamada, T. Suzuki, J. Oku, Preparation and Characterization of Hyperbranched Polyimide - Colloidal Silica Hybrids, Polym. Prep. Japan, 55 (2006) 5175-5176.

[14] H. B. Park, J.K. Kim, S.Y. Nam, Y.M. Lee, Imide-Siloxane Block Copolymer/Silica Hybrid Membranes: Preparation, Characterization and Gas Separation Properties, J. Membr. Sci., 220 (2003) 59-73.

[15] T. Suzuki, Y. Yamada, Y. Tsujita, Gas Transport Properties of 6FDA-TAPOB Hyperbranched Polyimide Membrane, Polymer, 45 (2004) 7167-7171.

[16] T. Suzuki, Y. Yamada, Physical and Gas Transport Properties of Novel Hyperbranched Polyimide – Silica Hybrid Membranes, Polym. Bull., 53 (2005) 139-146.

[17] T. Suzuki, Y. Yamada, K. Itahashi, 6FDA-TAPOB Hyperbranched Polyimide-

Silica Hybrids for Gas Separation Membranes, J. Appl. Polym. Sci., 109 (2008) 813-819.

[18] M.S. Boroglu, M.A. Gurkaynak, The Preparation of Novel Silica Modified Polyimide Membranes: Synthesis, Characterization, and Gas Separation Properties, Polym. Adv. Technol., 22 (2011) 545-553.

[19] M.G. García, J. Marchese, N.A. Ochoa, Effect of the Particle Size and Particle Agglomeration on Composite Membrane Performance, J. Appl. Polym. Sci., 118 (2010) 2417-2424.

[20] B.D. Freeman, Basis of Permeability/Selectivity Tradeoff Relations in Polymeric Gas Separation Membranes, Macromolecules, 32 (1992) 375-380.

[21] L.M. Robeson, Correlation of Separation Factor versus Permeability for Polymeric Membranes, J. Membr. Sci., 62 (1991) 165-185.

[22] L.M. Robeson, The Upper Bound Revisited, J. Membr. Sci., 320 (2008) 390-400.

Chapter 5

Physical and Gas Transport Properties of Asymmetric Hyperbranched Polyimide-Silica Hybrid Membranes

1. Introduction

In the synthesis of liner-type polyimides, we can obtain various kinds of polyimides with different structures by combining various monomers (diamines and dianhydrides). For the asymmetric type polyimides prepared from asymmetric dianhydrides and symmetric diamines, it has been reported that the resulting polyimides exhibited increased solubility, reduced viscosity, and higher glass transition temperatures (T_gs) than the symmetric type polyimides. The increased T_gs were ascribable to their rigid and bent structure, and the steric hindrance [1-4]. In general, it is said that the increase in gas permeability is also induced by the rigid molecular chain.

In this chapter, physical and gas transport properties of the asymmetric hyperbranched polyimide (HBPI) -silica hybrid membranes were investigated and compared with those of symmetric HBPI-silica hybrid membranes.

2. Experimental

2. 1 Materials

1,3,5-Tris(4-aminophenoxy)benzene (*TAPOB*) was synthesized by the reduction of 1,3,5-tris(4-nitrophenoxy)benzene with palladium carbon and hydrazine in methanol [5]. Asymmetric triamine monomer, 2,4,4'-(triaminodiphenyl)ether (*TADE*), and dianhydride monomer, 4,4'-(hexafluoroisopropylidene) diphthalic anhydride (*6FDA*), were kindly supplied from Wakayama Seika Kogyo Co. (Wakayama, Japan) and Daikin

Industries (Osaka, Japan), respectively. 3-Aminopropyltrimethoxysilane (*APTrMOS*) and 3-(triethoxysilyl) propyl succinic anhydride (*TEOSPSA*) were purchased from Sigma-Aldrich Co. LLC. (St. Louis, MO, USA) and Gelest Inc. (Morrisville, PA, USA), respectively. Tetramethoxysilane (*TMOS*) was purchased from AZmax, Co., Ltd (Tokyo, Japan). *N, N*-Dimethylacetamide (*DMAc*) used as a solvent was purchased from Nacalai Tesque (Kyoto, Japan). The chemical structures of the monomers, silane coupling agents, and silicon alkoxide are shown in Figure 5-1.

2.2 Polymerization

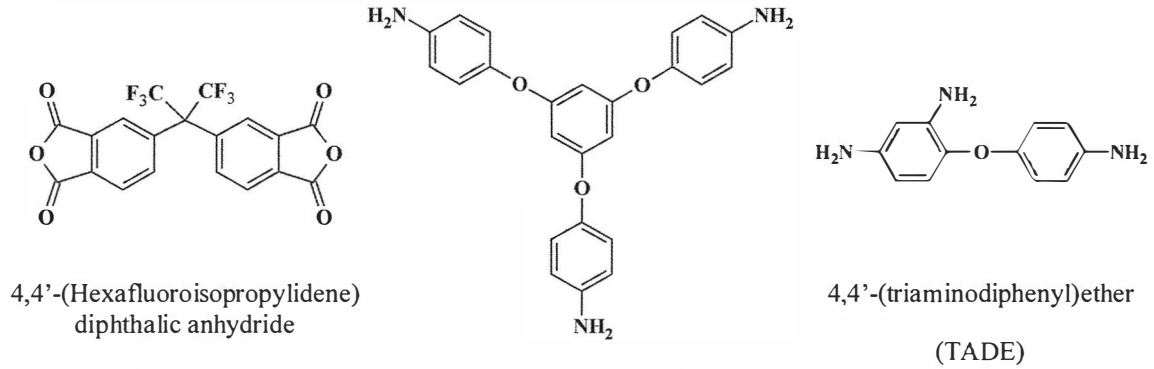

Figure 5-1 Chemical structures of monomers, silane coupling agents and silicon alkoxide.

2.2.1 Dianhydride-terminated hyperbranched polyamic acids (DA-HBPAAs)

Three mmol of 6FDA was dissolved in 30-40 ml of DMAc in a 100-ml three-neck flask under N_2 flow at room temperature. 1.6 mmol of triamine (TADE or TAPOB) in

20 ml of DMAc was then added dropwise through a syringe with stirring. The solid content of reaction mixtures was controlled to *ca.* 3.5 wt%. After stirring for 3 h, 0.4 mmol of APTrMOS as a coupling agent was added into the reaction mixture with further stirring for 1 h to afford asymmetric or symmetric DA-HBPAA.

2.2.2 Amine-terminated hyperbranched polyamic acids (AM-HBPAAs)

Three mmol of triamine (TADE or TAPOB) was dissolved in 30-34 ml of DMAc in a 100-ml three-neck flask under N_2 flow at room temperature. 3.0 mmol of 6FDA in 28-40 ml of DMAc was then added dropwise through a syringe with stirring. The solid content of reaction mixtures was controlled to *ca.* 3.5 wt%. After stirring for 3 h, 1.0 mmol of TEOSPSA as a coupling agent was added into the reaction mixture with further stirring for 1 h to afford asymmetric or symmetric AM-HBPAA.

2.3 Membrane formation

The asymmetric and symmetric HBPI-silica hybrid membranes were prepared by the reaction of asymmetric or symmetric HBPAAs with silicon alkoxide, TMOS, via sol–gel reaction, and then followed by thermal imidization. Appropriate amounts of TMOS and deionized water (TMOS : deionized water = 1 : 6 as a molar ratio) were added into the DMAc solution of the asymmetric or symmetric HBPAAs. The mixed solutions were stirred for 24 h and then cast on PET films and dried at 85°C for 3 h. These prepared films were peeled off and subsequently imidized and hybridized at 100°C for 1 h, 200°C for 1 h, and 300°C for 1 h in a heating oven under N_2 flow. The average thickness of the asymmetric or symmetric HBPI-silica hybrid membranes was about 30 μm. A schematic diagram for the preparation of asymmetric and symmetric HBPI-silica hybrid membranes is shown in Figure 5-2.

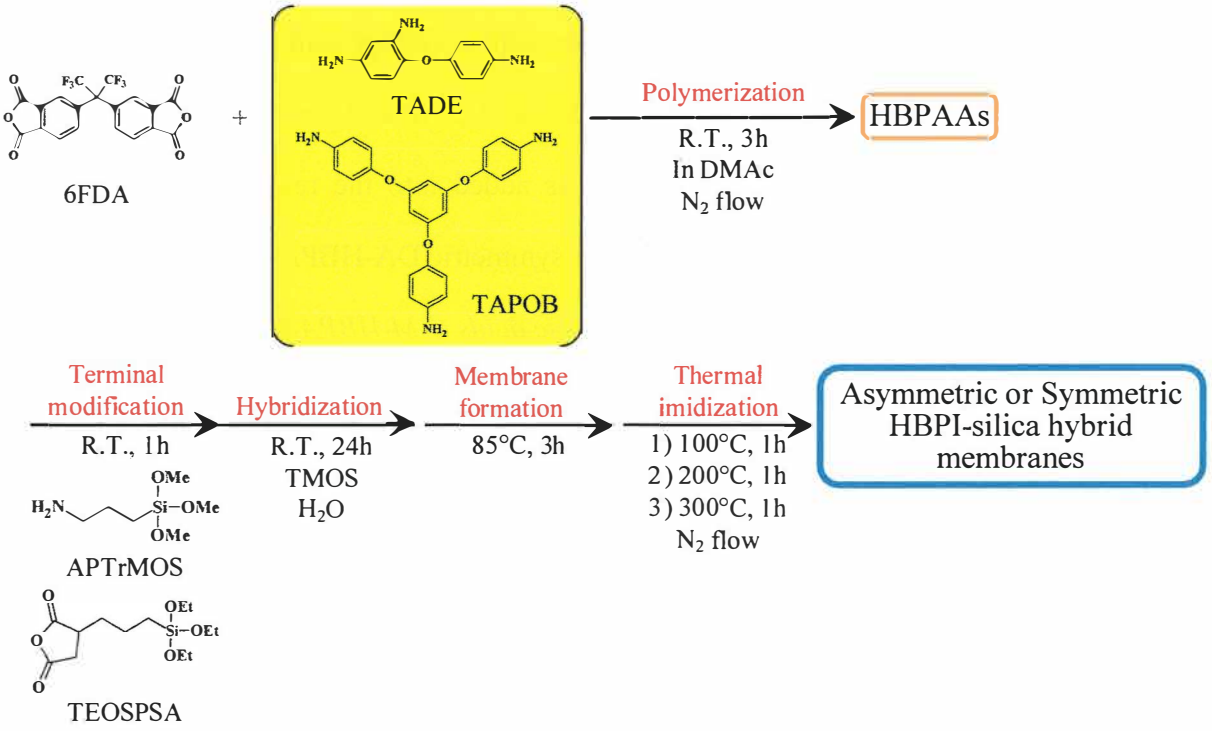

Figure 5-2 A schematic diagram for the preparation of asymmetric and symmetric HBPI-silica hybrid membranes.

2.4 Measurements

The inherent viscosity of HBPAAs was measured in a DMAc solution with a 0.5 g/dL concentration at 25°C with an Ubbelohde viscometer. Attenuated total reflection Fourier transform infrared (ATR FT-IR) spectra were recorded on a JASCO (Tokyo, Japan) FT/IR-4100 (Tokyo, Japan) at a wavenumber range of 550–4000 cm^{-1} and a resolution of 1 cm^{-1}. Ultraviolet-visible (UV-vis) optical transmittances were measured with a JASCO V-530 UV/vis spectrometer at wavelengths of 200–800 nm. Thermal mechanical analysis (TMA) measurements were carried out using a Seiko Instruments TMA/SS6100 (Chiba, Japan) at a heating rate of 5°C/min under N_2 flow. Dynamic mechanical analysis (DMA) measurements were performed with a Seiko Instruments DMA6100 at a heating rate of 5°C/min under N_2 flow; the load frequency was 1 Hz. Thermogravimetric-differential thermal analysis (TG-DTA) experiments were performed with a Seiko Instruments TG/DTA5200 at a heating rate of 10°C/min under

air flow. The densities (ρs) of HBPIs were measured by a floating method with bromoform and 2-propanol at 25°C. According to the group contribution method, the FFV of HBPIs can be estimated by the following equation [6]:

$$FFV = \frac{V_{sp} - 1.3V_w}{V_{sp}} \quad (1)$$

where V_{sp} (cm^3/mol) is the specific molar volume and V_w (cm^3/mol) is the van der Waals volume of the repeating unit. CO_2, O_2, N_2, and CH_4 permeation measurements were taken with a constant volume/variable pressure apparatus under 76 cmHg at 25°C. The permeability coefficient, P [cm^3(STP)cm/cm^2 s cmHg], was determined by the equation [7] :

$$P = \frac{22414}{A}\frac{L}{p}\frac{V}{RT}\frac{dp}{dt} \quad (2)$$

where A is the membrane area (cm^2), L is the membrane thickness (cm), p is the upstream pressure (cmHg), V is the downstream volume (cm^3), R is the universal gas constant (6236.56 cm^3 cmHg/mol K), T is the absolute temperature (K), and dp/dt is the permeation rate (cmHg/s). The gas permeability coefficient can be explained on the basis of the solution-diffusion mechanism, which is represented by the equation [7, 9] :

$$P = D \times S \quad (3)$$

where D (cm^2/s) is the diffusion coefficient and S [cm^3(STP)/cm^3_{polym} cmHg] is the solubility coefficient. The diffusion coefficient was calculated by the time-lag method represented by the equation [10] :

$$D = \frac{L^2}{6\theta t} \quad (4)$$

where θt (s) is the time-lag.

3. Results and discussion

3.1 Polymer synthesis

TADE has asymmetric structure in which two amino groups bind to one of the phenyl group of the diphenyl ether. The reactivity of the amino group in 2-position is lower than other two amino groups. Thus, it is considered that the degree of branching (DB) of the asymmetric HBPI is relatively low and the linearity is high. Chen et al. reported that the DB of symmetric AM-6FDA-TAPOB HBPI was 0.65 [11]. In this study, the DBs of asymmetric AM-6FDA-TAPB HBPI and the symmetric AM-6FDA-TAPOB HBPI measured by a same manner as Chen were 0.25 and 0.65, respectively. This result confirmed that the asymmetric HBPI is more linear than the symmetric HBPI.

The inherent viscosity (η_{inh}) values of HBPAA are shown in Table 5-1. In Table 5-1, it was recognized that the η_{inh} values of the asymmetric HBPAAs were lower than those of corresponding symmetric HBPAAs. Generally, it is said that the η_{inh} value of linear-

Table 5-1 Physical properties of the asymmetric and symmetric HBPI-silica hybrid films.

	η_{inh}[a] [dL/g]	Transmittance at 600nm [%]	TMA CTE[b] [ppm/°C]	DMA Tg [°C]	TG-DTA T_d^5 [°C]	TG-DTA Residue[c] [%]
Asymmetric DA-HBPI	0.27	69.4	47	350	471	0
10wt%SiO_2	-	88.0	41	390	486	10
20wt%SiO_2	-	89.3	33	394	492	20
30wt%SiO_2	-	92.9	28	N.D.[d]	503	30
Asymmetric AM-HBPI	0.56	20.1	45	384	455	0
10wt%SiO_2	-	24.5	37	385	470	9
20wt%SiO_2	-	34.7	31	386	478	21
30wt%SiO_2	-	51.9	25	N.D.[d]	495	30
Symmetric DA-HBPI	0.34	88.9	54	304	457	0
10wt%SiO_2	-	89.9	47	320	490	10
20wt%SiO_2	-	90.2	38	337	496	20
30wt%SiO_2	-	90.3	31	351	509	30
Symmetric DA-HBPI	0.60	50.8	53	366	466	0
10wt%SiO_2	-	54.4	47	379	477	7
20wt%SiO_2	-	66.8	41	378	481	20
30wt%SiO_2	-	76.3	31	N.D.[d]	495	33

[a] η_{inh} value on corresponding HBPAA.
[b] CTE at 100-150°C
[c] Determined from the residual at 800°C
[d] Not detected

type polymer is higher than that of hyperbranched polymer. Thus, it was expected that the η_{inh} value of asymmetric HBPAA with lower degree of branching was higher than that of symmetric HBPAA. However the opposite result was obtained. This might result from the fact that it is difficult to synthesize high molecular weight asymmetric HBPAA molecule because of low reactivity of the amino group in 2-position in TADE.

3.2 Polymer characterization

ATR FT-IR spectra of the asymmetric and symmetric pristine HBPIs and the asymmetric AM-HBPI-silica hybrid films are shown in Figure 5-3 (a, b). The bands observed around 1784 cm^{-1} (C=O asymmetrical stretching), 1721 cm^{-1} (C=O symmetrical stretching), 1360-1374 cm^{-1} (C-N stretching), and 718-721 cm^{-1} (C=O bending) are characteristic absorption bands of polyimides [11,12]. In contrast, no characteristic bands of polyamic acids around 1680 cm^{-1} were found. These results indicate that the asymmetric HBPIs are well imidized by thermal imidization at 300℃ as well as symmetric HBPIs. The bands around 1857 cm^{-1} in Figure 5-3 a) is attributed

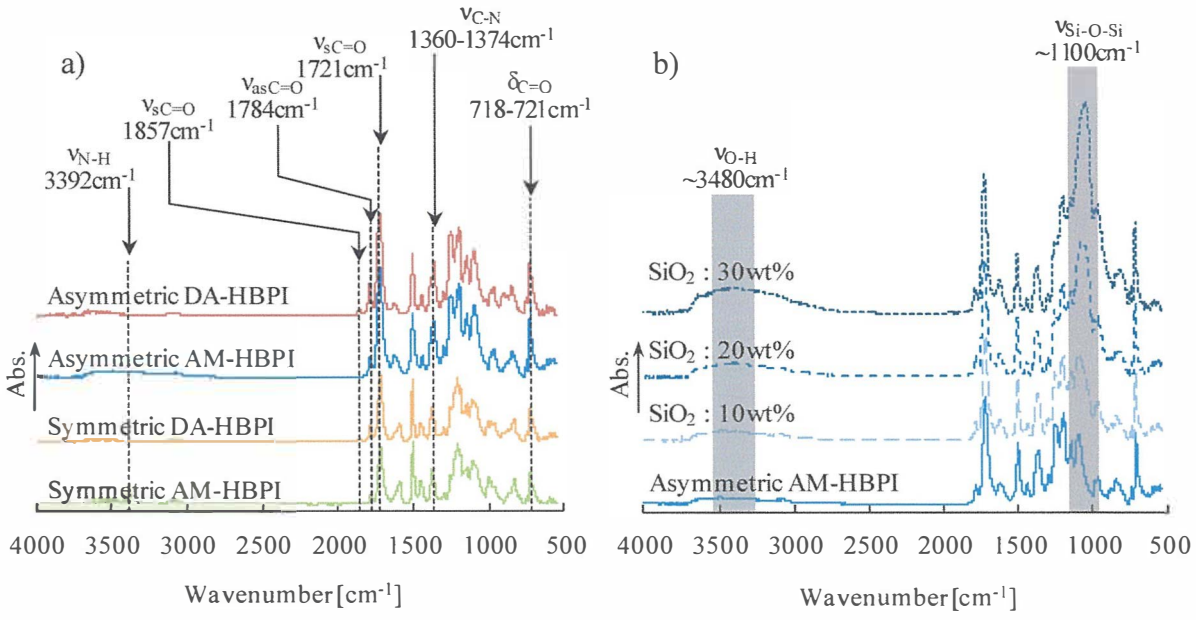

Figure 5-3 ATR FT-IR spectra of the (a) asymmetric and symmetric HBPIs and (b) asymmetric AM-HBPI-silica hybrids (SiO_2 content: 0-30wt%).

to the stretching of C=O of the terminal anhydride groups in the DA-HBPIs [11,13]. The characteristic band attributed to the stretching of N-H of the terminal amino groups in the AM-HBPIs around 3392cm^{-1} overlapped with the peak of the O-H groups, and could not be observed. For the HBPI-silica hybrid films (Figure 5-3 b)), it can be observed that the broad and strong absorption bands around 1100 cm^{-1} assigned to Si-O-Si stretching are enhanced with increasing SiO_2 content, indicating sufficient formation of the three-dimensional Si-O-Si network [14]. The broad absorption bands around 3480 cm^{-1} are likely attributed to silanol groups remaining in the silica domain.

The optical transmittances at 600nm are shown in Table 5-1 and plotted against silica content in Figure 5-4. The optical transmittances of the pristine asymmetric HBPI films are lower than that of the corresponding pristine symmetric HBPI films. This is because the molecular size of TADE, a triamine monomer of asymmetric HBPI, is smaller than TAPOB, a triamine monomer of symmetric HBPI, and therefore imide group density in a unit volume of asymmetric HBPI is higher than that of symmetric HBPI. The

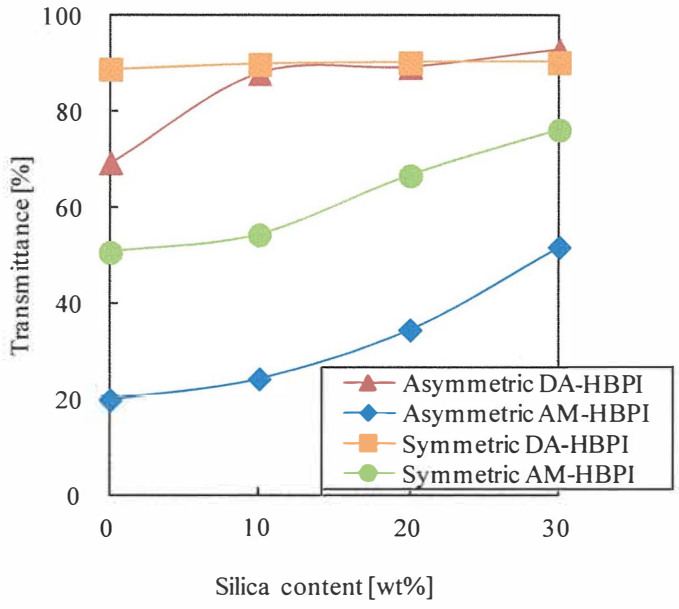

Figure 5-4 Optical transmittances of the asymmetric and symmetric HBPI-silica hybrid films at 600nm.

asymmetric and symmetric AM-HBPI films are colored to dark brown because of the partial thermal denaturation of terminal amino groups of the AM-HBPIs during thermal imidization [15]. However the optical transmittances of asymmetric and symmetric HBPI-silica hybrid films increased with increasing silica content, which might be attributed to decreased imide group density in a unit volume and favorable dispersion of silica. And this result indicated the good dispersion of silica component even in the asymmetric HBPI with high linearity. The fine and homogeneous dispersion of silica is brought not only by the characteristic hyperbranched structures of molecular chains but also by silane coupling agent which offer covalent bonds between organic and inorganic components [16].

The thermal properties of the asymmetric and symmetric HBPI-silica hybrids were investigated by TMA, DMA, and TG-DTA measurements. Coefficients of thermal expansion (CTEs) of the asymmetric and symmetric HBPI-silica hybrid films are listed in Table 5-1 and plotted against silica content in Figure 5-5. CTE values of the

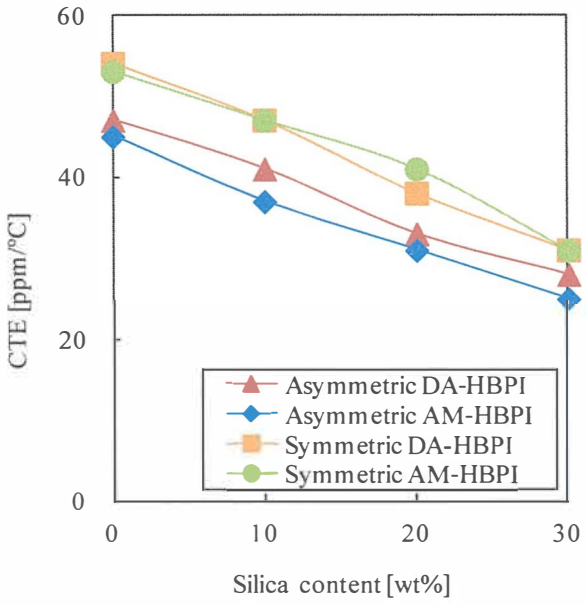

Figure 5-5 Coefficients of thermal expansion (CTEs) of the asymmetric and symmetric HBPI-silica hybrid films.

asymmetric HBPI-silica hybrid films were lower than those of symmetric HBPI-silica hybrid films. This result is probably caused by the rigidity of the asymmetric HBPI molecular chains. Although only one ether unit is contained in a TADE monomer, three ether units are contained in a TAPOB monomer. Additionally, the steric hindrance is arisen by the asymmetric structure of TADE. Thus, the asymmetric HBPI molecules are more rigid than the symmetric HBPI molecules. With increasing silica content, CTEs of the asymmetric and symmetric HBPI-silica hybrid films decreased. This is caused by the enhancement of the thermal mechanical stability of the HBPI matrix by the formation of a robust three-dimensional Si-O-Si network and the decreased mobility of the HBPI molecular chains by hybridization with silica.

The storage moduli (E's) and tan δ of the asymmetric and symmetric HBPI-silica hybrid films are shown in Figure 5-6 (a-d). Unfortunately, DMA measurement for the asymmetric DA-HBPI-silica hybrid film containing 30 wt% of SiO_2 could not be carried out because of its mechanical brittleness. In the glassy region, no remarkable difference between the asymmetric HBPI and the symmetric HBPI was observed. In contrast, in rubbery region, we can see that the E' values of the asymmetric HBPI-silica hybrid films were higher than those of corresponding symmetric HBPI-silica hybrid films. As in the case of CTE, this is attributed to the rigidity of asymmetric (TADE system) HBPI molecules. E's of the asymmetric and symmetric HBPI-silica hybrid films increased with increasing the silica content in both regions. This increase is caused by the increasing of inorganic behavior and the decreasing mobility of HBPI molecular chains by hybridization with silica.

Glass transition temperatures (T_gs) of the asymmetric and symmetric HBPI-silica hybrid films determined from the peak of tan δ are summarized in Table 5-1 and plotted against the silica content in Figure 5-7. The T_g value of the asymmetric pristine HBPI is

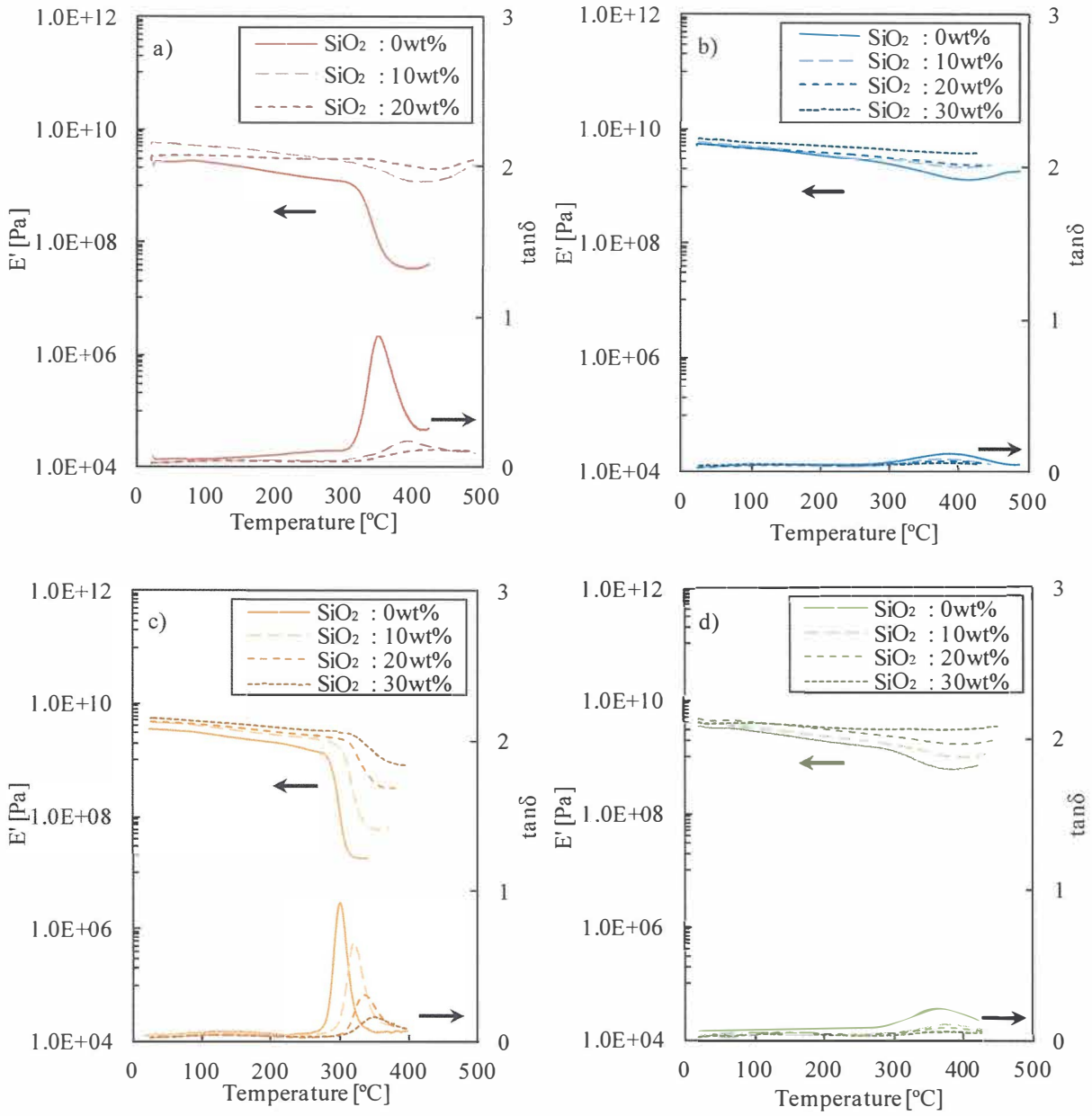

Figure 5-6 Storage moduli (E's) and tan δ of the a) asymmetric DA-HBPI-silica hybrid films, b)asymmetric AM-HBPI-silica hybrid films, c) symmetric DA-HBPI-silica hybrid films, and d) symmetric AM-HBPI-silica hybrid films.

higher than that of corresponding symmetric pristine HBPI. With increasing the silica content, T_gs shifted to a higher temperature along with a decrease of peak intensity and a broadening of the half-width of tan δ. This result indicates that T_gs increased with the increase of inorganic behavior and the decrease of mobility of the HBPI molecular chains caused by cross-linking through silica domains. Particularly, the T_g values of

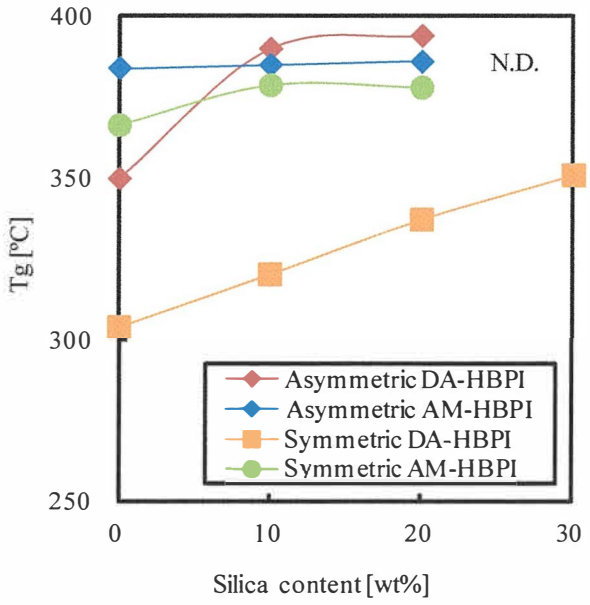

Figure 5-7 Glass transition temperatures (T_gs) of the asymmetric and symmetric HBPI-silica hybrid films derived from the peak top of tan δ.

asymmetric and symmetric DA-HBPI-silica hybrids increased with increasing silica content conspicuously. This is probably because that robust three-dimensional Si-O-Si network is easily formed via sol-gel reaction in the DA-HBPI-silica hybrids [15].

5% weight loss temperatures (T_d^5s) were investigated by TG-DTA and summarized in Table 5-1 along with the silica content determined from the residues at 800°C. The residues showed that all hybrid films contained an appropriate amount of silica, as expected. In Figure 5-8, T_d^5 values of the asymmetric and symmetric HBPI-silica hybrids are plotted against silica content. For the symmetric pristine HBPI, the T_d^5 value of the AM-HBPI was higher than that of corresponding DA-HBPI. On the other hand, in the case of asymmetric pristine HBPI, the T_d^5 value of the DA-HBPI was higher than that of corresponding AM-HBPI. T_d^5 values are affected by the amount of thermally unstable units in the molecule. For the symmetric HBPI, the T_d^5 value was probably controlled largely by the degradation of C-F bond in 6FDA component [15]. Thus, the T_d^5 value of the DA-HBPI with higher content of 6FDA was lower than that of AM-

HBPI. On the other hand, in the asymmetric HBPI, the rigidity of AM-HBPI molecule may have a major effect on the T_d^5 value. The AM-HBPI is more rigid than DA-HBPI because there are many branching units in the AM-HBPI molecular chains, and so the cross-linking reaction between silane coupling agents is hard to progress and many thermally unstable silanol groups remain in the asymmetric AM-HBPI molecular terminals. The T_d^5s values of the asymmetric and symmetric HBPI–silica hybrids increased with increasing silica content. This increased thermal stability of the HBPI–silica hybrid films resulted from the formation of cross-linking between the HBPI and the silica domain, the introduction of inorganic characteristics, and the radical trapping effect of silica. Even though the silica content increased, the T_d^5 of the asymmetric HBPI-silica hybrids did not increase so conspicuously as corresponding symmetric HBPI-silica hybrids. This was probably because there were more silanol groups left in the asymmetric HBPI-silica hybrids than the symmetric HBPI-silica hybrids due to the rigidity of the asymmetric HBPI molecular chains as the above mentioned discussion

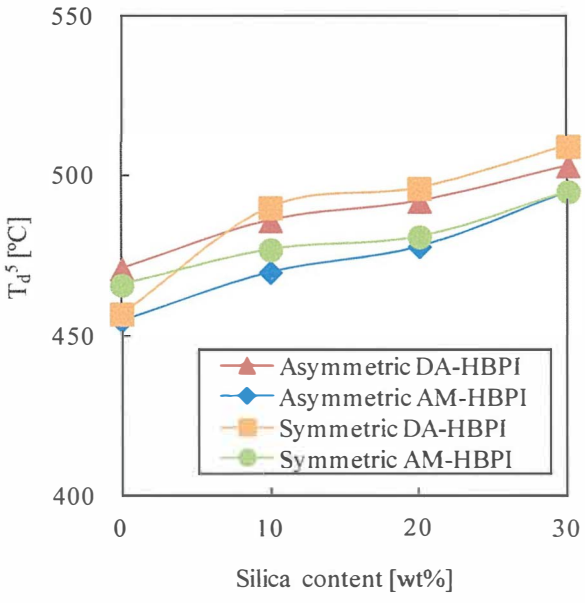

Figure 5-8 5% weight loss temperatures (T_d^5s) of the asymmetric and symmetric HBPI-silica hybrids.

about the TMA and DMA behaviour.

3.3 Gas transport properties

The gas permeability, diffusion, and solubility coefficients of the asymmetric and symmetric HBPI-silica hybrid membranes are summarized in Table 5-2 along with the fractional free volumes (FFVs) calculated from the group contribution method. And the CO_2 and CH_4 permeability, diffusion, and solubility coefficients are plotted against silica content in Figure 5-9 (a, b), Figure 5-10 (a, b), and Figure 5-11 (a, b). In general, it is well known that gas diffusivities of polymers strongly depend on the FFVs [17,18]. In this work, the gas permeabilities and FFVs of asymmetric HBPIs also tended to be higher than those of corresponding symmetric HBPIs. This was due to the higher rigidity of the asymmetric HBPI molecules. As shown in Table 5-2 and Figure 5-9 a),

Table 5-2 Gas transport properties of the asymmetric and symmetric HBPI-silica hybrid membranes at 76cmHg and 25°C

	FFV	$P\times10^{10}$ [cm^3(STP)cm/cm^2 s cmHg]				$D\times10^{8}$ [cm^2/s]				$S\times10^{2}$ [cm^3(STP)/cm^3 polym cmHg]			
		CO_2	O_2	N_2	CH_4	CO_2	O_2	N_2	CH_4	CO_2	O_2	N_2	CH_4
Asymmetric DA-HBPI	0.168	14	2.9	0.43	0.20	0.44	1.9	0.38	0.049	32	1.5	1.1	4.0
10wt%SiO_2		16	3.1	0.47	0.19	0.45	1.8	0.37	0.045	35	1.7	1.3	4.3
20wt%SiO_2		18	3.2	0.49	018	0.46	1.6	0.31	0.038	39	2.2	1.6	4.6
30wt%SiO_2		19	3.5	0.46	0.17	0.47	1.6	0.28	0.039	40	2.0	1.7	4.4
Asymmetric AM-HBPI	0.166	18	3.6	0.68	0.22	0.48	1.8	0.57	0.042	38	2.0	1.2	5.3
10wt%SiO_2		16	3.0	0.56	0.18	0.40	1.6	0.37	0.035	40	1.9	1.5	5.2
20wt%SiO_2		14	2.4	0.34	0.14	0.34	1.4	0.22	0.021	41	1.8	1.6	6.7
30wt%SiO_2		13	2.2	0.31	0.10	0.32	0.93	0.20	0.019	42	2.3	1.6	5.3
Symmetric DA-HBPI	0.161	7.4	1.5	0.23	0.098	0.30	1.4	0.25	0.028	25	1.1	0.92	3.5
10wt%SiO_2		10	2.0	0.31	0.13	0.35	1.5	0.29	0.026	30	1.4	1.1	5.0
20wt%SiO_2		13	2.1	0.32	0.16	0.37	1.3	0.25	0.030	35	1.7	1.3	5.2
30wt%SiO_2		23	3.0	0.46	0.24	0.57	1.7	0.29	0.040	41	1.8	1.6	6.0
Symmetric AM-HBPI	0.161	13	2.3	0.35	0.22	0.41	1.5	0.26	0.048	30	1.5	1.3	4.5
10wt%SiO_2		15	2.4	0.37	0.23	0.47	1.7	0.32	0.055	31	1.4	1.2	4.1
20wt%SiO_2		16	2.5	0.38	0.22	0.41	1.4	0.27	0.048	38	1.8	1.4	4.6
30wt%SiO_2		19	2.9	0.43	0.21	0.46	1.5	0.24	0.054	42	1.9	1.8	3.9

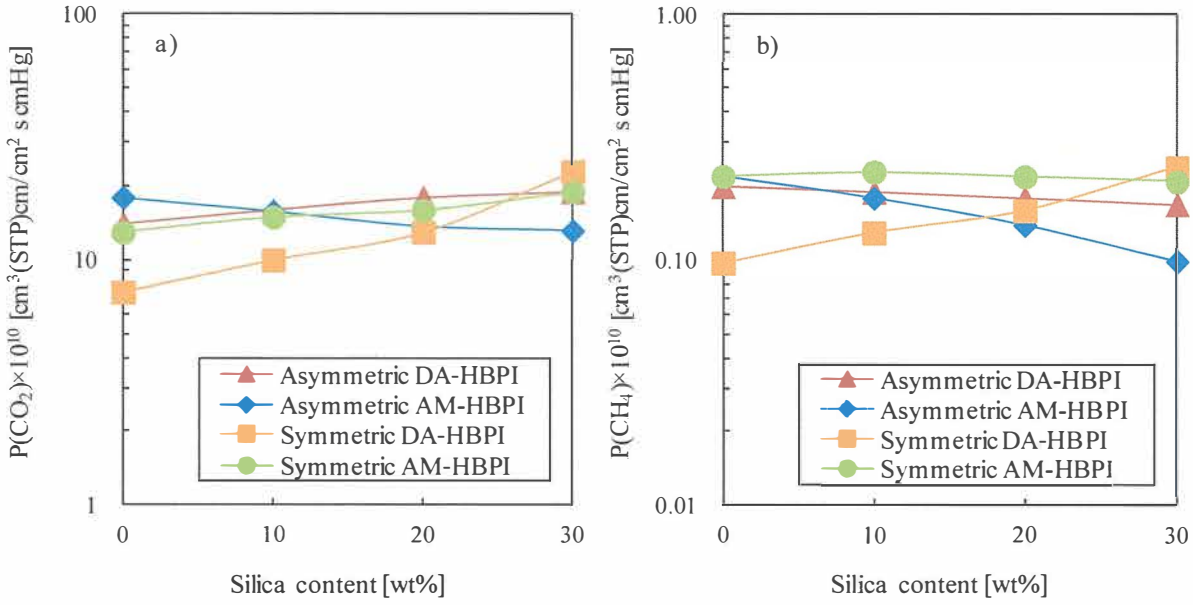

Figure 5-9 a) CO_2 and b) CH_4 permeability coefficients of the asymmetric and symmetric HBPI-silica hybrid membranes.

the CO_2 gas permeability coefficient of the asymmetric AM-HBPI-silica hybrid membranes decreased with increasing silica content. In addition, the increasing of the CO_2 gas permeability coefficient of the asymmetric DA-HBPI-silica hybrid membranes with increasing silica content was smaller than those of corresponding symmetric DA-HBPI-silica hybrid membranes. For the CH_4 gas transport property, from Table 5-2 and Figure 5-9 b), it was recognized that the CH_4 gas permeability of the asymmetric DA- and AM-HBPI-silica hybrid membranes decreased with increasing silica content conspicuously. And these results on permeability greatly reflect the change in the diffusivity coefficient (Figure 5-10 and Figure 5-11). In the previous research, Suzuki et al. found that the gas permeability coefficient and the CO_2/CH_4 permselectivity of the symmetric DA-HBPI-silica hybrid membranes prepared via sol-gel reaction using TMOS increased with increasing silica content, suggesting the additional formation of free volume holes and a Langmuir sorption site effective for gas transport and separation properties through hybridization with silica [19-21]. However, in the

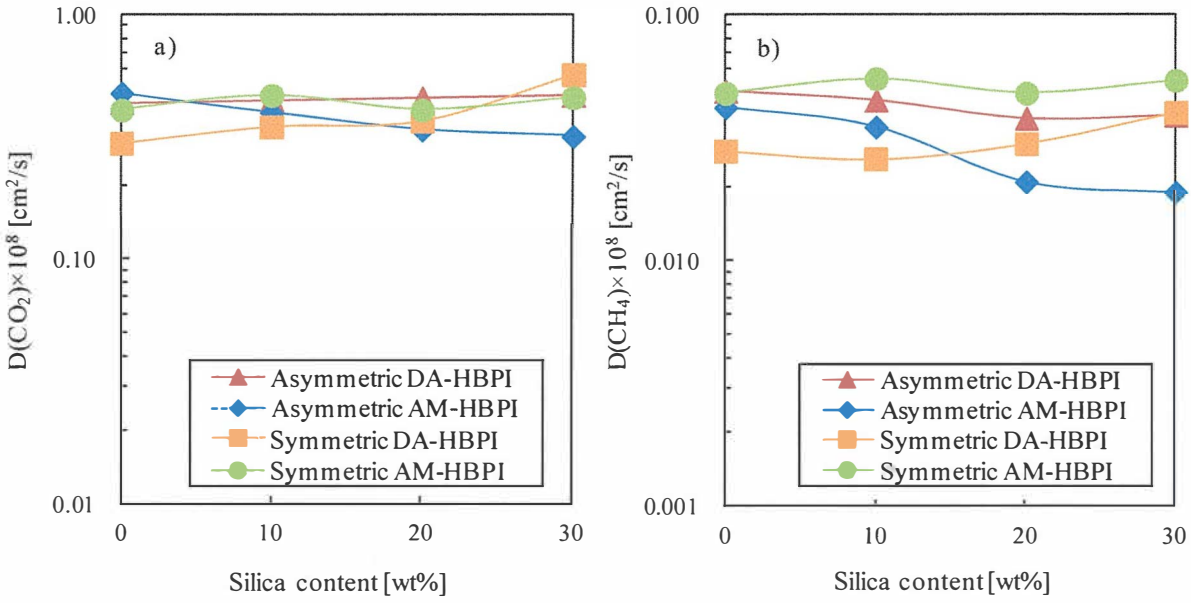

Figure 5-10 a) CO_2 and b) CH_4 diffusivity coefficients of the asymmetric and symmetric HBPI-silica hybrid membranes.

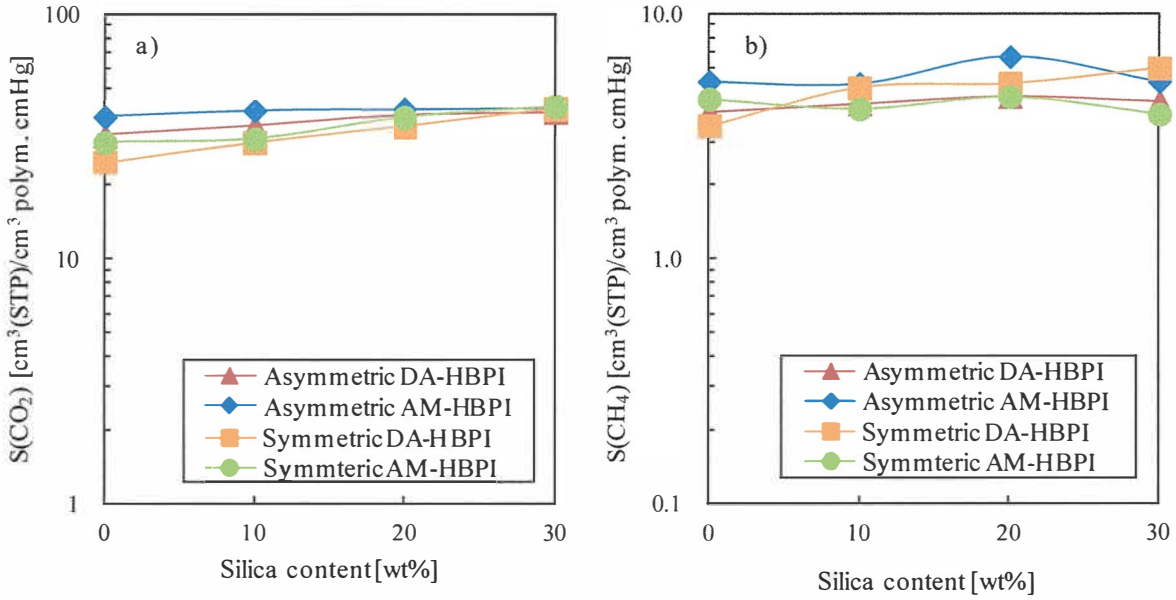

Figure 5-11 a) CO_2 and b) CH_4 solubility coefficients of the asymmetric and symmetric HBPI-silica hybrid membranes.

asymmetric HBPI-silica hybrids with the higher linearity of polymer chains, the dispersibility of silica component is not as good as in the symmetric HBPI-silica hybrids. Therefore, silica component is

aggregated to the size that affects the gas permeation but doesn't affect the optical transmittance. The more the size of a silica component is large, the more the diffusion path formed in the HBPI-silica interfacial region becomes long and tortuous. The effect of newly formed diffusion path was countered by the increase of total path of the gas. Similar gas transport properties have been reported in several other studies. Merkel et al. studied the effect of particle size on gas permeability of the superglassy polymer-silica nanocomposites. They reported the importance of using small particles to achieve the desired effect on gas transport in the polymer; the gas permeability increases linearly with decreasing silica particle size [22-24]. Dougnac et al. also reported similar results about the transport properties of the PA6-silica nanosphere composites [25]. In addition, as reported in chapter 4, it was thought that an effect of hybridization on gas permeability was hard to be taken in the AM-HBPI-silica hybrid membranes because of the rigidity of the AM-HBPI polymer chains which inhibit the progress of the sol-gel reaction. It was considered that the rigidity of asymmetric AM-HBPI was the highest of all examined HBPIs, and that the gas permeability decreased with increasing the silica content.

3.4 O_2/N_2 and CO_2/CH_4 selectivities

The ideal permselectivity for the combination of gases A and B [α(A/B)] is defined by the equation[26] :

$$\alpha(A/B)=\frac{P(A)}{P(B)}=\frac{D(A)}{D(B)}\times\frac{S(A)}{S(B)}=\alpha^{D}(A/B)\times\alpha^{S}(A/B) \qquad (5)$$

where $\alpha^{D}(A/B)$ is the diffusivity selectivity and $\alpha^{S}(A/B)$ is the solubility selectivity. The O_2/N_2 and CO_2/CH_4 selectivities of the HBPI-silica hybrid membranes are listed in Table 5-3, and O_2/N_2 and CO_2/CH_4 permselectivities are plotted against the O_2 and CO_2

Table 5-3 O_2/N_2 and CO_2/CH_4 selectivities of the asymmetric and symmetric HBPI-silica hybrid membranes at 76 cmHg and 25°C

	O_2/N_2 selectivity			CO_2/CH_4 selectivity		
	$\alpha(O_2/N_2)$	$\alpha^D(O_2/N_2)$	$\alpha^S(O_2/N_2)$	$\alpha(CO_2/CH_4)$	$\alpha^D(CO_2/CH_4)$	$\alpha^S(CO_2/CH_4)$
Asymmetric DA-HBPI	6.7	5.0	1.4	70	9.0	8.0
10wt%SiO_2	6.6	4.9	1.3	84	10.0	8.1
20wt%SiO_2	6.5	5.2	1.4	100	12	8.5
30wt%SiO_2	7.6	5.7	1.2	112	12	9.1
Asymmetric AM-HBPI	5.3	3.3	1.7	82	11	7.2
10wt%SiO_2	5.4	4.3	1.3	88	11	7.8
20wt%SiO_2	6.0	6.2	1.1	100	16	6.1
30wt%SiO_2	7.0	4.7	1.5	132	17	7.8
Symmetric DA-HBPI	6.8	5.8	1.2	75	11	7.0
10wt%SiO_2	6.6	5.2	1.3	79	13	5.9
20wt%SiO_2	6.7	5.3	1.3	82	12	6.8
30wt%SiO_2	6.6	5.8	1.1	95	14	6.7
Symmetric AM-HBPI	6.6	5.8	1.2	59	8.5	6.7
10wt%SiO_2	6.5	5.3	1.2	65	8.6	7.6
20wt%SiO_2	6.6	5.2	1.3	73	9.5	8.3
30wt%SiO_2	6.7	6.3	1.1	90	8.5	11

permeability coefficients in Figure 5-12 (a, b), respectively. In Figure 5-12 (a, b), the open symbols represent the data of the pristine HBPI, and the darkness of filled symbols increase with increasing silica content.

In general, there is a trade-off relationship between permeability and permselectivity; the gas permselectivity decreases with increasing the permeability, or *vice versa* [26]. In the previous study, Suzuki et al. reported that 1) the $\alpha(O_2/N_2)$ values of the symmetric DA-HBPI-silica hybrid membranes slightly decreased and the O_2 permeability increased with increasing silica content along with the upper bound trade-off line for O_2/N_2 separation demonstrated by Robeson [27,28], and 2) both $\alpha(CO_2/CH_4)$ values and CO_2 permeability of the symmetric DA-HBPI-silica hybrid membranes increased with increasing silica content. In this study, for the asymmetric AM-HBPI silica hybrid membranes, the plots of the O_2 permeability and O_2/N_2 permselectivity relationship shifted to the low permeability region with increasing silica content along with the

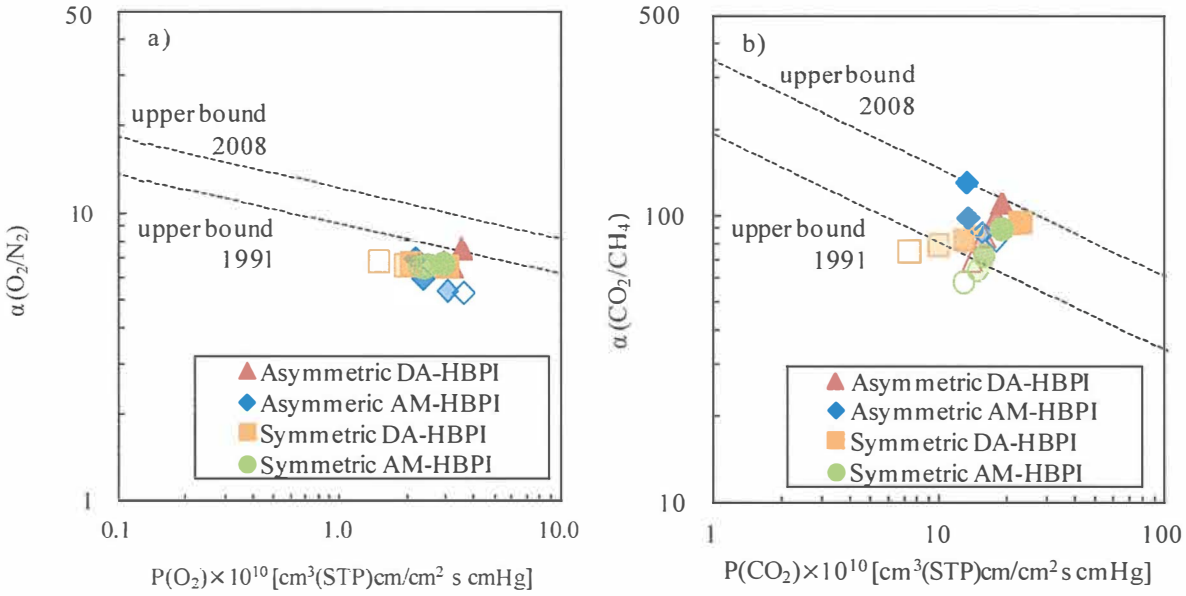

Figure 5-12 Ideal a) O_2/N_2 and b) CO_2/CH_4 selectivity of the asymmetric and symmetric HBPI-silica hybrid membranes plotted against O_2 and CO_2 permeability, respectively.

upper bound trade-off line (Figure 5-12 a)). On the other hand, the plots of the CO_2 permeability and CO_2/CH_4 permselectivity relationship shifted to the low permeability region with significant increase of permselectivity with the increase of silica content (Figure 5-12 b)). For this reason, it is considered that the free volume holes formed by hybridization with silica in the asymmetric AM-HBPI silica hybrid membranes have an excellent molecular sieving effect on CO_2/CH_4 selectivity because the CH_4 gas diffusivity coefficient decreased with increasing silica content conspicuously.

4. Conclusions

The asymmetric and symmetric HBPI-silica hybrid membranes were prepared via sol-gel reaction and their physical and gas transport properties were investigated. It is considered that the asymmetric HBPI molecular chain is more linear than the symmetric HBPI. ATR FT-IR spectra revealed satisfactory imidization and sufficient formation of a three-dimensional Si-O-Si network in all prepared films. The result of optical

transmittances indicated the fine and homogeneous dispersion of silica component even in the asymmetric HBPI hybrids with high linearity. From the DMA and TMA measurements, it was suggested that thermomechanical property and dimensional stability of the asymmetric HBPI-silica hybrids were higher than those of symmetric HBPI-silica hybrids because the rigidity of the asymmetric HBPI molecular chains. Besides, there were more silanol groups left in the asymmetric HBPI-silica hybrids than the symmetric HBPI-silica hybrids due to the rigidity of the asymmetric HBPI molecular chains. Thus, the T_d^5 values of the asymmetric HBPI-silica hybrids did not increase so conspicuously as corresponding symmetric HBPI-silica hybrids with increasing silica content. The CO_2, O_2, N_2, and CH_4 gas permeability coefficient of asymmetric AM-HBPI-silica hybrid membranes decreased with increasing silica content. This was because the dispersibility of a silica component in the asymmetric HBPI-silica hybrids with the high linearity of polymer chain is not as fine as in symmetric HBPI-silica hybrids, and therefore the long and tortuous diffusion path was newly formed by hybridization with silica. Nevertheless, the asymmetric HBPI-silica hybrids demonstrate superior CO_2/CH_4 selectivity due to the excellent molecular sieving effect of the newly formed free volume holes by incorporation with silica.

References

[1] M. Hasegawa, N. Sensui, Y. Shindo, R. Yokota, Structure and Properties of Novel Asymmetric Biphenyl Type Polyimides. Homo- and Copolymers and Blends, Macromolecules, 32 (1999) 387-396.

[2] P.M. Hergenrother, K.A. Watson, J.G. Smith, J.W. Connell, R. Yokota, Polyimides from 2,3,3',4'-Biphenyltetracarboxylic Dianhydride and Aromatic Diamines, Polymer, 43 (2002) 5077–5093.

[3] Q. Li, X. Fang, Z. Wang, L. Gao, M. Ding, Polyimides from Isomeric Oxydiphthalic Anhydrides, J. Polym. Sci. Part A: Polym. Chem., 41 (2003) 3249–3260.

[4] T. Sasaki, H. Moriuchi, S. Yano, R. Yokota, High Thermal Stable Thermoplastic–Thermosetting Polyimide Film by use of Asymmetric Dianhydride (a-BPDA), Polymer, 46 (2005) 6968–6975.

[5] T. Takeichi, J. K. Stille, Star and Liner Imide Oligomers Containing Reactive End Caps: Preparation and Thermal Properties, Macromolecules, 19 (1986) 2093-2102.

[6] D.W. V Krevelen (Eds.), Properties of Polymers, Elsevier, Amsterdam, 1990, 71-107 (Chapter 4).

[7] R.S. Prabhakar, B.D. Freeman, I. Roman, Gas and Vapor Sorption and Permeation in Poly(2,2,4-trifluoro-5-trifluoromethoxy-1,3-dioxole-co-tetrafluoro-ethylene), Macromolecules, 37 (2004) 7688-7697.

[8] N. Muruganandam, W.J. Koros, D.R. Paul, Gas Sorption and Transport in Substituted Polycarbonates, J. Polym. Sci. Part B: Polym. Phys., 25 (1987) 1999-2026.

[9] A. Morisato, H.C. Shen, S.S. Sankar, B.D.Freeman, I. Pinnau, C.G. Casillas, Polymer Characterization and Gas Permeability of Poly(1-trimethylsilyl-1-propyne) [PTMST], Poly(1-phenyl-1-propyne) [PPP], and PTMSP/PPP Blends, J. Polym. Sci. Part B: Polym. Phys., 34 (1996) 2209-2222.

[10] D.H. Weinkauf, H.D. Kim, D.R. Paul, Gas Transport Properties of Liquid Crystalline Poly(p-phenyleneterephthalamide), Macromolecules, 25 (1992) 788-796.

[11] H. Chen, J. Yin, Synthesis and Characterization of Hyperbranched Polyimides with Good Organosolubility and Thermal Properties Based on New Triamine and Conventional Dianhydrides, J. Polym. Sci. Part A: Polym. Chem., 40 (2002) 3804-3814.

[12] J. Fang, H. Kita, K. Okamoto, Gas Permeation Properties of Hyperbranched Polyimide membranes, J. Membr. Sci., 182 (2001) 245-256.

[13] J. Fang, H. Kita, K. Okamoto, Hyperbranched Polyimides for Gas Separation Applications. 1. Synthesis and Characterization, Macromolecules, 33 (2000) 4639-4646.

[14] C. Hibshman, C.J. Cornelius, E.J. Marand, The Gas Separation Effects of Annealing Polyimide–Organosilicate Hybrid Membranes, J. Membr. Sci., 211 (2003) 25-40.

[15] M. Miki, Y. Yamada, Structure-Gas Transport Property Relationships of Hyperbranched Polyimide-silica Hybrid Membranes, J. Photopolym. Technol., 261 (2013) 319-26.

[16] N. Tomokiyo, Y. Yamada, T. Suzuki, J. Oku, Preparation and Characterization of Hyperbranched Polyimide - Colloidal Silica Hybrids, Polym. Prep. Japan, 55 (2006) 5175-5176.

[17] J.Y. Park, D.R. Paul, Correlation and Prediction of Gas Permeability in Glassy Polymer Membrane Materials via a Modified Free Volume Based Group Contribution Method, J. Membr. Sci., 125 (1997) 23-39.

[18] A. Thran, G. Kroll, F. Faupel, Correlation Between Fractional Free Volume and Diffusivity of Gas Molecules in Glassy Polymers, J. Polym. Sci. Part B: Polym. Phys., 37 (1999) 3344-3358.

[19] T. Suzuki, Y. Yamada, Physical and Gas Transport Properties of Novel Hyperbranched Polyimide – Silica Hybrid Membranes, Polym. Bull., 53 (2005) 139-146.

[20] T. Suzuki, Y. Yamada, K. Itahashi, 6FDA-TAPOB Hyperbranched Polyimide-Silica Hybrids for Gas Separation Membranes, J. Appl. Polym. Sci., 109 (2008) 813-819.

[21] T. Suzuki, Y. Yamada, Y. Tsujita, Gas Transport Properties of 6FDA-TAPOB Hyperbranched Polyimide Membrane, Polymer, 45 (2004) 7167-7171.

[22] T.C. Merkel, B.D. Freeman, R.J. Spontak, Z. He, I. Pinnau, P. Meakin, A.J. Hill, Ultrapermeable, Reverse-Selective Nanocomposite Membranes, Science, 296 (2002) 519-522.

[23] T.C. Merkel, L.G. Toy, A.L. Andrady, H. Gracz, E.O. Stejskal, Investigation of Enhanced Free Volume in Nanosilica-Filled Poly(1-trimethylsilyl-1-propyne) by ^{129}Xe NMR Spectroscopy, Macromolecules, 36 (2003) 353-358.

[24] A.L. Andrady, T.C. Merkel, L.G.Toy, Effect of Particle Size on Gas Permeability of Filled Superglassy Polymers, Macromolecules, 37 (2004) 4329-4331.

[25] V.N. Dougnac, B.C. Peoples, R. Quijada, The Effect of Nanospheres on the Permeability of PA6/SiO_2 Nanocomposites, Polym. Int., 60 (2011) 1600-1606.

[26] B.D. Freeman, Basis of Permeability/Selectivity Tradeoff Relations in Polymeric Gas Separation Membranes, Macromolecules, 32 (1992) 375-380.

[27] L.M. Robeson, Correlation of Separation Factor versus Permeability for Polymeric Membranes, J. Membr. Sci., 62 (1991) 165-185.

[28] L.M. Robeson, The Upper Bound Revisited, J. Membr. Sci., 320 (2008) 390-400.

Chapter 6

Gas Transport Mechanism of Hyperbranched Polyimide-Silica Hybrid / Composite Membranes

1. Introduction

Polyimide-silica hybrids and composites can be prepared by the sol-gel process or the addition of colloidal silica. The sol-gel reaction is achieved by addition of silicon alkoxide to polyamic acid (polyimide precursor) solution, and subsequently the hydrolysis and polycondensation with an appropriate acid or base catalyst; the addition of colloidal silica is commonly just mixing colloidal silica particles with the polyamic acid solution. Generally, it is said that colloidal silica has dense structure and silica prepared via sol-gel reaction has amorphous three-dimensional network structure with nanopores.

The dispersion of silica components in polyimide matrix has a significant impact on the properties of hybrids and composites. The modification of polyimide molecular terminals is one of the most effective method to enhance the compatibility between polyimide and silica and, thereby, to improve the dispersibility of the silica components. Hybrid materials which have strong chemical interaction between organic and inorganic components such as covalent bonds can be obtained by use of polyimides with terminal modification. On the other hand, we can obtain composite materials which show weak or no interactions between the two components by use of polyimides without terminal modification.

In this chapter, the physical and gas transport properties of hyperbranched polyimide-silica hybrid (HBPI-silica HBD) and hyperbranched polyimide-silica composite (HBPI-

silica CPT) membranes prepared with silicon alkoxide or colloidal silica were investigated to discuss and propose the gas transport mechanism in the HBPI-silica HBD and CPT membranes.

2. Experimental

2.1 Materials

1,3,5-Tris(4-aminophenoxy)benzene (*TAPOB*) was synthesized by the reduction of 1,3,5-tris(4-nitrophenoxy)benzene with palladium carbon and hydrazine in methanol [1]. Dianhydride, 4,4'-(hexafluoroisopropylidene) diphthalic anhydride (*6FDA*), was kindly supplied by Daikin Industries (Osaka, Japan). 3-Aminopropyltrimethoxysilane (*APTrMOS*) was purchased from Sigma-Aldrich Co. LLC. (St. Louis, MO, USA). Tetramethoxysilane (*TMOS*) was purchased from AZmax, Co., Ltd (Tokyo, Japan) and colloidal silica was obtained from Nissan Chemical Industries, Ltd (Tokyo, Japan). *N, N*-Dimethylacetamide (*DMAc*) used as a solvent was purchased from Nacalai Tesque (Kyoto, Japan). The chemical structures of monomers, silane coupling agent, and silica sources are shown in Figure 6-1.

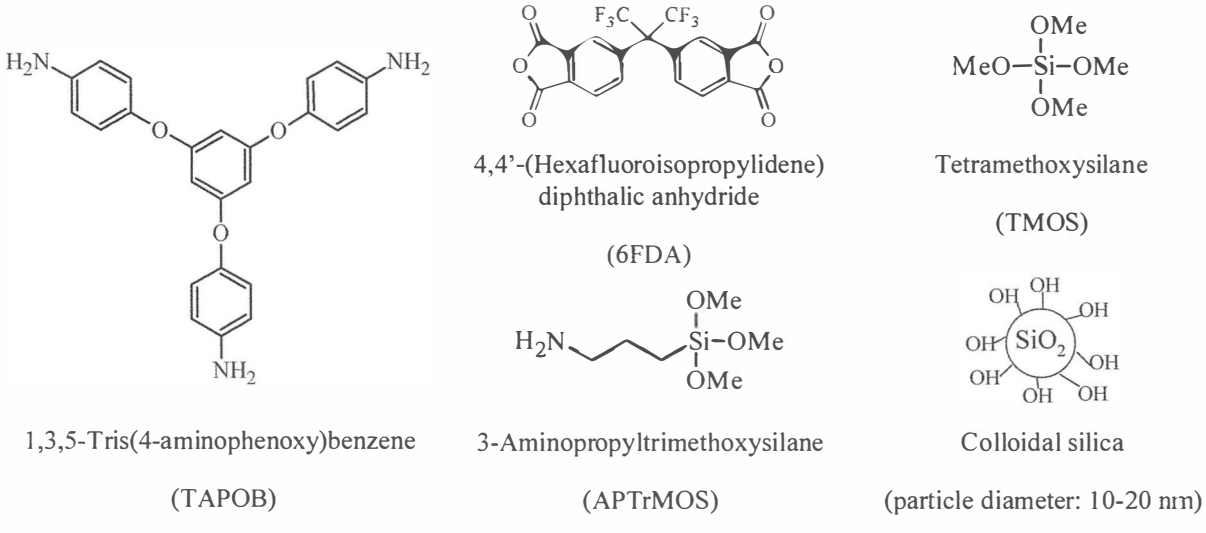

Figure 6-1 Chemical structures of monomers, silane coupling agent, and silica sources.

2.2 Polymerization

Three mmol of 6FDA was dissolved in 40 ml of DMAc in a 100-ml three-neck flask under N_2 flow at room temperature. To this solution, 1.6 mmol of TAPOB in 20 ml of DMAc was then added dropwise through a syringe with stirring for 3 h to afford hyperbranched polyamic acids (HBPAAs). Subsequently, for the HBPAAs to be used for the preparation of HBPI-silica HBDs, 0.4 mmol of the silane coupling agent, APTrMOS, was added into the reaction mixture to modify the terminal groups of the HBPAAs with further stirring for 1 h.

2.3 Membrane formation

2.3.1 TMOS system HBPI-silica HBD and CPT membranes

The TMOS system HBPI-silica HBD and CPT membranes were prepared to react HBPAAs with silicon alkoxide, TMOS, by sol–gel reaction, and then followed by thermal imidization. Appropriate amounts of TMOS and deionized water (TMOS : deionized water = 1 : 6 as a molar ratio) were added into the DMAc solution of the HBPAAs. HBPAAs modified with APTrMOS were used for the preparation of HBPI-silica HBDs; on the other hand, unmodified HBPAAs were used for the preparation of HBPI-silica CPTs. The mixed solutions were stirred for 24 h and then cast on PET films and dried at 85°C for 3 h. The prepared films were peeled off and subsequently imidized at 100°C for 1 h, 200°C for 1 h, and 300°C for 1 h in a heating oven under N_2 flow. The average thickness of the prepared HBPI-silica HBD and CPT membranes was about 30 μm. A schematic diagram for the preparation of TMOS system HBPI-silica HBD and CPT membranes is shown in Figure 6-2.

2.3.2 Colloidal silica system HBPI-silica HBD and CPT membranes

The colloidal silica system HBPI-silica HBD and CPT membranes were prepared by mixing HBPAAs and colloidal silica, and then followed by thermal imidization.

Appropriate amounts of colloidal silica dispersed in DMAc was added into the DMAc solution of the HBPAAs. As is the case with TMOS system, HBPAAs modified with APTrMOS were used for the preparation of HBPI-silica HBDs; on the other hand, unmodified HBPAAs were used for the preparation of HBPI-silica CPTs. Shortly after mixing the HBPAAs and colloidal silica, the prepared solutions were cast on PET films and dried at 85°C for 3 h. The prepared films were peeled off and subsequently imidized at 100°C for 1 h, 200°C for 1 h, and 300°C for 1 h in a heating oven under N_2 flow. The average thickness of the prepared HBPI-silica HBD and CPT membranes was about 30 μm. A schematic diagram for the preparation of colloidal silica system HBPI-silica HBD and CPT membranes is shown in Figure 6-2.

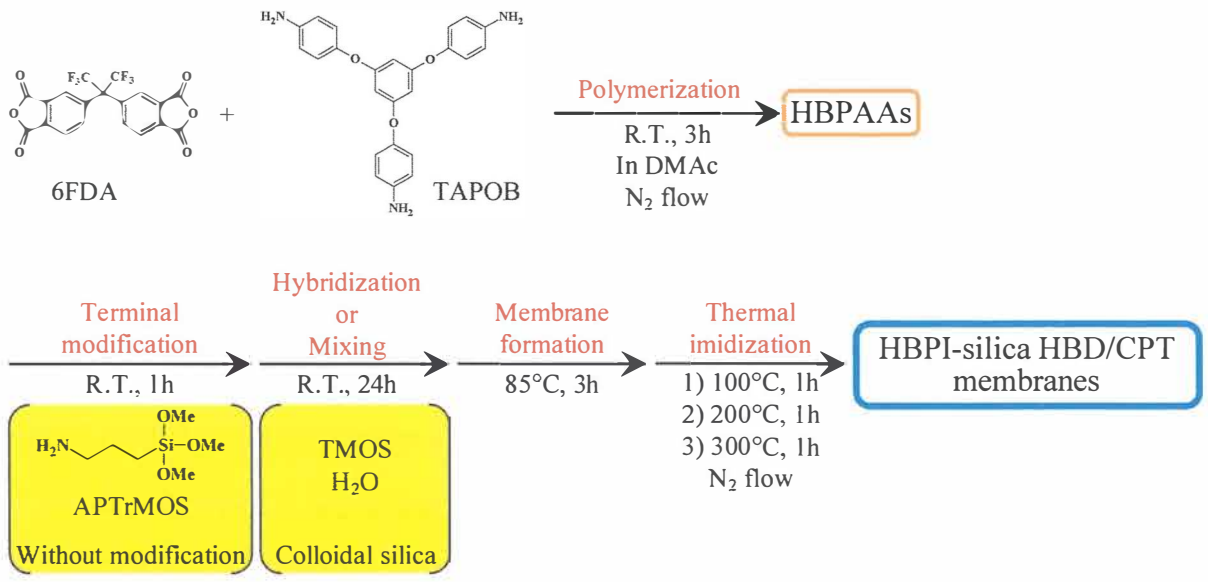

Figure 6-2 A schematic diagram for the preparation of HBPI-silica HBD and CPT membranes.

2.4. Measurements

Attenuated total reflection Fourier transform infrared (ATR FT-IR) spectra were recorded on a JASCO (Tokyo, Japan) FT/IR-4100 at a wavenumber range of 550–4000 cm^{-1} and a resolution of 1 cm^{-1}. Transmission electron microscopy (TEM) micrographs of ultrathin sections of the HBPI-silica HBD and CPT films were recorded with a

Hitachi High-Technologies (Tokyo, Japan) H-7650 with an acceleration voltage of 100 kV. Ultraviolet-visible (UV-vis) optical transmittances were measured with a JASCO V-530 UV/vis spectrometer at wavelengths of 200–800 nm. Thermogravimetric-differential thermal analysis (TG-DTA) experiments were performed with a Seiko Instruments (Chiba, Japan) TG/DTA5200 at a heating rate of 10°C/min under air flow. Dynamic mechanical analysis (DMA) measurements were performed with a Seiko Instruments DMA6100 at a heating rate of 5°C/min under N_2 flow; the load frequency was 1 Hz. Thermal mechanical analysis (TMA) measurements were carried out using a Seiko Instruments TMA/SS6100 at a heating rate of 5°C/min under N_2 flow. CO_2, O_2, N_2, and CH_4 permeation measurements were taken with a constant volume/variable pressure apparatus under 76 cmHg at 25°C. The permeability coefficient, P [cm^3(STP)cm/cm^2 s cmHg], was determined by the equation [2] :

$$P = \frac{22414}{A}\frac{L}{p}\frac{V}{RT}\frac{dp}{dt} \qquad (1)$$

where A is the membrane area (cm^2), L is the membrane thickness (cm), p is the upstream pressure (cmHg), V is the downstream volume (cm^3), R is the universal gas constant (6236.56 cm^3 cmHg/mol K), T is the absolute temperature (K), and dp/dt is the permeation rate (cmHg/s). The gas permeability coefficient can be explained on the basis of the solution-diffusion mechanism, which is represented by the equation [3, 4]:

$$P = D \times S \qquad (2)$$

where D (cm^2/s) is the diffusion coefficient and S [cm^3(STP)/cm^3_{polym} cmHg] is the solubility coefficient. The diffusion coefficient was calculated by the time-lag method represented by the equation [5]:

$$D = \frac{L^2}{6\theta t} \qquad (3)$$

where θt (s) is the time-lag. Wide angle X-ray diffractometry (WAXD) were recorded at room temperature by using Rigaku Co. (Tokyo, Japan) RINT2500 in the 2 theta range of 5 - 35° with a scan rate of 2°/min. Cu Kα (wavelength λ = 0.154nm) radiation was used. The average *d*-spacing value was determined from Bragg's equation:

$$d = \frac{\lambda}{2\sin\theta} \tag{4}$$

3. Results and Discussion

3.1 Polymer characterization

The ATR FT-IR spectra of the HBPI-silica HBD and CPT films are shown in Figure 6-3 (a, b). The bands observed around 1784 cm^{-1} (C=O asymmetrical stretching), 1722 cm^{-1} (C=O symmetrical stretching), 1375 cm^{-1} (C-N stretching), and 720 cm^{-1} (C=O bending) are characteristic absorption bands of polyimides. In contrast, the characteristic band of polyamic acids around 1680 cm^{-1} is not found. These results

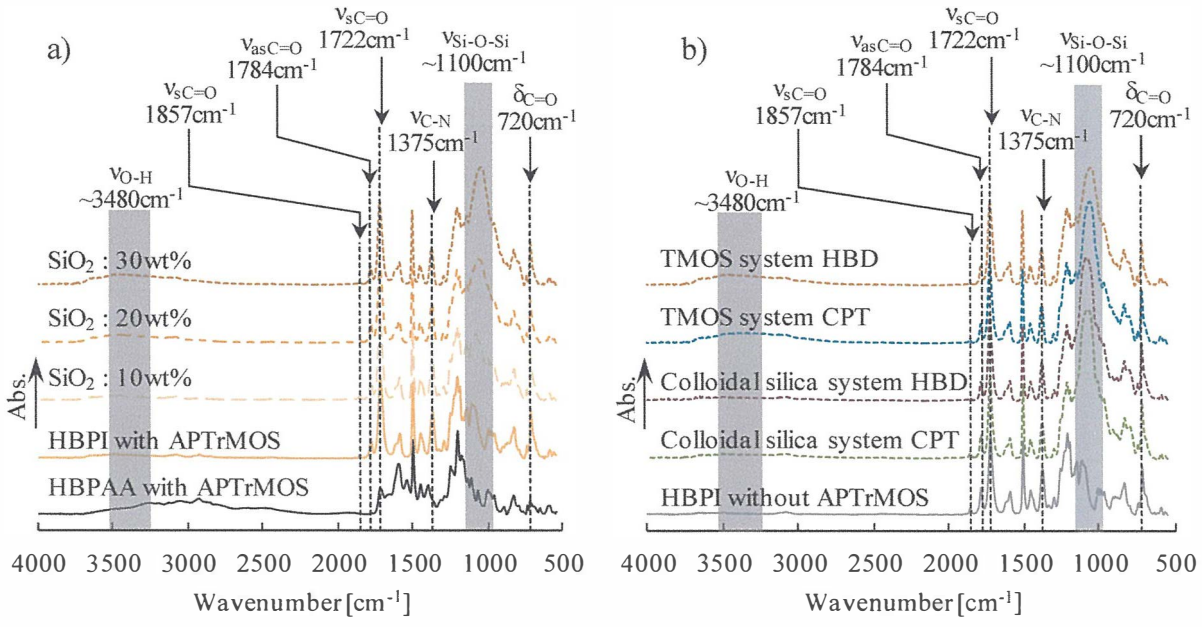

Figure 6-3 ATR FT-IR spectra of the a) TMOS system HBPI-silica HBDs (SiO_2 content : 0-30wt%) and b) HBPI-silica HBDs and CPTs (SiO_2 content : 30wt%).

indicate that the prepared films are well imidized. The bands around 1857 cm^{-1} are attributed to the stretching of C=O of the terminal anhydride groups in the HBPI molecules [6,7]. For the TMOS system HBPI-silica HBDs (Figure 6-3 a), it can be seen that the broad and strong absorption bands around 1100 cm^{-1} assigned to Si-O-Si stretching are enhanced with increasing SiO_2 content, indicating the sufficient formation of the three-dimensional Si-O-Si network [8]. The broad absorption bands around 3480 cm^{-1} are likely attributed to silanol groups remaining in the silica domain. In comparison of the TMOS system and the colloidal silica system (Figure 6-3 b), the absorption bands around 3480 cm^{-1} of TMOS system are stronger than those of colloidal silica system, suggesting that much more silanol groups remain in the TMOS system HBDs and CPTs than colloidal silica system HBDs and CPTs. It is also recognized that the absorption bands around 1100cm^{-1} of colloidal silica system are sharper and shifted slightly toward higher wavenumber region than those of TMOS system, suggesting the presence of rigid Si-O-Si bodings of colloidal silica system.

The TEM micrographs of the TMOS system HBPI-silica HBD and CPT are shown in

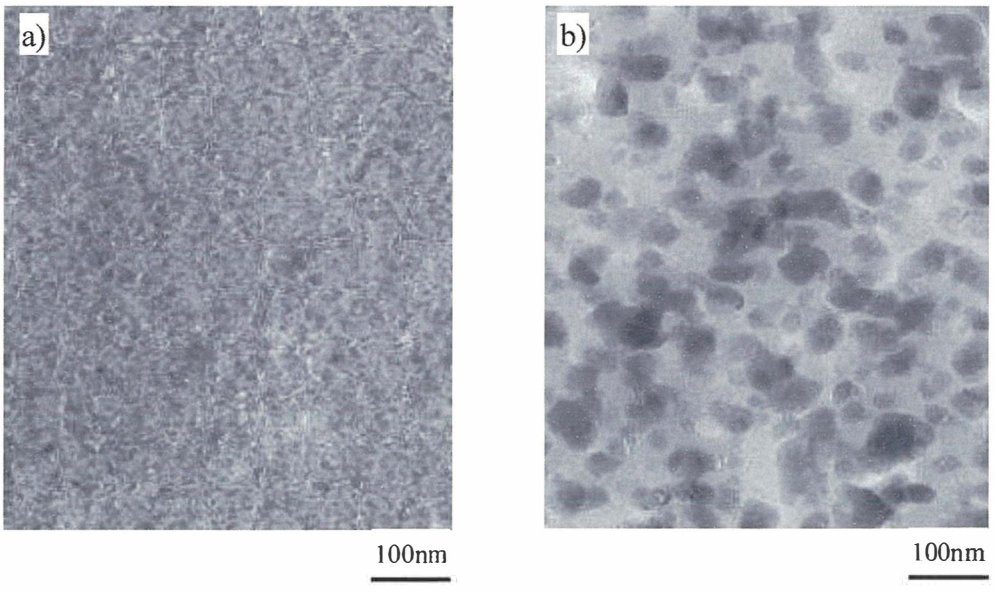

Figure 6-4 TEM micrographs of the TMOS system HBPI-silica a) HBD and b) CPT.

Figure 6-4. The TEM data revealed that the silica moiety in the HBPI-silica HBD dispersed finely due to the strong interaction between HBPI and silica.

The optical transmittances at 600nm are shown in Table 6-1 and plotted against silica

Table 6-1 Physical properties of the HBPI-silica hybrid and composite films.

		Transmittance at 600nm [%]	TG-DTA		DMA	TMA
			T_d^5 [°C]	Residue [a] [wt%]	Tg [°C]	CTE [b] [ppm/°C]
modified HBPI		88.9	457	0	304	56
TMOS system HBD	10wt%SiO_2	89.9	490	10	320	47
	20wt%SiO_2	90.2	496	20	338	31
	30wt%SiO_2	90.3	509	30	351	25
colloidal silica system HBD	10wt%SiO_2	88.5	477	9	299	47
	20wt%SiO_2	89.4	482	19	299	40
	30wt%SiO_2	89.5	488	30	304	36
unmodified HBPI		90.8	499	0	281	51
TMOS system CPT	10wt%SiO_2	84.1	478	10	284	42
	20wt%SiO_2	78.2	488	18	285	33
	30wt%SiO_2	79.4	500	29	289	25
colloidal silica system CPT	10wt%SiO_2	76.9	479	9	279	44
	20wt%SiO_2	71.4	484	17	282	38
	30wt%SiO_2	69.8	491	28	287	31

[a] Determined from the residual at 800°C

[b] CTE at 100-150°C

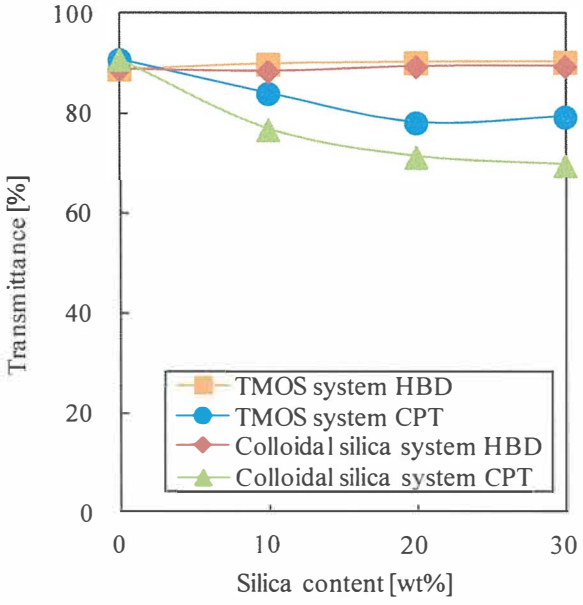

Figure 6-5 Optical transmittances of the HBPI-silica HBD and CPT films at 600nm.

content in Figure 6-5. The hybrid films maintain high transparency similar to the corresponding pristine HBPI up to high silica content. This result might be attributed to the decreased imide group density in a unit volume and the favorably fine dispersion of silica without aggregation. The fine and homogeneous dispersion of silica in the hybrid films is brought by silane coupling agents which offer covalent bonds between organic and inorganic components [9]. On the other hand, the transparency of composite films decreased severely with increasing silica content. This probably results from the low affinity of HBPI and silica moiety which leads to the aggregation of the silica components, consequently the light scattering occurs in the visible light region.

The thermal properties of the HBPI-silica HBDs and CPTs were investigated by TG-DTA, DMA, and TMA measurements. The 5% weight loss temperatures (T_d^5s) of the HBPI-silica hybrids were investigated by TG-DTA and summarized in Table 6-1 along with silica content determined from the residues at 800°C. The residues showed that all hybrids contained an appropriate amount of silica, as expected. In Figure 6-6, the T_d^5

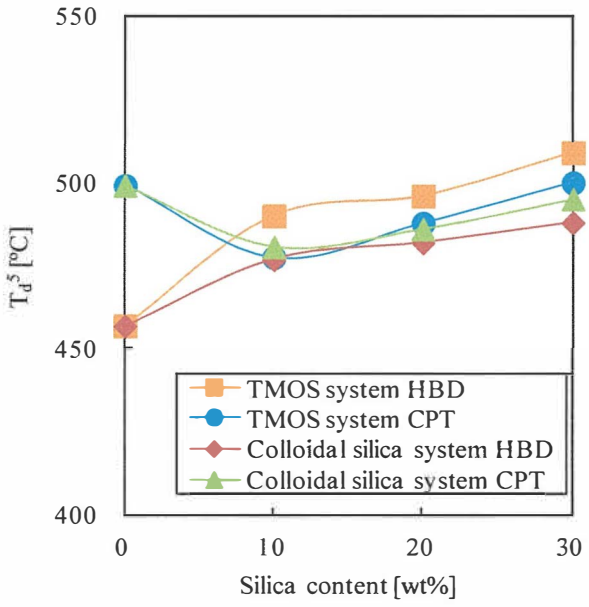

Figure 6-6 5% weight loss temperatures (T_d^5s) of the HBPI-silica HBDs and CPTs.

values of the HBPI-silica HBDs and CPTs are plotted against the silica content. The T_d^5 of the pristine HBPI modified with APTrMOS was lower than that of the unmodified pristine HBPI because C-N bonds formed by the addition of APTrMOS are less thermally stable [10]. The T_d^5 values of the HBPI-silica HBDs increased with increasing silica content due to the formation of cross-linking mediated by the silica domain, the introduction of inorganic characteristics, and the radical trapping effect of silica. Especially, the T_d^5 values of the TMOS system HBPI-silica HBDs increased remarkably because of the significant contribution of the formation of cross-linking between the HBPI and the silica domain by using much silanol groups remaining in the amorphous silica. For the colloidal silica system, the cross-linking reaction is hard to occur because there are not so many silanol groups on the surface of silica particles as silica prepared via sol-gel reaction. In the HBPI-silica CPTs, the T_d^5 values of both TMOS and colloidal silica system decreased in the low silica content region. This result might arise from the influence of the dehydration from the unreacted silanol groups remaining in the silica domain derived from sol-gel reaction or on the surface of silica particle. By contrast, in the higher silica content region, the T_d^5 values of both TMOS and colloidal silica system increased with increasing the silica content due to the strong influence of the introduction of inorganic characteristics and the radical trapping effect of silica.

The storage moduli (E's) and tan δ of the HBPI-silica HBD and CPT films are shown in Figure 6-7 (a-d). Only for the TMOS system HBPI-silica HBDs, the shift of T_g (peak of the tan δ) to higher temperature region along with a decrease of peak intensity and a broadening of the half-width of tan δ was observed. These results indicate the strong interaction of the modified HBPI and silica prepared via sol-gel reaction. In Figure 6-8(a, b), E's in the rubbery region and glassy region are plotted against the silica content. In the glassy region, no remarkable difference between these films was observed. In

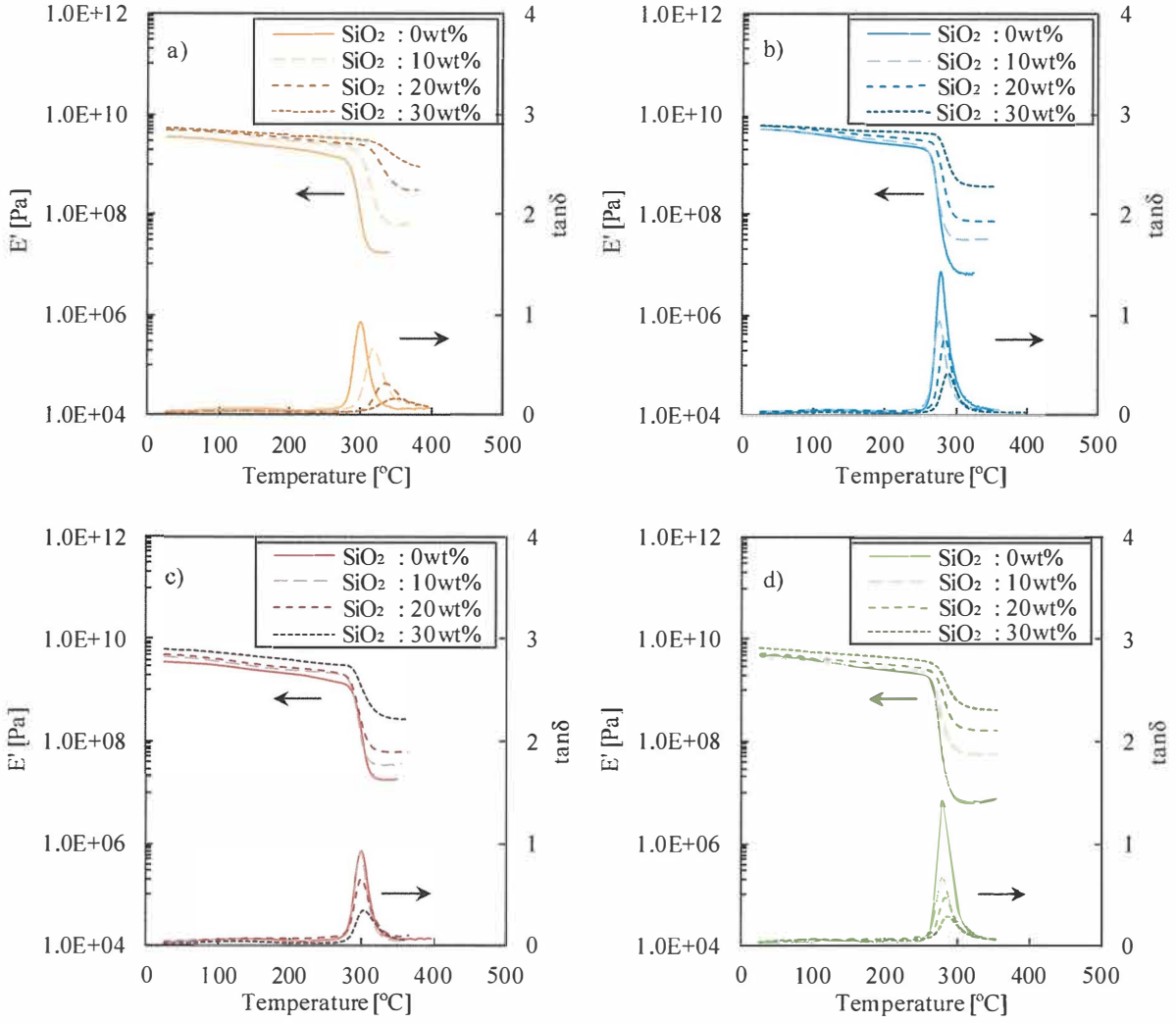

Figure 6-7 Strage moduli (E's) and tan δ of the a) TMOS system HBPI-silica HBD films, b) TMOS system HBPI-silica CPT films, c) colloidal silica system HBPI-silica HBD films, and d) colloidal silica system HBPI-silica CPT films.

contrast, in the rubbery region, the E's of the TMOS system HBPI-silica HBD films were higher than those of corresponding other films. This result indicates that in the rubbery region, the mobility of the molecular chains of the TMOS system HBPI-silica HBD is much lower than others because much more covalent bonds are formed between the modified HBPI and the silica moiety prepared via sol-gel reaction. This result also supports the above mentioned discussion about the T_d^5 behaviour.

The glass transition temperatures (T_gs) of the HBPI-silica HBD and CPT films determined from the peak of tan δ are summarized in Table 6-1 and plotted against

silica content in Figure 6-9. In Figure 6-9, it can be seen that only T_gs of TMOS system HBPI-silica HBDs increased with increasing the silica content. This result also confirms the difference of the affinity of the HBPI molecular chain and the silica moiety; the

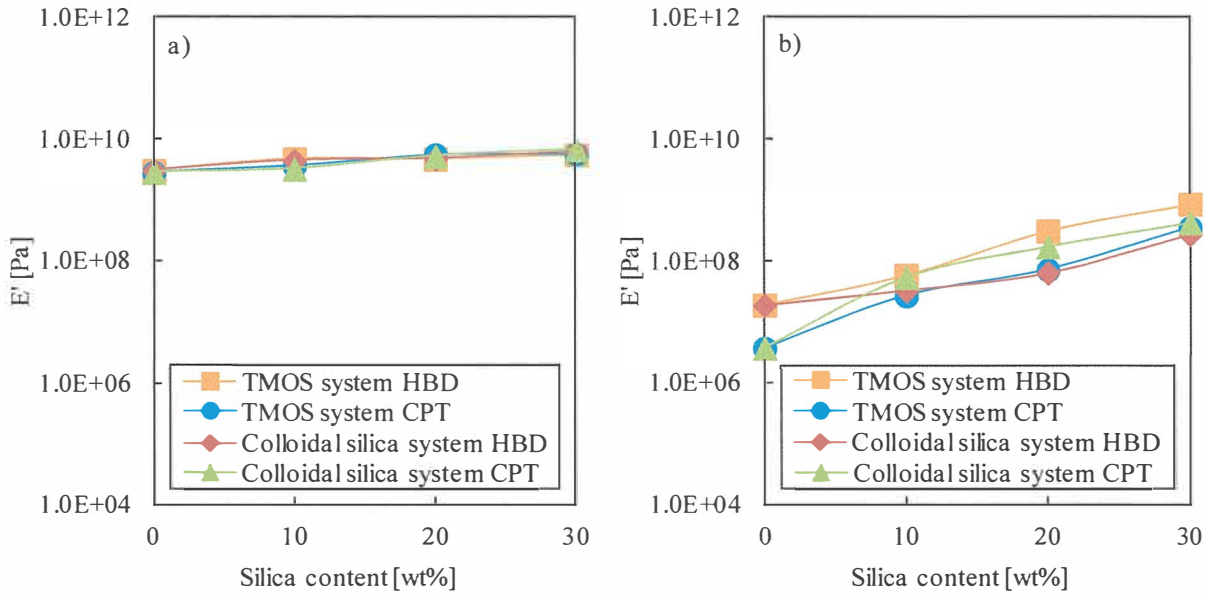

Figure 6-8 Strage moduli (E's) in the a) glassy region and b) rubbery region of the HBPI-silica HBD and CPT films plotted against silica content..

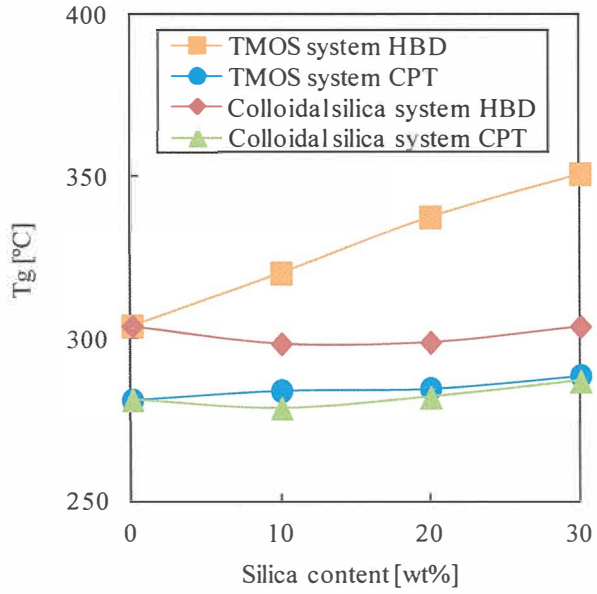

Figure 6-9 Glass transition temperatures (T_gs) of the HBPI-silica HBD and CPT films derived from the peak of tan δ.

molecular mobility decreased in the TMOS system HBPI-silica HBDs because of the strong interaction between two components through much cross-links.

The coefficients of thermal expansion (CTEs) from 100 to 150°C of the HBPI-silica HBD and CPT films are listed in Table 6-1. The CTE values of all hybrid and composite films decreased with increasing silica content attributed to the introduction of inorganic characteristics. In the TMOS system, the CTE values decreased conspicuously without dependence on hybrids or composites because the inorganic characteristics of silica domain appear strongly due to the three-dimensional entanglement of the HBPI molecules and the silica moiety.

3.2 Gas transport properties

The gas permeability, diffusion, and solubility coefficients of the HBPI-silica HBD and CPT membranes are summarized in Table 6-2, and the CO_2 permeability, diffusion, and solubility coefficients are plotted against the silica content in Figure 6-10 (a-c). As shown in Table 6-2 and Figure 6-10, the gas permeability coefficients of the TMOS

Table 6-2 Gas transport properties of the HBPI-silica HBD and CPT membranes at 76cmHg and 25°C

		$P\times10^{10}$ [cm^3(STP)cm/cm^2 s cmHg]				$D\times10^{8}$ [cm^2/s]				$S\times10^{2}$ [cm^3(STP)/cm^3 polym cmHg]			
		CO_2	O_2	N_2	CH_4	CO_2	O_2	N_2	CH_4	CO_2	O_2	N_2	CH_4
modified HBPI		7.4	1.5	0.23	0.098	0.30	1.4	0.25	0.028	25	1.1	0.92	3.5
TMOS system HBD	10wt%SiO_2	10	2.0	0.31	0.13	0.35	1.5	0.29	0.026	30	1.4	1.1	5.0
	20wt%SiO_2	13	2.1	0.32	0.16	0.37	1.3	0.25	0.030	35	1.7	1.3	5.2
	30wt%SiO_2	23	3.0	0.46	0.24	0.57	1.7	0.29	0.040	41	1.8	1.6	6.0
Colloidal silica system HBD	10wt%SiO_2	8.0	1.7	0.27	0.12	0.42	1.8	0.33	0.048	19	0.97	0.80	2.5
	20wt%SiO_2	8.1	1.6	0.30	0.12	0.37	1.5	0.33	0.049	22	1.1	0.91	2.5
	30wt%SiO_2	8.4	1.9	0.27	0.13	0.40	1.6	0.35	0.041	21	1.3	0.77	3.2
unmodified HBPI		3.8	0.86	0.11	0.046	0.19	0.87	0.14	0.012	21	0.99	0.81	3.9
TMOS system CPT	10wt%SiO_2	4.9	1.0	0.13	0.048	0.23	0.95	0.15	0.011	22	1.1	0.88	4.3
	20wt%SiO_2	7.0	1.3	0.18	0.067	0.25	0.97	0.16	0.012	28	1.4	1.1	5.4
	30wt%SiO_2	17	2.7	0.39	0.13	0.51	1.8	0.29	0.026	33	1.5	1.4	5.0
Colloidal silica system CPT	10wt%SiO_2	4.8	1.1	0.15	0.063	0.23	1.1	0.19	0.021	21	0.96	0.77	3.0
	20wt%SiO_2	4.9	1.1	0.15	0.066	0.26	1.0	0.21	0.022	19	1.0	0.71	3.0
	30wt%SiO_2	5.1	1.1	0.15	0.070	0.26	1.1	0.21	0.023	20	0.97	0.74	3.0

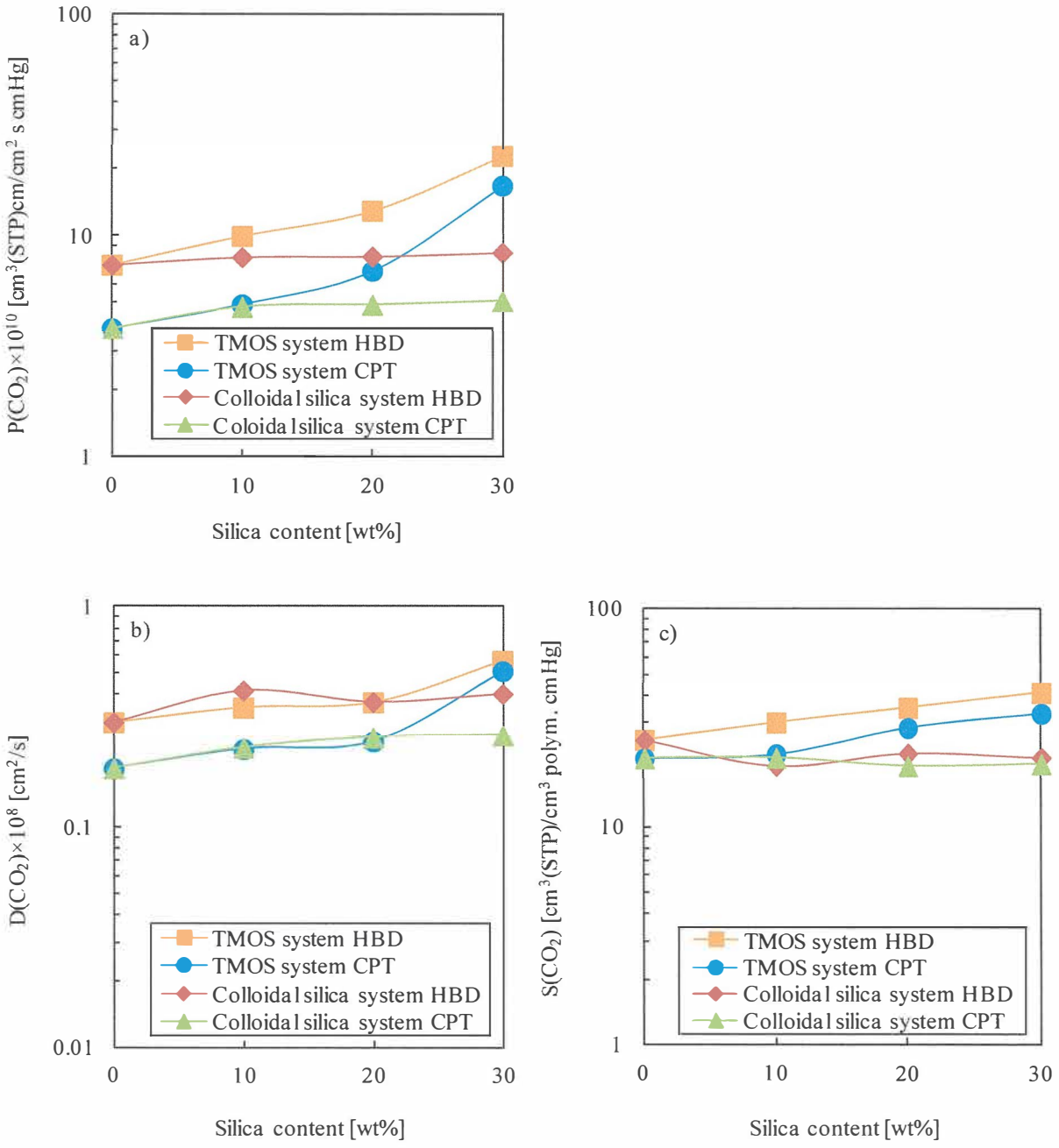

Figure 6-10 CO_2 a) permeability, b) diffusion and c) solubility coefficients of the HBPI-silica HBD and CPT membranes.

system HBPI-silica HBD and CPT membranes increased with increasing the silica content due to the contributions of both diffusion coefficient and solubility coefficient. This result indicates the additional formation of free volume holes and a Langmuir sorption site effective for gas transport properties through hybridization or mixing with silica [11-13]. By contrast, the gas permeability coefficients of the colloidal silica system

HBPI-silica HBD and CPT membranes increased very little with increasing the silica content. From these results, it was revealed that the gas transport behavior of the HBPI-silica HBD and CPT membranes was controlled largely by a silica source (sol-gel reaction with TMOS or colloidal silica) than a preparation method (hybrid or composite). Generally, it is well known that the introduction of the dense inorganic particles to polymer matrix increases the gas barrier properties of polymer films. For example, the permeability coefficients of the composite membrane with only 2 wt% addition of montmorillonite is less than half of those of pristine polyimide for various gases. This decrease of permeability coefficients was explained by the increase of the total path of gas [14]. Gases cannot diffuse through the dense inorganic filler. On the other hand, Park et al. pointed out that the gas transport of siloxane containing polyimide membrane could occur through the porous silica network and/or the path in the interfacial region between silica networks and the organic matrix [15]. Similar gas transport properties have been reported in several other studies. Merkel et al. reported the increased gas permeabilities of the high-free-volume glassy polymer due to the incorporation of nanosilica particles. They concluded that the polymer chains around the nanosilica particles were unable to pack efficiently, resulting in a low-density polymer-nanoparticle interfacial region which allows permeation of gases[16-18]. Hill suggested the theoretical model to quantitatively interpret Merkel et al.'s experiments [19,20]. He concluded that the incorporation of nanoinclusion leads to the formation of a polymer-segment depletion layer at the inclusion-polymer interface, and that the accompanying increase in free volume increased the bulk permeability and selectivity due to a significant increase in the local penetrant diffusivity. Zhang et al. also reported the improvement of the permeability of poly(vinyl alcohol) / 1,2-bis(triethoxysilyl)ethane hybrid membranes, and suggested that the amorphous region in the hybrid membranes increased with

increasing silica content [21]. The increased solubilities of the TMOS system HBPI-silica HBD and CPT membranes suggest that the Langmuir-type sorption site is additionally formed by the incorporation of silica domains. There are so many sorption sites in the TMOS system HBPI-silica HBD and CPT membranes because the silica domain prepared via the sol-gel reaction is porous and its specific surface area is large [22].

3.3 O_2/N_2 and CO_2/CH_4 selectivities

The ideal permselectivity for the combination of gases A and B [α(A/B)] is defined by the following equation [23]:

$$\alpha(A/B)=\frac{P(A)}{P(B)}=\frac{D(A)}{D(B)}\times\frac{S(A)}{S(B)}=\alpha^{D}(A/B)\times\alpha^{S}(A/B) \qquad (5)$$

where $\alpha^{D}(A/B)$ is the diffusivity selectivity and $\alpha^{S}(A/B)$ is the solubility selectivity. The O_2/N_2 and CO_2/CH_4 selectivities of the HBPI-silica HBD and CPT membranes are listed in Table 6-3, and CO_2/CH_4 permselectivity is plotted against the CO_2 permeability coefficient in Figure 6-11. In Table 6-3, the O_2/N_2 permselectivity slightly decreased with increasing silica content i.e. O_2 permeability. This behavior is consistent with the

Table 6-3 O_2/N_2 and CO_2/CH_4 selectivities of the HBPI-silica HBD and CPT membranes at 76 cmHg and 25°C

		O_2/N_2 selectivity			CO_2/CH_4 selectivity		
		$\alpha(O_2/N_2)$	$\alpha^{D}(O_2/N_2)$	$\alpha^{S}(O_2/N_2)$	$\alpha(CO_2/CH_4)$	$\alpha^{D}(CO_2/CH_4)$	$\alpha^{S}(CO_2/CH_4)$
modified HBPI		6.8	5.8	1.2	75	11	7.0
TMOS system HBD	10wt%SiO_2	6.6	5.2	1.3	79	13	5.9
	20wt%SiO_2	6.7	5.3	1.3	82	12	6.8
	30wt%SiO_2	6.6	5.8	1.1	95	14	6.7
Colloidal silica system HBD	10wt%SiO_2	6.5	5.5	1.2	67	8.8	7.6
	20wt%SiO_2	5.4	4.4	1.2	66	7.6	8.7
	30wt%SiO_2	7.2	4.4	1.6	64	9.9	6.5
unmodified HBPI		7.8	6.4	1.2	83	15	5.3
TMOS system CPT	10wt%SiO_2	7.9	6.3	1.2	102	20	5.0
	20wt%SiO_2	7.3	6.0	1.2	104	20	5.3
	30wt%SiO_2	7.0	6.2	1.1	129	20	6.6
Colloidal silica system CPT	10wt%SiO_2	7.1	5.7	1.3	76	11	6.9
	20wt%SiO_2	7.2	5.0	1.5	74	11	6.4
	30wt%SiO_2	7.0	5.4	1.3	73	11	6.5

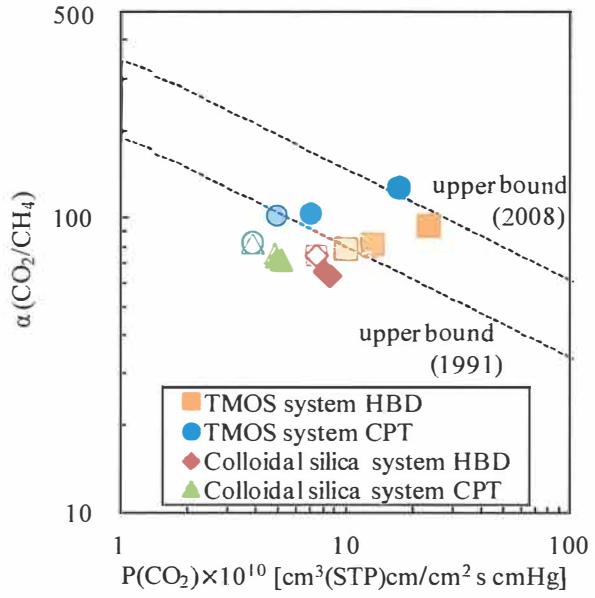

Figure 6-11 Ideal CO_2/CH_4 permselectivity [$\alpha(CO_2/CH_4)$] of HPBI-silica HBD and CPT membranes plotted against CO_2 permeability coefficient.

general understanding that more permeable polymers are generally less selective, and *vice versa* [23]. Hence, it can be concluded that free volume holes formed by hybridization or mixing with silica are not sufficiently effective to separate O_2 and N_2 that have similar kinetic diameters and shapes. For the CO_2/CH_4 permselectivity, in Figure 6-11, we can see the different tendency depending on the silica source. $\alpha(CO_2/CH_4)$ of the HBPI-silica HBD and CPT with colloidal silica slightly decrease with increasing CO_2 permeability along with the upper bound trade-off line for CO_2/CH_4 separation demonstrated by Robeson [24, 25], suggesting that the free volume formed in the colloidal silica system is not competent to separate CO_2 and CH_4. By contrast, both the CO_2 permeability and the CO_2/CH_4 permselectivity of the TMOS system HBPI-silica HBD and CPT membranes increased with increasing silica content. This result revealed that the free volume having CO_2/CH_4 separation ability was formed by hybridization or mixing via sol-gel reaction with TMOS.

The WAXD measurements were performed to scrutinize the difference between the

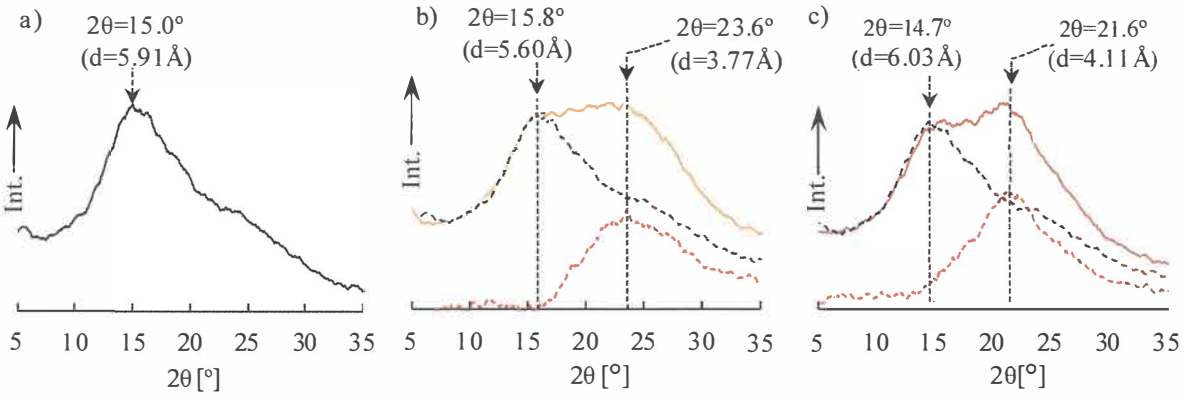

Figure 6-12 WAXD patterns of the a) pristine HBPI, b) TMOS system HBPI-silica HBD (SiO_2 content : 30wt%), and c) colloidal silica system HBPI-silica HBD (SiO_2 content : 30wt%).

TMOS system and colloidal silica system HBD and CPT membranes. Figure 6-12 shows the diffraction patterns of the a) pristine HBPI, b) TMOS system HBPI-silica HBD, and c) colloidal silica system HBPI-silica HBD. In the spectrum of the HBPI base polymer, the broad peak was found around 2θ=15.0°. The *d*-spacings can be calculated by applying the scattering angles (2θ) of the peaks into the Bragg's equation, $n\lambda=2d\sin\theta$. The *d*-spacings determined from this manner represent approximate average intersegmental distance of polyimide molecules [26-28]. Both TMOS system and colloidal silica system hybrids show two diffraction peaks. From Figure 6-12 b) and c), the intersegmental distance (*d*-spacing) of the HBPI molecule is narrowed by hybridization with silica derived from TMOS, whereas, slightly spread by hybridization with colloidal silica. The narrowing of the intersegmental distance in the HBPI-silica HBD with silica derived from TMOS may arise from the cross-linking formed between the HBPI molecular terminals and silanol groups remaining in the silica domain. On the other hand, the *d*-spacing of the HBPI molecule in the colloidal silica system HBPI-silica HBDs is expanded slightly than pristine HBPI because the nanosilica particles disrupt the polymer chain packing. The peak around 21-24° is caused by the diffraction of silica

moiety. It was confirmed that the silica domains prepared via sol-gel reaction with TMOS were more amorphous than colloidal silica due to the lower and broader peak of WAXD pattern. Comparing the *d*-spacing attributed to the silica moiety and the kinetic diameters of studied gases (CO_2 : 3.3 Å, O_2 : 3.5 Å, N_2 : 3.6 Å, CH_4 : 3.8 Å), it cannot be denied that the gases permeate through amorphous silica prepared by sol-gel reaction that have molecular sieving function.

3.4 Gas transport mechanism

From the results of gas permeability and selectivity in the HBPI-silica HBD and CPT membranes, the gas transport mechanism in the HBPI-silica HBD and CPT membranes was considered as shown in Figure 6-13.

In the TMOS system HBPI-silica HBD and CPT membranes (Figure 6-13(a, b)), gases can permeate through not only the newly formed diffusion path around the HBPI-silica interfacial region but also inside the porous nanosilica components because the amorphous silica is formed by sol-gel reaction. Consequently, the gas permeability increases with increasing silica content. Furthermore, the CO_2/CH_4 permselectivity of the HBPI-silica HBD and CPT membranes increased with increasing silica content because the porous nanosilica formed by sol-gel reaction have molecular sieving effects.

On the other hand, in the colloidal silica system HBPI-silica HBD and CPT membranes (Figure 6-13 (c, d)), large voids without CO_2/CH_4 separation ability are formed around the HBPI-silica interfacial region because of the weak interaction of HBPI and silica nanoparticles. Gases permeate through the tortuous diffusion path formed between HBPI and silica component since it cannot permeate through the dense colloidal silica phase. Therefore, few effects were found in permeability and CO_2/CH_4 permselectivity in the colloidal silica system HBPI-silica HBD and CPT membranes.

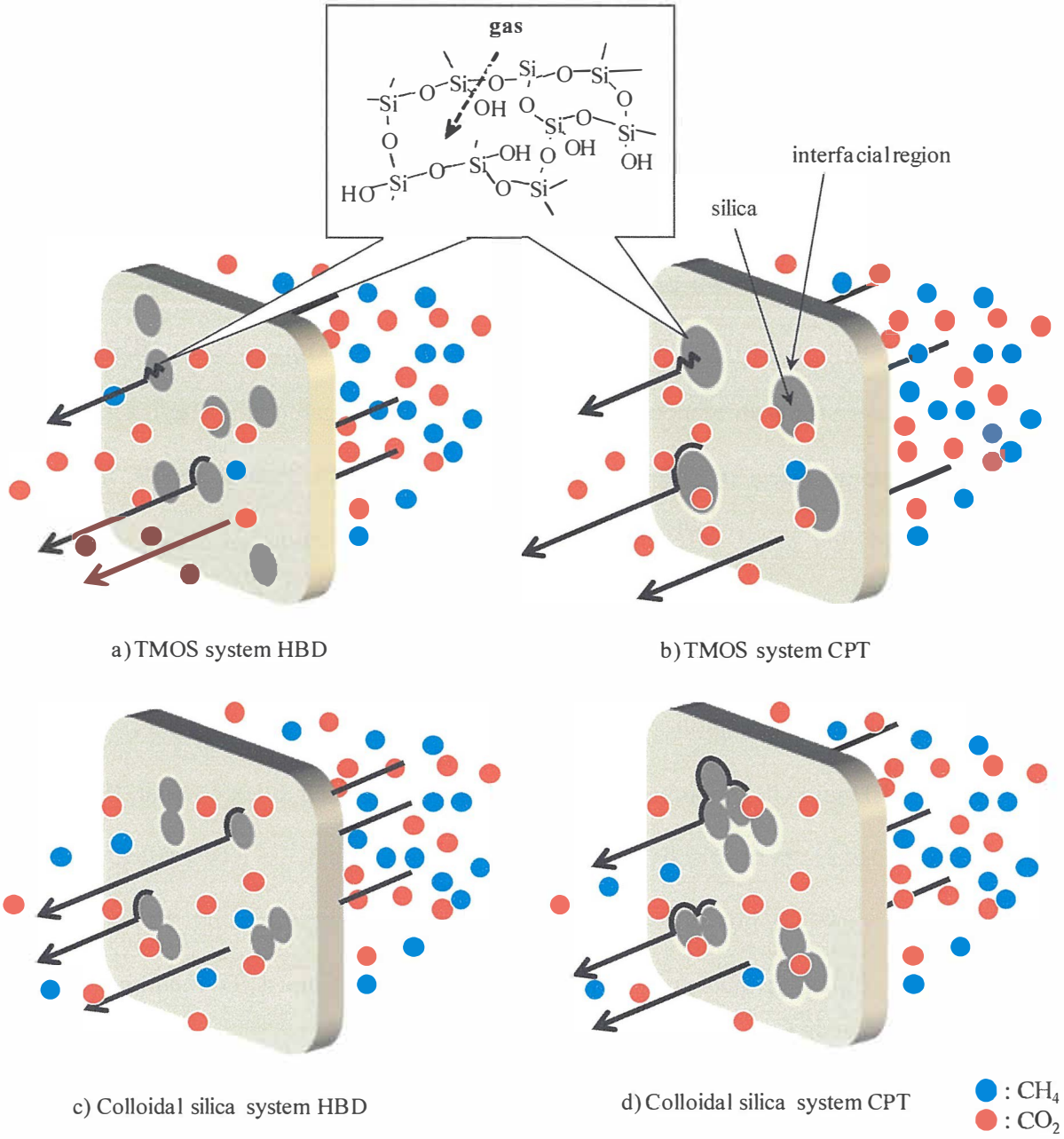

Figure 6-13 A Schematic image of gas transport mechanism through the HBPI-silica HBD and CPT membranes.

4. Conclusions

HBPI-silica HBD and CPT membranes were prepared via sol-gel reaction or the addition of colloidal silica and their general and gas transport properties were investigated. The ATR FT-IR spectra revealed satisfactory imidization and sufficient

formation of three-dimensional Si-O-Si networks in all prepared films. And these spectra also revealed the existence of the silanol groups in the TMOS system hybrids and composites. The HBPI-silica HBD films maintain high transparency similar to the corresponding pristine HBPIs at high silica content, indicating the favorable dispersion of silica. The T_d^5 values of all prepared HBPI-silica HBDs and CPTs increased with increasing the silica content due to the formation of cross-linking between HBPI and silica domain, the strong influence of the introduction of inorganic characteristics, and the radical trapping effect of silica. From the DMA and TMA measurements, it was found out that the most effective influence of the induction of silica to the thermomechanical property is obtained in the TMOS system HBPI-silica HBD because the interaction of the HBPI and the silica domain is stronger than other hybrids and composites. The gas permeability and CO_2/CH_4 permselectivity of the TMOS system HBPI-silica HBD and CPT membranes increased with increasing silica content. On the other hand, CO_2/CH_4 permselectivity of the colloidal silica system HBPI-silica HBD and CPT membranes slightly decreased with increasing CO_2 permeability. From these results, the gas transport mechanism in the HBPI-silica HBD and CPT membranes is proposed as follows; The increase of gas permeability and CO_2/CH_4 permselectivity of the TMOS system HBPI-silica HBD and CPT membranes are caused by the contribution of both of additional formation of free volume elements around polymer-silica interfacial region which provides diffusion path and Langmuir-type sorption site for gas molecules, and the formation of amorphous silica via sol-gel reaction which have molecular sieving function.

References

[1] T. Takeichi, J. K. Stille, Star and Liner Imide Oligomers Containing Reactive

End Caps: Preparation and Thermal Properties, Macromolecules, 19 (1986) 2093-2102.

[2] R.S. Prabhakar, B.D. Freeman, I. Roman, Gas and Vapor Sorption and Permeation in Poly(2,2,4-trifluoro-5-trifluoromethoxy-1,3-dioxole-co-tetrafluoroethylene), Macromolecules, 37 (2004) 7688-7697.

[3] N. Muruganandam, W.J. Koros, D.R. Paul, Gas Sorption and Transport in Substituted Polycarbonates, J. Polym. Sci. Part B: Polym. Phys., 25 (1987) 1999-2026.

[4] A. Morisato, H.C. Shen, S.S. Sankar, B.D.Freeman, I. Pinnau, C.G. Casillas, Polymer Characterization and Gas Permeability of Poly(1-trimethylsilyl-1-propyne) [PTMST], Poly(1-phenyl-1-propyne) [PPP], and PTMSP/PPP Blends, J. Polym. Sci. Part B: Polym. Phys., 34 (1996) 2209-2222.

[5] D.H. Weinkauf, H.D. Kim, D.R. Paul, Gas Transport Properties of Liquid Crystalline Poly(p-phenyleneterephthalamide), Macromolecules, 25 (1992) 788-796.

[6] H. Chen, J. Yin, Synthesis and Characterization of Hyperbranched Polyimides with Good Organosolubility and Thermal Properties Based on New Triamine and Conventional Dianhydrides, J. Polym. Sci. Part A: Polym. Chem., 40 (2002) 3804-3814.

[7] J. Fang, H. Kita, K. Okamoto, Hyperbranched Polyimides for Gas Separation Applications. 1. Synthesis and Characterization, Macromolecules, 33 (2000) 4639-4646.

[8] C. Hibshman, C.J. Cornelius, E. Marand, The Gas Separation Effects on Annealing Polyimide-Organosilicate Hybrid Membranes, J. Membr. Sci., 211 (2003) 25-40.

[9] N. Tomokiyo, Y. Yamada, T. Suzuki, J. Oku, Preparation and Characterization of Hyperbranched Polyimide - Colloidal Silica Hybrids, Polym. Prep. Japan, 55 (2006) 5175-5176.

[10] M. Miki, T. Suzuki, Y. Yamada, Structure–Property Relationships of Hyperbranched Polyimide–Silica Hybrid Membranes with Different Degrees of

Modification, J. Appl. Polym. Sci., 130 (2013)54-62.

[11] T. Suzuki, Y. Yamada, K. Itahashi, 6FDA-TAPOB Hyperbranched Polyimide-Silica Hybrids for Gas Separation Membranes, J. Appl. Polym. Sci., 109 (2008) 813-819.

[12] T. Suzuki, Y. Yamada, Y. Tsujita, Gas transport properties of 6FDA-TAPOB hyperbranched polyimide membrane, Polymer, 45 (2004) 7167-7171.

[13] T. Suzuki, Y. Yamada, Physical and Gas Transport Properties of Novel Hyperbranched Polyimide – Silica Hybrid Membranes, Polym. Bull., 53 (2005) 139-146.

[14] K. Yano, A. Usuki, A. Okada, Synthesis and Properties of Polyimide-Clay Hybrid Films, J. Polym. Sci. Part A: Polym. Chem., 35 (1997) 2289-2294.

[15] H.B. Park, J.K. Kim, S.Y. Nam, Y.M. Lee, Imide-siloxane block copolymer/silica hybrid membranes : preparation, characterization and gas separation properties, J. Membr. Sci., 220 (2003) 59-73.

[16] T.C. Merkel, B.D. Freeman, R.J. Spontak, Z. He, I. Pinnau, P. Meakin, A.J. Hill, Ultrapermeable, Reverse-Selective Nanocomposite Membranes, Science, 296 (2002) 519-522.

[17] T.C. Merkel, L.G. Toy, A.L. Andrady, H. Gracz, E.O. Stejskal, Investigation of Enhanced Free Volume in Nanosilica-Filled Poly(1-trimethylsilyl-1-propyne) by 129Xe NMR Spectroscopy, Macromolecules, 36 (2003) 353-358.

[18] A.L. Andrady, T.C. Merkel, L.G. Toy, Effect of Particle Size on Gas Permeability of Filled Superglassy Polymers, Macromolecules, 37 (2004) 4329-4331.

[19] R.J. Hill, Diffusive Permeability and Selectivity of nanocomposite Membranes, Ind. Eng. Chem. Res., 45 (2006) 6890-6898.

[20] R.J. Hill, Reverse-Selective Diffusion in nanocomposite Membranes, Phy. Rev. Lett., 96 (2006) 216001-1-26001-4.

[21] Q.G. Zhang, Q.L. Liu, A.M. Zhu, Y. Xiong, X.H Zhang, Characterization and Permeation Performance of Novel Organic-Inorganic Hybrid Membranes of Poly(vinyl Alcohol)/1,2-Bis(triethoxysilyl)ethane, J. Phys. Chem. B, 112 (2008) 16559–16565.

[22] K. Okamoto, K. Tanaka, H. Kita, M. Ishida, M. Kakimoto, Y. Imai, Gas Permeability and Permselectivity of Polyimides Prepared from 4,4'-Diaminotriphenylamine, Polym. J., 24 (1992) 451-457.

[23] B.D. Freeman, Basis of Permeability/Selectivity Tradeoff Relations in Polymeric Gas Separation Membranes, Macromolecules, 32 (1992) 375-380.

[24] L.M. Robeson, Correlation of separation factor versus permeability for polymeric membranes, J. Membr. Sci., 62 (1991) 165-185.

[25] L.M. Robeson, The upper bound revisited, J. Membr. Sci., 320 (2008) 390-400.

[26] J. Fang, H. Kita, K. Okamoto, Gas Permeation Properties oh Hyperbranched Polyimide Membranes, J. Membr. Sci., 182 (2001) 245-256.

[27] T.H. Kim, W.J. Koros, G.R. Husk, K.C. O'brien, Relationship between gas separation properties and chemical structure in a series of aromatic polyimides, J. Membr. Sci., 37 (1988) 45-62.

[28] R.F. Boehme, G.S. Cargill III, X-ray scattering measurements demonstrating in-plane anisotropy in Kapton polyimide films, in: K.L. Mittal (Eds.), Polyimides, Plenum Press, New York, 1984.

Chapter 7

Study on Nanostructure-Gas Transport Property Relationship of Hyperbranched Polyimide-Silica Hybrid Membranes

1. Introduction

In chapter 2 to chapter 6, a variety of hyperbranched polyimide (HBPI)-silica hybrid membranes were prepared and their physical and gas transport properties were investigated to clarify the structure-gas transport property relationship.

In this chapter, the nanostructures of HBPI-silica hybrids were examined by several methods to discuss the gas transport mechanism.

2. Experimental

2.1 Materials

1,3,5-Tris(4-aminophenoxy)benzene (*TAPOB*) was synthesized by the reduction of 1,3,5-tris(4-nitrophenoxy)benzene with palladium carbon and hydrazine in methanol [1]. Dianhydride, 4,4'-(hexafluoroisopropylidene) diphthalic anhydride (*6FDA*), was kindly supplied by Daikin Industries (Osaka, Japan). 3-Aminopropyltrimethoxysilane (*APTrMOS*) and 3-(triethoxysilyl) propyl succinic anhydride (*TEOSPSA*) were purchased from Sigma-Aldrich Co. LLC. (St. Louis, MO, USA) and Gelest Inc. (Morrisville, PA, USA), respectively. Tetramethoxysilane (*TMOS*) and methyltrimethoxysilane (*MTMS*) were purchased from AZmax, Co., Ltd (Tokyo, Japan). Colloidal silica was obtained from Nissan chemical industries, Ltd (Tokyo, Japan). *N, N*-Dimethylacetamide (*DMAc*) used as a solvent was purchased from Nacalai Tesque

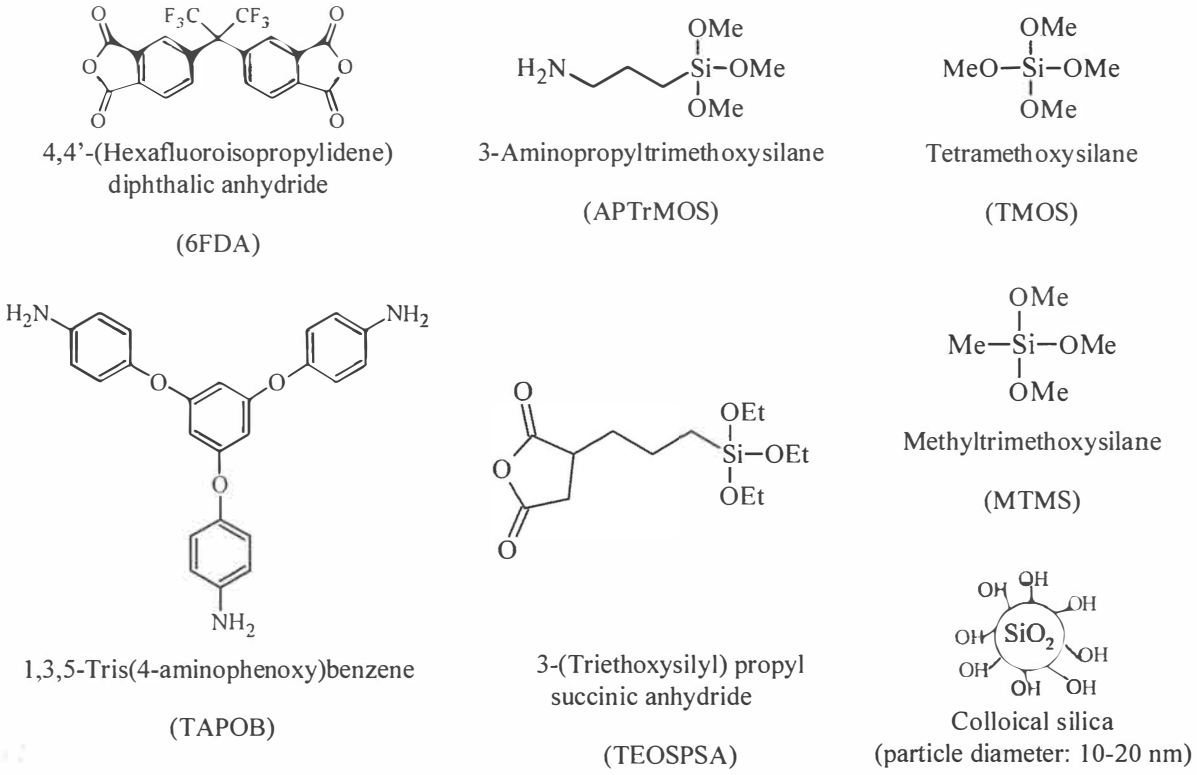

Figure 7-1 Chemical structures of monomers, silane coupling agents, and silica sources.

(Kyoto, Japan). The chemical structures of monomers, silane coupling agents, and silica sources are shown in Figure 7-1.

2.2 Polymerization

2.2.1 Dianhydride-terminated hyperbranched polyamic acids (DA-HBPAAs)

Three mmol of 6FDA was dissolved in 40 ml of DMAc in a 100-ml three-neck flask under N_2 flow at room temperature. 1.6 mmol of TAPOB in 20 ml of DMAc was then added dropwise through a syringe with stirring. The monomer content of reaction mixtures was controlled to *ca.* 3.5 wt%. After stirring for 3 h, 0.4 mmol of APTrMOS as a coupling agent was added into the reaction mixture with further stirring for 1 h to afford DA-HBPAA.

2.2.2 Amine-terminated hyperbranched polyamic acids (AM-HBPAAs)

Three mmol of TAPOB was dissolved in 34 ml of DMAc in a 100-ml three-neck

flask under N_2 flow at room temperature. 3.0 mmol of 6FDA in 40 ml of DMAc was then added dropwise through a syringe with stirring. The monomer content of reaction mixtures was controlled to *ca.* 3.5 wt%. After stirring for 3 h, 1.0 mmol of TEOSPSA as a coupling agent was added into the reaction mixture with further stirring for 1 h to afford AM-HBPAA.

2.3 Membrane formation

2.3.1 Sol-gel system HBPI-silica hybrids

The sol-gel system HBPI-silica hybrids were prepared by thermal imidization and sol-gel reaction with two kinds of silicon alkoxides, TMOS and MTMS. Appropriate amounts of silicon alkoxides, TMOS or MTMS, and deionized water (silicon alkoxides : deionized water = 1 : 6 as a molar ratio) were added into the DMAc solution of the HBPAAs. The mixed solutions were stirred for 24 h and then cast on PET films and dried at 85°C for 3 h. The prepared films were peeled off and subsequently imidized at 100°C for 1 h, 200°C for 1 h, and 300°C for 1 h in a heating oven under N_2 flow. The average thickness of the prepared HBPI-silica hybrid membranes was about 30 μm. A schematic diagram for the preparation of sol-gel system HBPI-silica hybrid membranes is shown in Figure 7-2.

2.3.2 Colloidal silica system HBPI-silica hybrids

Colloidal silica system HBPI-silica hybrids were prepared by blending HBPAAs and colloidal silica, and then followed by thermal imidization. Appropriate amounts of colloidal silica dispersed in DMAc was added into the DMAc solution of the HBPAAs. Shortly after mixing the HBPAAs and colloidal silica, the prepared solutions were cast on PET films and dried at 85°C for 3 h. The prepared films were peeled off and subsequently imidized at 100°C for 1 h, 200°C for 1 h, and 300°C for 1 h in a heating oven under N_2 flow. The average thickness of the prepared HBPI-silica hybrid

membranes was about 30 μm. A schematic diagram for the preparation of colloidal silica system HBPI-silica hybrid membranes is shown in Figure 7-2.

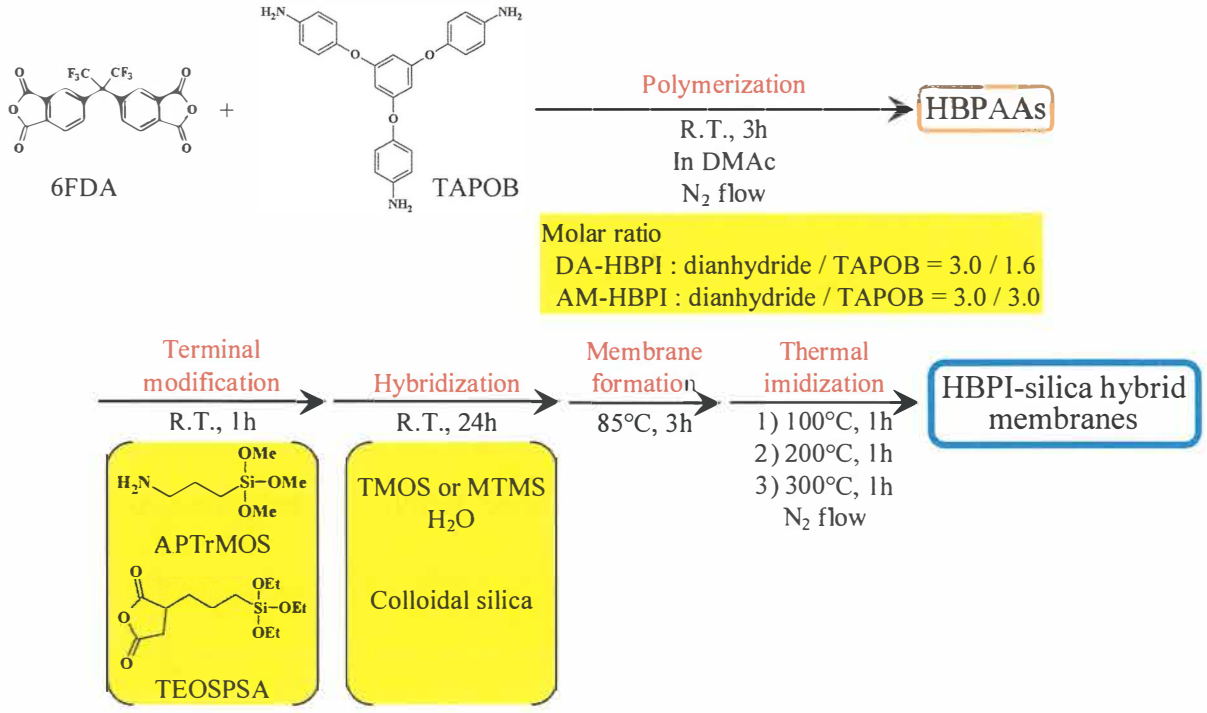

Figure 7-2 A schematic diagram for the preparation of DA- and AM-HBPI-silica hybrid membranes.

2.4 Measurements

CO_2, O_2, N_2, and CH_4 permeation measurements were taken with a constant volume/variable pressure apparatus under 76 cmHg at 25°C. The permeability coefficient, P [cm^3(STP)cm/cm^2 s cmHg], was determined by the equation [2] :

$$P = \frac{22414}{A}\frac{L}{p}\frac{V}{RT}\frac{dp}{dt} \qquad (1)$$

where A is the membrane area (cm^2), L is the membrane thickness (cm), p is the upstream pressure (cmHg), V is the downstream volume (cm^3), R is the universal gas constant (6236.56 cm^3 cmHg/mol K), T is the absolute temperature (K), and dp/dt is the permeation rate (cmHg/s). The gas permeability coefficient can be explained on the basis of the solution-diffusion mechanism, which is represented by the equation [3,4]:

$$P = D \times S \quad (2)$$

where D (cm^2/s) is the diffusion coefficient and S [$cm^3(STP)/cm^3_{polym}$ cmHg] is the solubility coefficient. The diffusion coefficient was calculated by the time-lag method represented by the equation [5]:

$$D = \frac{L^2}{6\theta t} \quad (3)$$

where θt (s) is the time-lag.

The densities (ρs) of the HBPI-silica hybrids were measured by a floating method with bromoform and 2-propanol at 25°C. According to the group contribution method, the fractional free volume (FFV) of the pristine HBPIs can be estimated by the following equation [6] :

$$FFV = \frac{V_{sp} - 1.3V_w}{V_{sp}} \quad (4)$$

where V_{sp} (cm^3/mol) is the specific molar volume and V_w (cm^3/mol) is the van der Waals volume of the repeat unit. Nitrogen adsorption/desorption measurements were carried out using a Quantachrome Instruments (Boynton Beach, Fl, USA) Autosorp-1 after degassing at 300 °C for 30min. Before measurements, the HBPI-silica hybrids were baked at 650°C for 8h to pyrolyze the HBPI moiety. Wide angle X-ray diffractometry (WAXD) were recorded at room temperature by using a Rigaku (Tokyo, Japan) RINT2500 in the 2 theta range of 5 - 35° with a scan rate of 2°/min. Cu Kα (wavelength λ = 0.154nm) radiation was used. The average *d*-spacing value was determined from Bragg's equation:

$$d = \frac{\lambda}{2\sin\theta} \quad (5)$$

Positron annihilation lifetime spectroscopy (PALS) experiments were performed by

using of 0.4-MBq ^{22}Na sealed in thin Kapton foil as positron source. The samples composed of 10 mm*10 mm size HBPI-silica hybrid films stacked to 1 mm in thickness were placed in a cell and subjected to vacuum at room temperature.

3. Results and Discussion

3.1 Gas permeability

Figure 7-3 shows the relationship between 1/FFV and gas diffusivity coefficient of the HBPI membranes reported in chapter 2, 3, and 5. As mentioned in chapter 2, it is well known that the gas diffusivities of polymers are strongly correlated to their FFVs [7,8]. From Figure 7-3, it is confirmed that the distinct correlation between log D and inverse FFV can be seen for the HBPI membranes reported in this thesis; the larger the FFV is, the larger diffusion coefficient is.

The gas permeability, diffusion, and solubility coefficients of the HBPI-silica hybrid membranes are summarized in Table 7-1, and the CO_2 permeability, diffusion, and

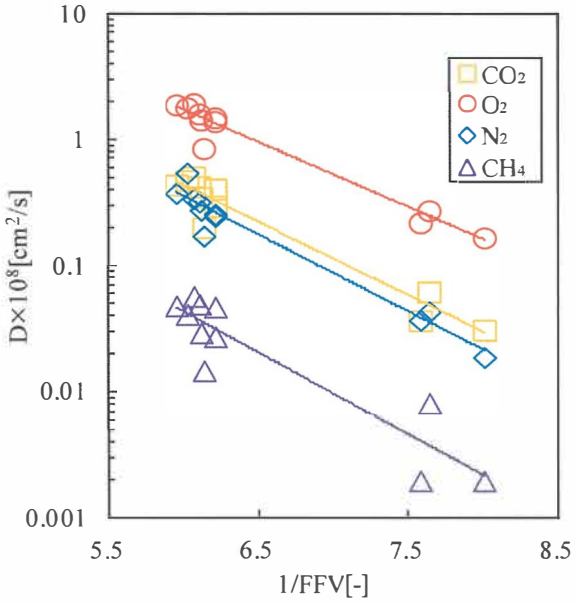

Figure 7-3 Relationship between 1/FFV and CO_2 gas diffusivity coefficient (D) of the HBPI membranes.

solubility coefficients are plotted against silica content in Figure 7-4 (a-c). As shown in Table 7-1 and Figure 7-4, the gas permeability coefficients of the TMOS system HBPI-silica hybrid membranes increased with increasing the silica content due to the contributions of the diffusion coefficient and the solubility coefficient. In contrast, for the MTMS system HBPI-silica hybrid membranes, significant increase of gas permeability coefficients was mainly caused by the enormous improvement of gas diffusivity. In addition, the gas permeability coefficients of the colloidal silica system HBPI-silica hybrid membranes increased very little with increasing the silica content.

To discuss the reason for these results, densities of the HBPI-silica hybrids and BET surface area of the silica moiety of HBPI-silica hybrids were measured. In Figure 7-5,

Table 7-1 Gas transport properties of the HBPI-silica hybrid membranes at 76cmHg and 25°C

	$P\times10^{10}$ [cm^3(STP)cm/cm^2 s cmHg]				$D\times10^{8}$ [cm^2/s]				$S\times10^{2}$ [cm^3(STP)/cm^3 polym cmHg]				BET surface area [a] [m^2/g]
	CO_2	O_2	N_2	CH_4	CO_2	O_2	N_2	CH_4	CO_2	O_2	N_2	CH_4	
DA-HBPI	7.4	1.5	0.23	0.098	0.30	1.4	0.25	0.028	25	1.1	0.92	3.5	-
TMOS system hybrid													
10wt%SiO_2	10	2.0	0.31	0.13	0.35	1.5	0.29	0.026	30	1.4	1.1	5.0	-
20wt%SiO_2	13	2.1	0.32	0.16	0.37	1.3	0.25	0.030	35	1.7	1.3	5.2	-
30wt%SiO_2	23	3.0	0.46	0.24	0.57	1.7	0.29	0.040	41	1.8	1.6	6.0	178
MTMS system hybrid													
10wt%SiO_2	23	4.4	0.75	0.45	1.0	3.8	0.83	0.13	23	1.2	0.90	3.6	-
20wt%SiO_2	53	9.5	1.9	1.5	2.6	8.7	2.2	0.42	21	1.1	0.90	3.7	-
30wt%SiO_2	99	18	4.1	4.1	5.4	16	4.8	1.2	19	1.1	0.86	3.4	272
40wt%SiO_2	158	28	7.6	10	9.9	28	9.3	3.7	16	1.0	0.82	2.7	-
50wt%SiO_2	251	46	14	20	17	46	17	6.8	15	1.0	0.79	3.0	-
Colloidal silica system hybrid													
10wt%SiO_2	8.0	1.7	0.27	0.12	0.42	1.8	0.33	0.048	19	0.97	0.80	2.5	-
20wt%SiO_2	8.1	1.6	0.30	0.12	0.37	1.5	0.33	0.049	22	1.1	0.91	2.5	-
30wt%SiO_2	8.4	1.9	0.27	0.13	0.40	1.6	0.35	0.041	21	1.3	0.77	3.2	122
AM-HBPI	13	2.3	0.35	0.22	0.41	1.5	0.26	0.048	30	1.5	1.3	4.5	-
TMOS system hybrid													
10wt%SiO_2	15	2.4	0.37	0.23	0.47	1.7	0.32	0.055	31	1.4	1.2	4.1	-
20wt%SiO_2	16	2.5	0.38	0.22	0.41	1.4	0.27	0.048	38	1.8	1.4	4.6	-
30wt%SiO_2	19	2.9	0.43	0.21	0.46	1.5	0.24	0.054	42	1.9	1.8	3.9	186

[a] BET surface area of the silica moiety

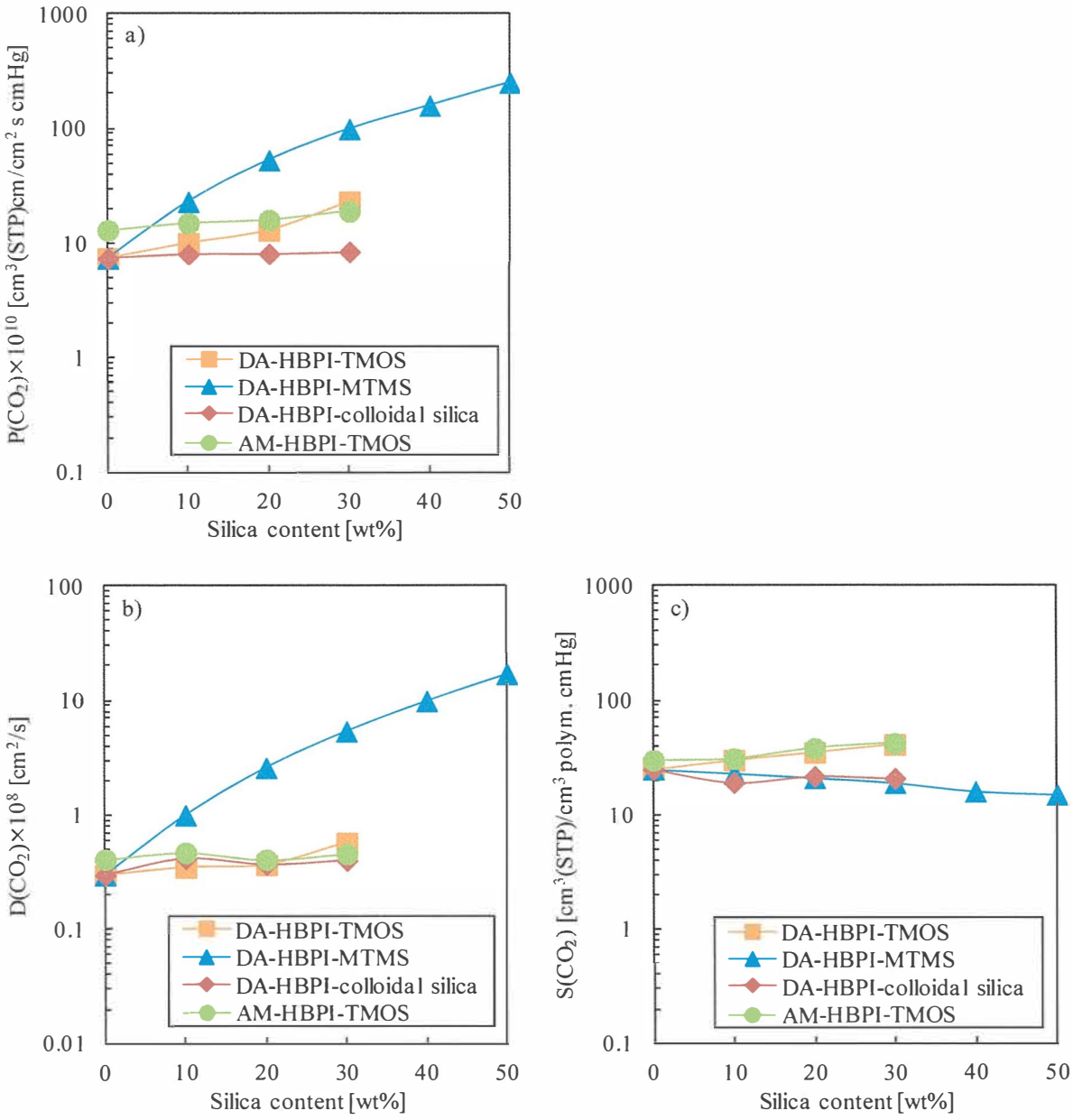

Figure 7-4 CO_2 a) permeability, b) diffusion, and c) solubility coefficients of the HBPI-silica hybrid membranes.

the densities of TMOS system and colloidal silica system DA-HBPI-silica hybrids were plotted against silica content. The densities of colloidal silica system DA-HBPI-silica hybrids increased with increasing silica content linearly and the density of silica moiety was estimated to be 1.92 g/cm^3 by the extrapolation method. In contrast, the increase of the density of TMOS system DA-HBPI-silica hybrids became small gradually with

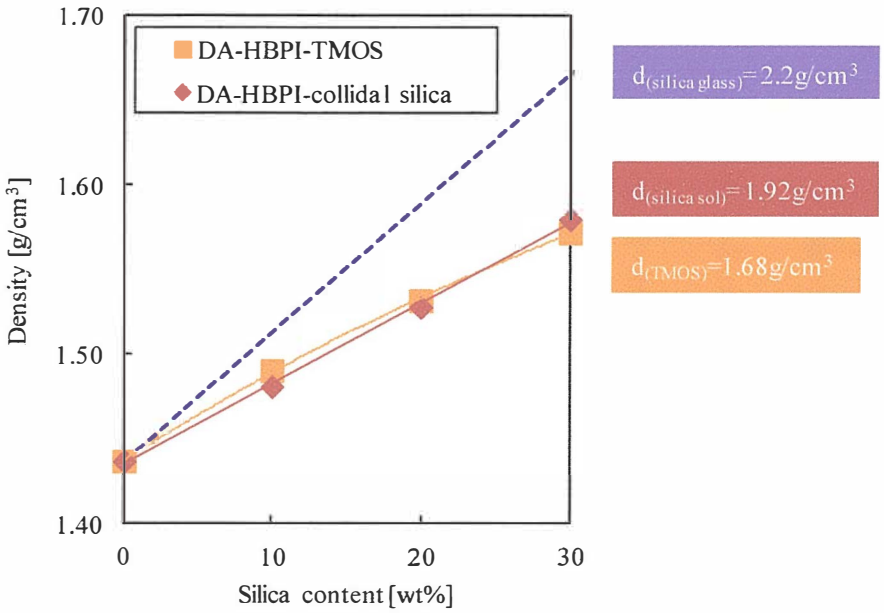

Figure 7-5 The density of the DA-HBPI-silica hybrids.

increasing silica content and the density of silica was estimated to be 1.68 g/cm^3. These values were smaller than that of silica glass (2.2 g/cm^3), suggesting the incomplete polycondensation reaction to form SiO_2 structure. In addition, these results indicate that silica formed in the TMOS system HBPI-silica hybrid is porous and amorphous than that of in the colloidal silica system HBPI- silica hybrid.

The BET surface area of silica moiety of HBPI-silica hybrids obtained from nitrogen adsorption/desorption measurements were summarized in Table 7-1, and CO_2 diffusion and solubility coefficients are plotted against BET surface area in Figure 7-6 (a, b). We can see that diffusion coefficient increased with increasing BET surface area (Figure 7-6 a)). This result indicates the additional formation of diffusion path inside the porous silica network and/or in the interfacial region between silica networks and the organic matrix through hybridization via sol-gel reaction. In addition, solubility coefficients of TMOS system HBPI-silica hybrid membranes were higher than those of MTMS system and colloidal silica system HBPI-silica hybrid membranes, suggesting the formation of Langmuir sorption site effective for gas transport properties through hybridization via

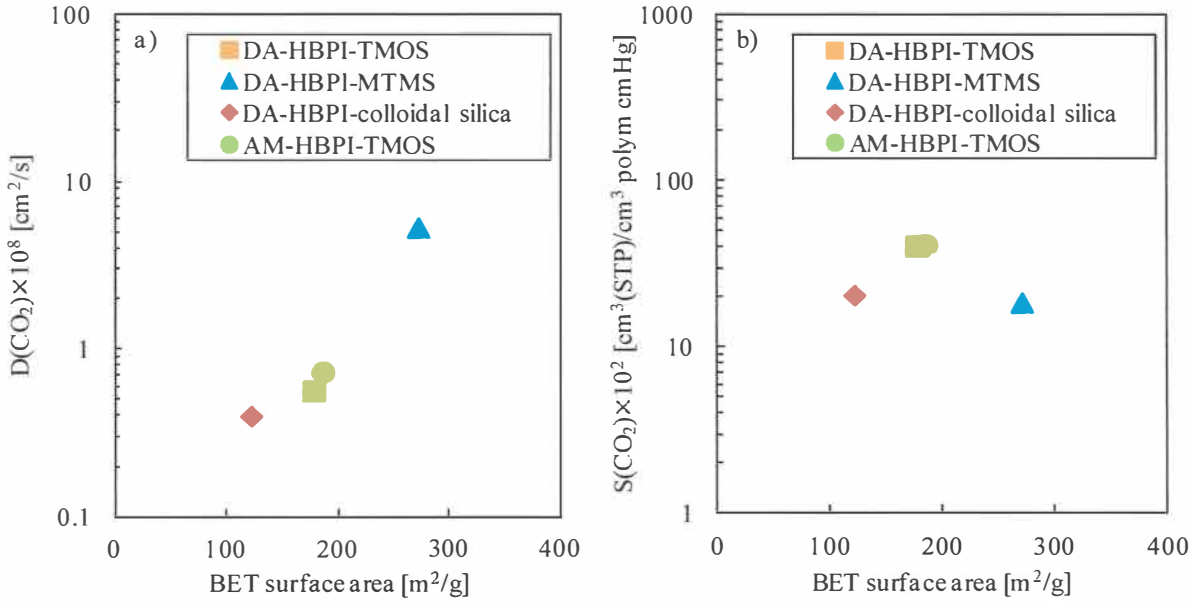

Figure 7-6 CO_2 a) diffusion and b) solubility coefficient of the HBPI-silica hybrid membranes plotted against BET surface area of silica moiety.

sol-gel reaction with TMOS [9-11]. Although amorphous silica network is also formed in the MTMS system HBPI-silica hybrids, methyl unit present in the silica domain is considered to inhibit the adsorption of gases.

3.2 Gas selectivity

The WAXD measurements were performed to investigate the morphology of the HBPI-silica hybrids. The WAXD measurement is one of the most important non-destructive tools to analyze the crystal structure. In recent years, WAXD is widely used as a technique of evaluating the ordered structure of polyimide [12-17]. According to their previous studies, the WAXD pattern of polyimide consisted of two diffraction peaks; the first peak was associated with intramolecular (along the chain axis) chain order, while the second one was caused by the diffraction of a poor molecular packing combined with the amorphous halo[15-17]. The *d*-spacings calculated from the second peak by using the Bragg's equation, $n\lambda=2d\sin\theta$, represent approximate average intersegmental distance of polymeric molecules.

Figure 7-7(a-e) shows the diffraction patterns of pristine HBPI and HBPI-silica hybrid films. In Figure 7-7(a-e), we can see that different diffraction patterns are observed according to the composition of HBPI-silica hybrid films. The *d*-spacings determined from the Bragg's equation are summarized in Table 7-2. For the pristine DA- and AM-HBPI (Figure 7-6 a) and e)), only one broad peak was found around 2θ=15.0° and 16.0°, respectively. These broad peaks are caused by the diffraction of the poor molecular packing combined with the amorphous halo of the HBPI. Both TMOS system and colloidal silica system HBPI-silica hybrid films show two diffraction peaks, and MTMS system HBPI-silica hybrid film shows three diffraction peaks. The diffraction peak of amorphous SiO_2 was reported to be observed around 2θ=21.8-23.0° [18,19].

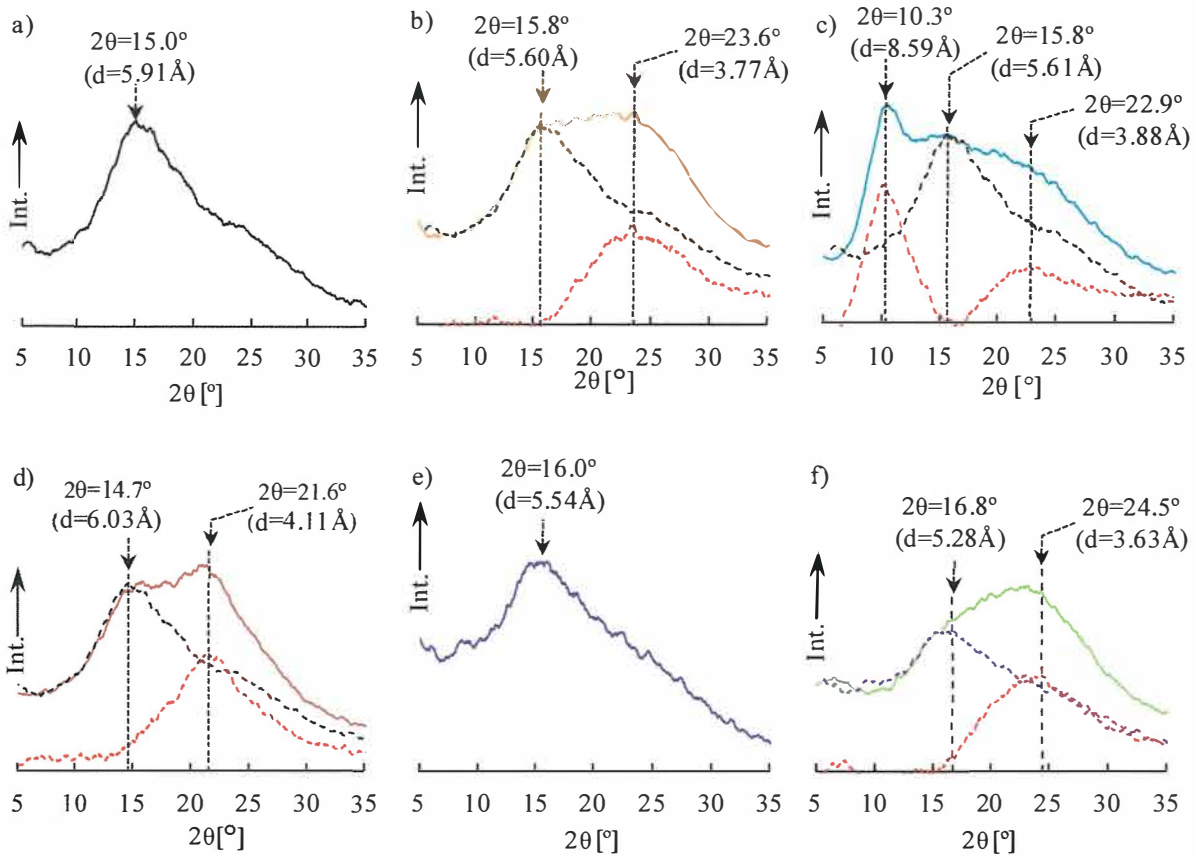

Figure 7-7 WAXD patterns of the a) pristine DA-HBPI, b) TMOS system DA-HBPI-silica hybrid, c) MTMS system DA-HBPI-silica hybrid, d) colloidal silica system DA-HBPI-silica hybrid, e) pristine AM-HBPI, and f) TMOS system AM-HBPI-silica hybrid.

Table 7-2 The *d*-spacing and average diameter of free volume holes of the HBPI-silica hybrids.

	WAXD						PALS	
	Diffraction peak [°]			*d*-Spacing [Å]			Life time [ns]	Average diameter of free volume holes [Å]
DA-HBPI		15.0			5.91		2.431	6.44
TMOS system hybrid [a]	23.6	15.8		3.77	5.60		2.341	6.30
MTMS system hybrid [a]	22.9	15.8	10.3	3.88	5.61	8.59	1.355 4.514	4.34 9.04
Colloidal silica system hybrid [a]	21.6	14.7		4.11	6.03		2.270	6.18
AM-HBPI		16.0			5.54		2.354	6.32
TMOS system hybrid [a]	24.5	16.8		3.63	5.28		2.206	6.08

[a] SiO_2 content : 30 wt%

Therefore it is thought that these plural peaks are attributed to the HBPI (2θ=14.7-16.8°) and silica domain (2θ=10.3, 21.6-24.5°).

Figure 7-8 shows the relationship between *d*-spacing and CO_2/CH_4 diffusivity selectivity of the HBPI-silica hybrid membranes. The *d*-spacing used in Figure 7-8 is the biggest one obtained for each sample, and the open symbols and the filled symbols represent the data of the pristine HBPIs and the HBPI-silica hybrids, respectively. In

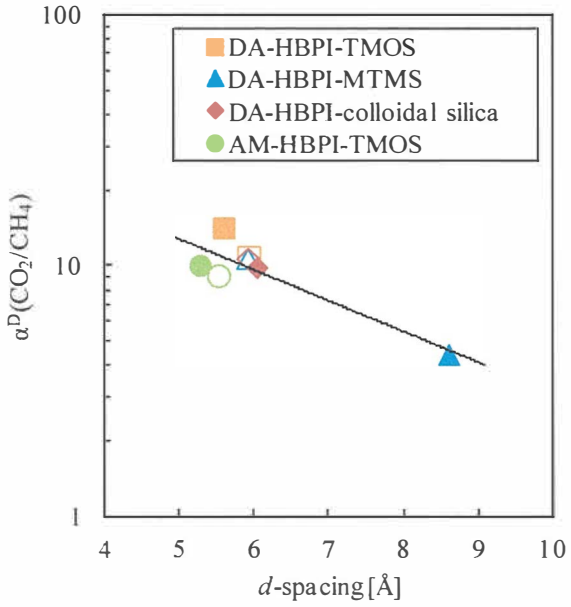

Figure 7-8 CO_2/CH_4 diffusivity selectivity [$\alpha^D(CO_2/CH_4)$] of the HBPI-silica hybrid membranes plotted against the d-spacing determined from WAXD measurement.

Figure 7-8, we can see that the diffusivity selectivity increased with decreasing the *d*-spacing, and that the *d*-spacing was narrowed by hybridization with silica derived from TMOS. In addition, CO_2/CH_4 diffusivity selectivity was controlled by the biggest *d*-spacing obtained for each sample. From these results, it can be said that the HBPI–silica hybrid membranes possess the CO_2/CH_4 separation ability attributed to a size-selective molecular sieving effect brought by the incorporation of silica. In addition, comparing the *d*-spacing attributed to the silica moiety and the kinetic diameters of studied gases (CO_2 : 3.3 Å, O_2 : 3.5 Å, N_2 : 3.6 Å, CH_4 : 3.8 Å), it cannot be denied that the gases permeate through amorphous silica prepared by sol-gel reaction.

The positron annihilation lifetime spectroscopy (PALS) was also employed for the estimation of the average diameters of free volume holes. In this technique, a positron from a radioactive source is injected into a polymer sample; forms a spin parallel bound state with an electron, which is called ortho-positronium (*o*-Ps). The *o*-Ps is easy to be captured in free volume holes. The lifetime of an *o*-Ps particle captured in free volume holes depends on the electron density in its local environment. A correlation between the measured lifetime of *o*-Ps and the size of the void volume is used to determine the average diameters of free volume holes [20,21]. The average diameters of free volume holes measured by PALS were listed in Table 7-2. For all examined membranes except the MTMS system HBPI-silica hybrid membrane, only one life time was observed. It is thought that these life times are attributed to the free volume holes in the HBPI moiety. The reason that the life time attributed to silica component was not observed in the TMOS system and colloidal silica system HBPI-silica hybrid was because the morphology of the silica component might be unsuitable for the PALS examination. For the MTMS system HBPI-silica hybrids, two life times were observed, considering that both of these life times is arise from the silica component derived from MTMS. It is

considered that the life time attributed to HBPI moiety in the MTMS system HBPI-silica hybrid is overlapped by other two life times and cannot be observed.

The relationship between CO_2/CH_4 diffusivity selectivity of the HBPI-silica hybrid membranes and the average diameter of free volume holes determined from PALS was shown in Figure 7-9. The average diameter of free volume holes used in Figure 7-9 is the biggest one obtained for each sample, and the open symbols and the filled symbols represent the data of the pristine HBPI and HBPI-silica hybrid, respectively. As is the case in the WAXD measurement, the diffusivity selectivity increased with decreasing the average diameter of free volume holes and the average diameter of free volume holes was narrowed by hybridization with silica derived from TMOS. This result also supports the suggestion that the HBPI–silica hybrid membranes possess the CO_2/CH_4 separation ability attributed to a size-selective molecular sieving effect brought by the incorporation of silica.

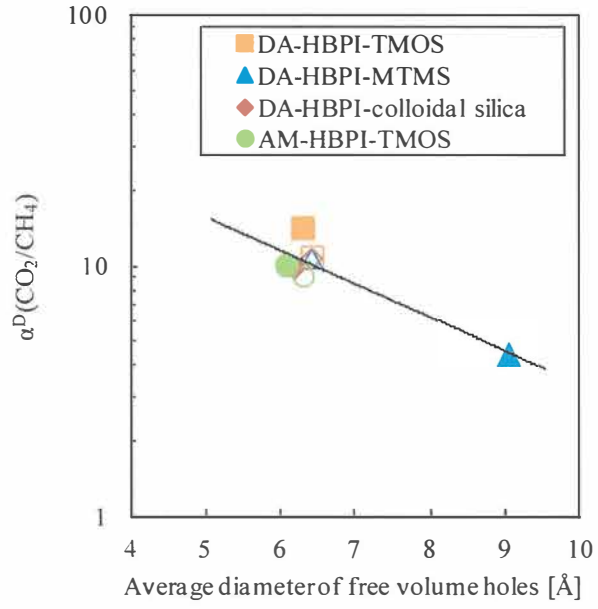

Figure 7-9 CO_2/CH_4 diffusivity selectivity $[\alpha^D(CO_2/CH_4)]$ of the HBPI-silica hybrid membranes plotted against the average diameter of free volume holes determined from PALS

In Figure 7-10, we can see the linear correlation between the average diameter of free volume holes estimated from PALS and the *d*-spacing determined from WAXD. Originally, the average diameter of free volume holes estimated from PALS and the *d*-spacing determined from WAXD is used for different purposes. However, for the HBPI-silica hybrid membranes, it can be alleged that both methods are valuable for the evaluation of the gas permeation property.

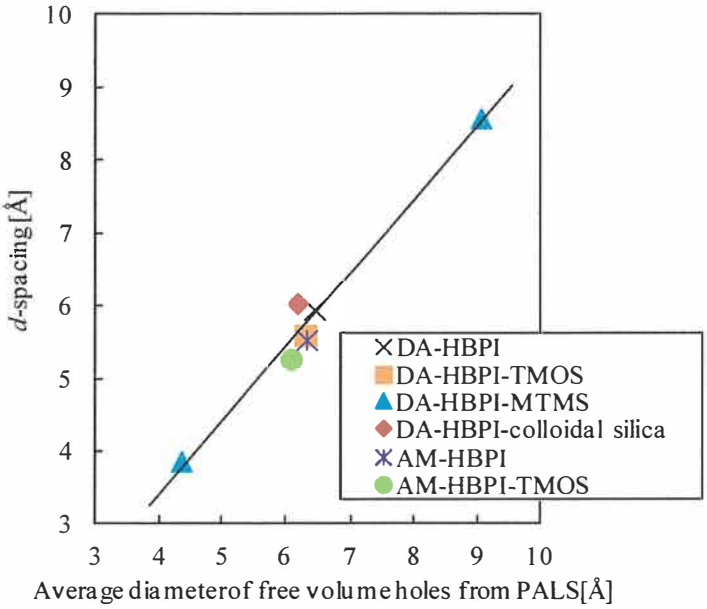

Figure 7-10 The relationship between the average diameter of free volume holes estimated from PALS and the *d*-spacing determined from WAXD.

4. Conclusions

To evaluate the nanostructure of HBPI-silica hybrids, several methods such as nitrogen adsorption/desorption measurement, WAXD measurement, and PALS experiment were applied. From the relationship between FFV and gas diffusivity, it was confirmed that the larger the FFV was, the larger diffusion coefficient was. From the measurements of nitrogen adsorption isotherms, wide angle X-ray diffractometry

(WAXD), and positron annihilation lifetime spectroscopy (PALS), it was suggested that the HBPI-silica hybrid membranes possessed the CO_2/CH_4 separation ability attributed to a size-selective molecular sieving effect brought by the incorporation silica. The linear correlation was found between the *d*-spacing determined from WAXD and the average diameter of free volume holes estimated from PALS. Therefore, both WAXD measurement and PALS experiment are valuable for the evaluation of the gas permeation property.

References

[1] T. Takeichi, J. K. Stille, Star and Liner Imide Oligomers Containing Reactive End Caps: Preparation and Thermal Properties, Macromolecules, 19 (1986) 2093-2102.

[2] R.S. Prabhakar, B.D. Freeman, I. Roman, Gas and Vapor Sorption and Permeation in Poly(2,2,4-trifluoro-5-trifluoromethoxy-1,3-dioxole-co-tetrafluoroethylene), Macromolecules, 37 (2004) 7688-7697.

[3] N. Muruganandam, W.J. Koros, D.R. Paul, Gas Sorption and Transport in Substituted Polycarbonates, J. Polym. Sci. Part B: Polym. Phys., 25 (1987) 1999-2026.

[4] A. Morisato, H.C. Shen, S.S. Sankar, B.D.Freeman, I. Pinnau, C.G. Casillas, Polymer Characterization and Gas Permeability of Poly(1-trimethylsilyl-1-propyne) [PTMST], Poly(1-phenyl-1-propyne) [PPP], and PTMSP/PPP Blends, J. Polym. Sci. Part B: Polym. Phys., 34 (1996) 2209-2222.

[5] D.H. Weinkauf, H.D. Kim, D.R. Paul, Gas Transport Properties of Liquid Crystalline Poly(p-phenyleneterephthalamide), Macromolecules, 25 (1992) 788-796.

[6] D.W. V Krevelen (Eds.), Properties of Polymers, Elsevier, Amsterdam, 1990, 71-107 (Chapter 4).

[7] S. Ando, T. Matsuura, S. Sasaki, Coloration of Aromatic Polyimides and

Electronic Properties of Their Source Materials, Polym. J., 29 (1997) 69-76.

[8] J.Y. Park, D.R. Paul, Correlation and Prediction of Gas Permeability in Glassy Polymer Membrane Materials via a Modified Free Volume based Group Contribution Method, J. Membr. Sci., 125 (1997) 23-39.

[9] T. Suzuki, Y. Yamada, K. Itahashi, 6FDA-TAPOB Hyperbranched Polyimide-Silica Hybrids for Gas Separation Membranes, J. Appl. Polym. Sci., 109 (2008) 813-819.

[10] T. Suzuki, Y. Yamada, Y. Tsujita, Gas transport properties of 6FDA-TAPOB hyperbranched polyimide membrane, Polymer, 45 (2004) 7167-7171.

[11] T. Suzuki, Y. Yamada, Physical and Gas Transport Properties of Novel Hyperbranched Polyimide – Silica Hybrid Membranes, Polym. Bull., 53 (2005) 139-146.

[12] J. Fang, H. Kita, K. Okamoto, Gas Permeation Properties oh Hyperbranched Polyimide Membranes, J. Membr. Sci., 182 (2001) 245-256.

[13] T.H. Kim, W.J. Koros, G.R. Husk, K.C. O'brien, Relationship between gas separation properties and chemical structure in a series of aromatic polyimides, J. Membr. Sci., 37 (1988) 45-62.

[14] R.F. Boehme, G.S. Cargill III, X-ray scattering measurements demonstrating in-plane anisotropy in Kapton polyimide films, in: K.L. Mittal (Eds.), Polyimides, Plenum Press, New York, 1984.

[15] H.B. Park, J.K. Kim, S.Y. Nam, Y.M. Lee, Imide-Siloxane Block Copolymer/Silica Hybrid Membranes: Preparation, Characterization and Gas Separation Properties, J Membr. Sci., 220 (2003) 59-73.

[16] C. Joly, S. Goizet, J.C. Schrotter, J. Sanchez, M. Escoubes, Sol-Gel Polyimide-Silica Composite Membranes: Gas Transport Properties, J Membr. Sci., 130 (1997) 63-74.

[17] C. Joly, M. Smaihi, L. Porcar, R.D. Noble, Polyimide-Silica Composite Materials: How Does Silica Influence Their Microstructure and Gas Permeation Properties?, Chem. Mater., 11 (1999) 2331-2338.

[18] S. Musić1, N. Filipović-Vinceković, L. Sekovanić, Precipitation of Amorphous SiO_2 Particles and Their Properties, Braz. J. Chem. Eng., 28 (2011) 89-94.

[19] J.R. Martinez, S. Palomares, G. Ortega-Zarzosa, F. Ruiz, Y. Chumakov, Rietveld Refinement of Amorphous SiO_2 Prepared via Sol–Gel Method, Mater. Lett., 60 (2006) 3526-3529.

[20] A. Shimazu, T. Miyazaki, S. Katayama, Y. Ito, Permeability, Permselectivity, and Penetrant-Induced Plasticization in Fluorinated Polyimides Studied by Positron Lifetime Measurements, J. Polym. Sci. Part B: Polym. Phys., 41 (2003) 308–318.

[21] T.C. Merkel, B.D. Freeman, R.J. Spontak, Z. He, I. Pinnau, P. Meakin, A.J. Hill, Ultrapermeable, Reverse-Selective Nanocomposite Membranes, Science, 296 (2002) 519-522.

Chapter 8

Study on Physical and Gas Transport Properties of Polyimide-Silica Hybrid Membranes Treated with CO_2 Gas

1. Introduction

Aromatic polyimides have been of great interest in gas separation membranes because of their excellent mechanical and thermal property, and high gas permeability and selectivity. However, exposure to CO_2 gas causes plasticization or swelling of the polyimide membrane, as well as another polymeric membrane, which greatly diminishes the separating efficiency of the membrane. Recent work demonstrates that cross-linking a polyimide inhibits the plasticization [1-3]. Besides, Shimazu et al. reported that for polyimide-C4 hydrocarbon system the formation of cluster by penetrant and the strong interaction of penetrant with the surrounding polymer may lead to a decreasing of diffusivity [4,5]. Both the hyperbranched structure and the hybridization are techniques for forming the cross-linked structure in polymer chains, and the cross-linked structure is expected to be effective for the CO_2 plasticization resistance.

In this chapter, physical and gas transport properties of the hyperbranched polyimide (HBPI) -silica and the linear-type polyimide-silica hybrid membranes treated with CO_2 gas were investigated to estimate the influence of the molecular structure and the hybridization on the stability of gas transport property.

2. Experimental

2.1 Materials

1,3,5-Tris(4-aminophenoxy)benzene (*TAPOB*) was synthesized by the reduction of 1,3,5-tris(4-nitrophenoxy)benzene with palladium carbon and hydrazine in methanol [6] . 1,3-Bis(4-aminophenoxy)benzene (*TPER*) was obtained from Wakayama Seika Kogyo Co., Ltd (Wakayama, Japan). Dianhydride, 4,4'-(hexafluoroisopropylidene) diphthalic anhydride (*6FDA*), was kindly supplied by Daikin Industries (Osaka, Japan). 3-Aminopropyltrimethoxysilane (*APTrMOS*) was purchased from Sigma-Aldrich Co. LLC. (St. Louis, MO, USA). Tetramethoxysilane (*TMOS*) and methyltrimethoxysilane (*MTMS*) were purchased from AZmax, Co., Ltd (Tokyo, Japan). *N, N*-Dimethylacetamide (*DMAc*) used as a solvent was purchased from Nacalai Tesque (Kyoto, Japan). The chemical structures of monomers, silane coupling agent and silicon alkoxides are shown in Figure 8-1.

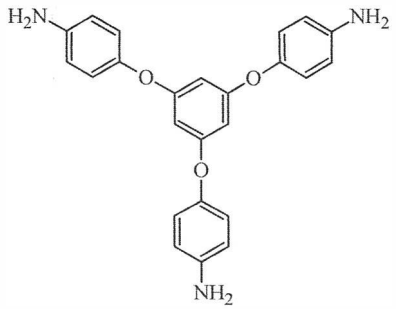

1,3,5-Tris(4-aminophenoxy)benzene

(TAPOB)

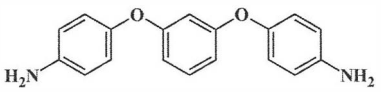

1,3-Bis(4-aminophenoxy)benzene

(TPER)

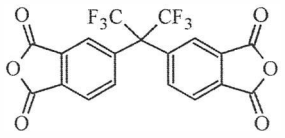

4,4'-(Hexafluoroisopropylidene) diphthalic anhydride

(6FDA)

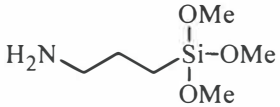

3-Aminopropyltrimethoxysilane

(APTrMOS)

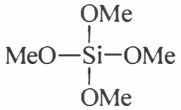

Tetramethoxysilane

(TMOS)

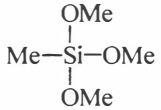

Methyltrimethoxysilane

(MTMS)

Figure 8-1 Chemical structures of monomers, silane coupling agent and silicon alkoxides.

2.2 Polymerization

2.2.1 6FDA-TAPOB hyperbranched polyamic acid (HBPAA)

Three mmol of 6FDA was dissolved in 40 ml of DMAc in a 100-ml three-neck flask under N_2 flow at room temperature. To this solution, 1.6 mmol of TAPOB in 20 ml of DMAc was added dropwise through a syringe with stirring. After stirring for 3 h, 0.4 mmol of APTrMOS was added into the reaction mixture with further stirring for 1 h to afford 6FDA-TAPOB HBPAA.

2.2.2 6FDA-TPER liner-type polyamic acid

Three mmol of 6FDA was dissolved in 9 ml of DMAc in a 50-ml three-neck flask under N_2 flow at room temperature. To this solution, 2.75 mmol of TPER was added with stirring. The reaction mixture was further stirred for 3 h. After that, 0.5 mmol of APTrMOS was added into the reaction mixture with further stirring for 1 h to afford 6FDA-TPER liner-type polyamic acid.

2.3 Membrane formation

The 6FDA based HBPI and liner-type polyimide–silica hybrids were prepared via sol-gel reaction with two kinds of silicon alkoxides, TMOS and/or MTMS, and thermal imidization. Appropriate amounts of TMOS and/or MTMS and water (silicon alkoxides : deionized water = 1 : 6 as a molar ratio) were added into the DMAc solution of the polyamic acids. For TMOS/MTMS combined system, TMOS and MTMS were added to achieve equivalent weight fraction of silica components arising from TMOS and MTMS. The mixed solutions were stirred for 24 h and cast on PET films and dried at 85°C for 3 h. The prepared films were peeled off and subsequently imidized and hybridized at 100°C for 1 h, 200°C for 1 h, and 300°C for 1 h in a heating oven under N_2 flow. The average thickness of the obtained membranes was about 30 μm. KAPTON 100H® film was purchased from DU PONT-TORAY CO., LTD. (Tokyo, Japan), and

used as received. U-VERNISH-A® was purchased from Ube Industries, Ltd. (Tokyo, Japan), and used after film formation and thermal imidization.

2.4 CO_2 treatment

The HBPI and liner-type polyimide-silica hybrid films were put in the autoclave and exposed to a mixture gas of CO_2 and N_2 at 50°C for 168 h. The treatment pressure was 2.5 MPa for CO_2 and the total pressure was 6.0 MPa. A schematic diagram for the preparation and CO_2 treatment of polyimide-silica hybrid membranes is shown in Figure 8-2.

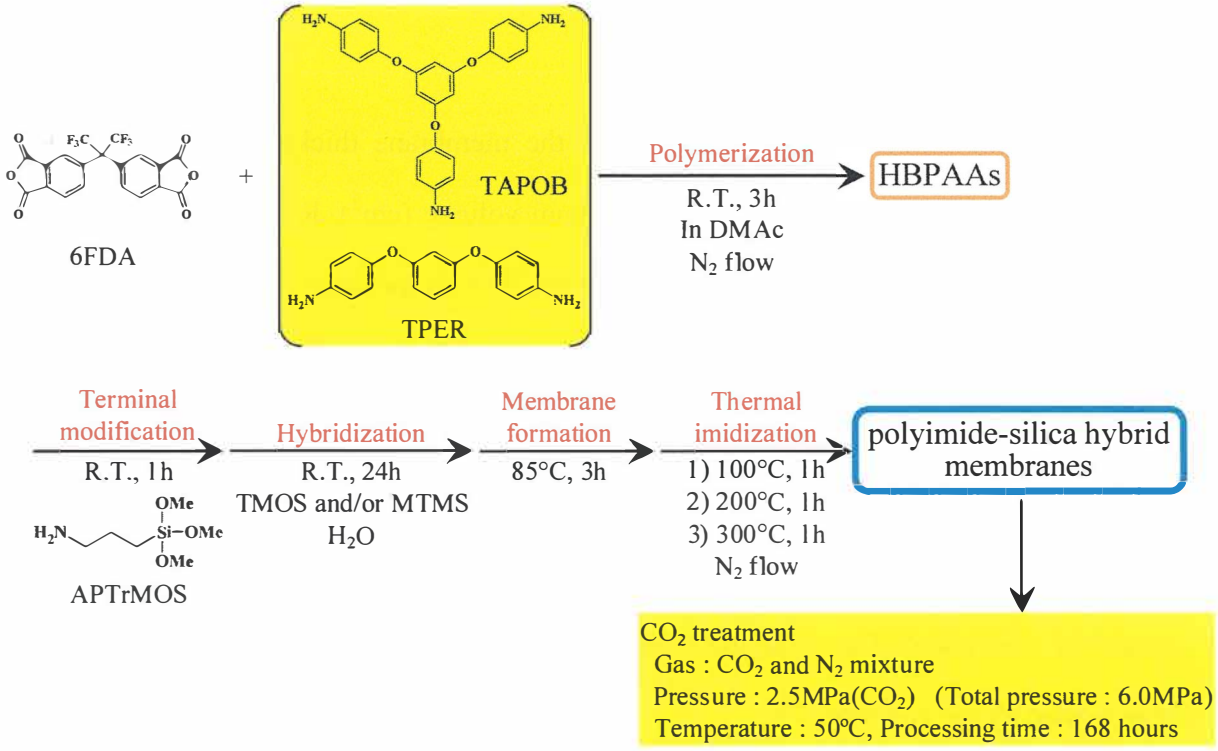

Figure 8-2 A schematic diagram for the preparation and CO_2 treatment of polyimide-silica hybrid membranes

2.5 Measurements

Attenuated total reflection Fourier transform infrared (ATR FT-IR) spectra were recorded on a JASCO (Tokyo, Japan) FT/IR-4100 at a wavenumber range of 550--4000 cm^{-1} and a resolution of 1 cm^{-1}. Ultraviolet-visible (UV-vis) optical transmittances were

measured with a JASCO V-530 UV/vis spectrometer at wavelengths of 200–800 nm. Thermogravimetric-differential thermal analysis (TG-DTA) experiments were performed with a Seiko Instruments (Chiba, Japan) TG/DTA5200 at a heating rate of 10°C/min under air flow. The mechanical properties were measured at room temperature on a Tokyo Testing Machine Inc. (Aichi, Japan) Little Senster LSC5/30 with a crosshead speed of 5 mm/min. CO_2 and CH_4 permeation measurements were taken with a constant volume/variable pressure apparatus at 76 cmHg and 25°C. The permeability coefficient, P [cm^3(STP)cm/cm^2 s cmHg], was determined by the equation [7] :

$$P = \frac{22414}{A}\frac{L}{p}\frac{V}{RT}\frac{dp}{dt} \qquad (1)$$

where A is the membrane area (cm^2), L is the membrane thickness (cm), p is the upstream pressure (cmHg), V is the downstream volume (cm^3), R is the universal gas constant (6236.56 cm^3 cmHg/mol K), T is the absolute temperature (K), and dp/dt is the permeation rate (cmHg/s). The gas permeability coefficient can be explained on the basis of the solution-diffusion mechanism, which is represented by the equation [8,9] :

$$P = D \times S \qquad (2)$$

where D(cm^2/s) is the diffusion coefficient and S [cm^3(STP)/cm^3_{polym} cmHg] is the solubility coefficient. The diffusion coefficient was calculated by the time-lag method represented by the equation [10] :

$$D = \frac{L^2}{6\theta t} \qquad (3)$$

where θt (s) is the time-lag.

3. Results and Discussion

3.1 Polymer characterization

In this study, the HBPIs were prepared from polycondensation reaction of a dianhydride, 6FDA, and a triamine, TAPOB. For 6FDA-TAPOB system, the hyperbranched structure polymer can be easily obtained because of the high reactivity of 6FDA monomer and equivalent reactivity of three amino groups of TAPOB [11].

The ATR FT-IR spectra of the 6FDA based polyimides before and after CO_2 treatment are shown in Figure 8-3. The bands observed around 1784 cm^{-1} (C=O asymmetrical stretching), 1722 cm^{-1} (C=O symmetrical stretching), 1375 cm^{-1} (C-N stretching), and 720 cm^{-1} (C=O bending) of the control samples are characteristic absorption bands of polyimides [12,13]. In contrast, the characteristic band of polyamic acids around 1680 cm^{-1} is not found. These results indicate that the prepared films are well imidized. The bands around 1857 cm^{-1} observed in the 6FDA-TAPOB HBPIs are attributed to the terminal anhydride groups of HBPI moleculer chains which contain a lot of molecular terminals. For the hybrid system, the bands observed around 1100 cm^{-1},

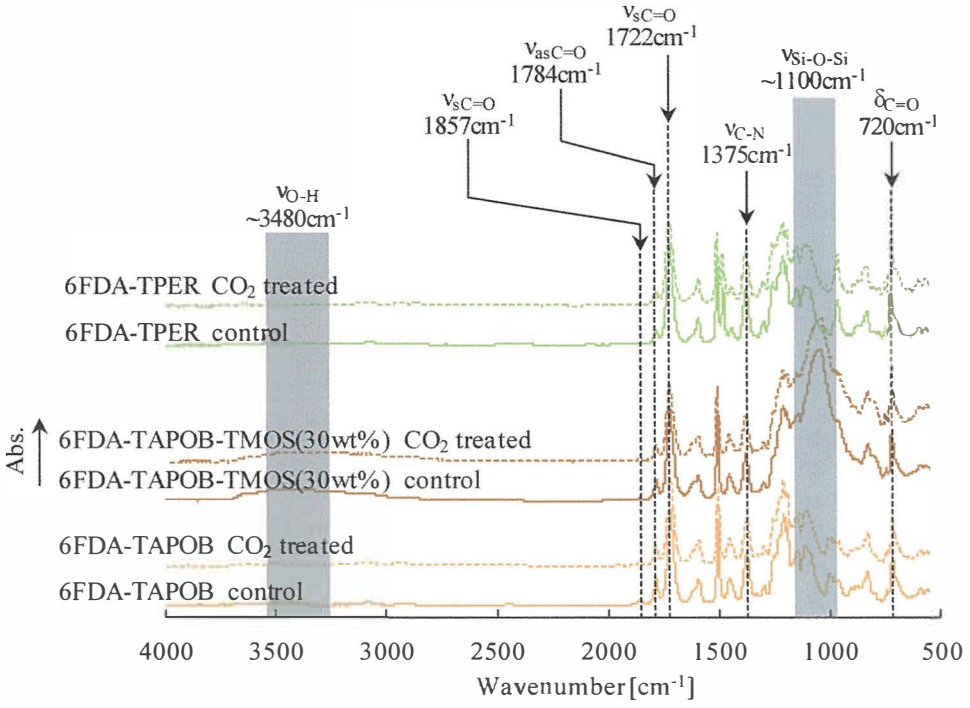

Figure 8-3 ATR FT-IR spectra of the 6FDA-based polyimides before and after CO_2 treatment.

assigned to Si-O-Si stretching [14], increased with increased silica content, indicating sufficient formation of the three-dimensional Si-O-Si network. In addition, there was no marked difference in ATR FT-IR spectra before and after CO_2 treatment. This experimental result indicates that CO_2 treatment had no influence on the polyimide molecular chain and the three-dimensional Si-O-Si network themselves.

Optical transmittances of the HBPI-silica hybrid films before and after CO_2 treatment are summerized in Table 8-1 with those of typical linear-type polyimide-silica hybrid films. The HBPI-silica hybrid films had good transparency better than liner-type polyimide-silica hybrid films, indicating high homogeneity and favorable dispersion of

Table 8-1 Physical properties of the polyimide-silica hybrid films before and after CO_2 treatment

	Transmittance	TG-DTA			Mechanical properties		
	at 600nm	Tg	T_d^5	Residue [a]	E	σ	ε
	[%]	[°C]	[°C]	[wt%]	[GPa]	[MPa]	[%]
Control							
6FDA-TAPOB	88.2	288	467	0	2.1	50.6	2.6
TMOS 10wt%SiO_2	88.4	302	481	8	2.1	44.6	2.3
30wt%SiO_2	91.3	332	494	29	2.4	22.9	0.9
MTMS 10wt%SiO_2	89.8	285	475	5	1.9	44.1	2.6
30wt%SiO_2	88.0	295	483	28	1.6	19.4	1.2
50wt%SiO_2	95.2	N.D.[b]	501	49	1.1	6.60	0.6
TMOS/MTMS 30wt%SiO_2	91.3	311	493	30	2.2	18.8	1.2
6FDA-TPER	90.0	245	499	0	1.9	101	14
TMOS 30wt%SiO_2	48.7	253	512	31	3.1	101	4.3
KAPTON 100H®	76.3	N.D.[b]	557	0	2.5	300	89
U-VERNISH-A®	84.1	N.D.[b]	567	0	2.2	140	93
CO_2 treated							
6FDA-TAPOB	86.2	292	439	0	2.4	80.4	4.9
TMOS 10wt%SiO_2	86.0	310	457	6	2.5	75.0	3.7
30wt%SiO_2	87.4	N.D.[b]	474	28	3.0	38.5	1.2
MTMS 10wt%SiO_2	88.1	290	456	6	2.0	75.0	5.2
30wt%SiO_2	92.4	303	478	30	1.6	28.5	2.1
50wt%SiO_2	95.0	N.D.[b]	499	49	0.95	6.28	1.0
TMOS/MTMS 30wt%SiO_2	91.2	317	476	28	2.3	21.5	1.4
6FDA-TPER	89.8	231	490	0	1.9	88.2	16
TMOS 30wt%SiO_2	51.8	254	504	29	3.2	111	7.1
KAPTON 100H®	77.3	N.D.[b]	545	0	2.5	302	99
U-VERNISH-A®	84.5	N.D.[b]	559	0	2.5	143	52

[a] Determined from the residual at 800°C

[b] Not detected

silica nanoparticle. These results are arising from not only the covalent bond parts between the organic and inorganic components formed by APTrMOS but also the characteristic hyperbranched structure of molecular chains [15]. Transmittances of all the examined films did not change even after CO_2 treatment. This result also suggests that CO_2 treatment had no influence on the polyimide molecular chains and the three-dimensional Si-O-Si network themselves.

Glass transition temperatures (T_gs) and 5% weight loss temperatures (T_d^5s) of the 6FDA based polyimides before and after CO_2 treatment were investigated by TG-DTA and summarized in Table 8-1 in addition to the silica content determined from the residual at 800ºC. The residual showed that all hybrid membranes contained an appropriate amount of silica, as expected. In Figure 8-4, T_g and T_d^5 values of the prepared polyimide-silica hybrids before and after CO_2 treatment are plotted against silica content. The filled symbols and the open symbols represent the data of the control samples and the CO_2 treated samples, respectively. For MTMS system 6FDA-TAPOB HBPI-silica hybrid (SiO_2=50wt%), KAPTON 100H® and U-VERNISH-A®, T_gs were not detected because of their rigid molecular chains. After CO_2 treatment, T_g of the pristine 6FDA-TAPOB HBPI increased slightly while that of the pristine 6FDA-TPER decreased. This result indicates that in the 6FDA-TAPOB HBPI, the restraints of the micro-Brownian motion or the densification of polyimide molecular chain are caused by CO_2 treatment. In contrast, plasticization seems to be caused in the 6FDA-TPER liner-type polyimide. In the hybrid membranes, the changes of T_gs before and after CO_2 treatment decreased with increasing silica content. This fact suggests that stiffening of the three-dimensional Si-O-Si network was caused by CO_2 treatment. T_d^5s of all samples decreased after CO_2 treatment. The T_d^5 value change of the 6FDA-TAPOB base polymer was larger than that of 6FDA-TPER, because parts of the moleculer

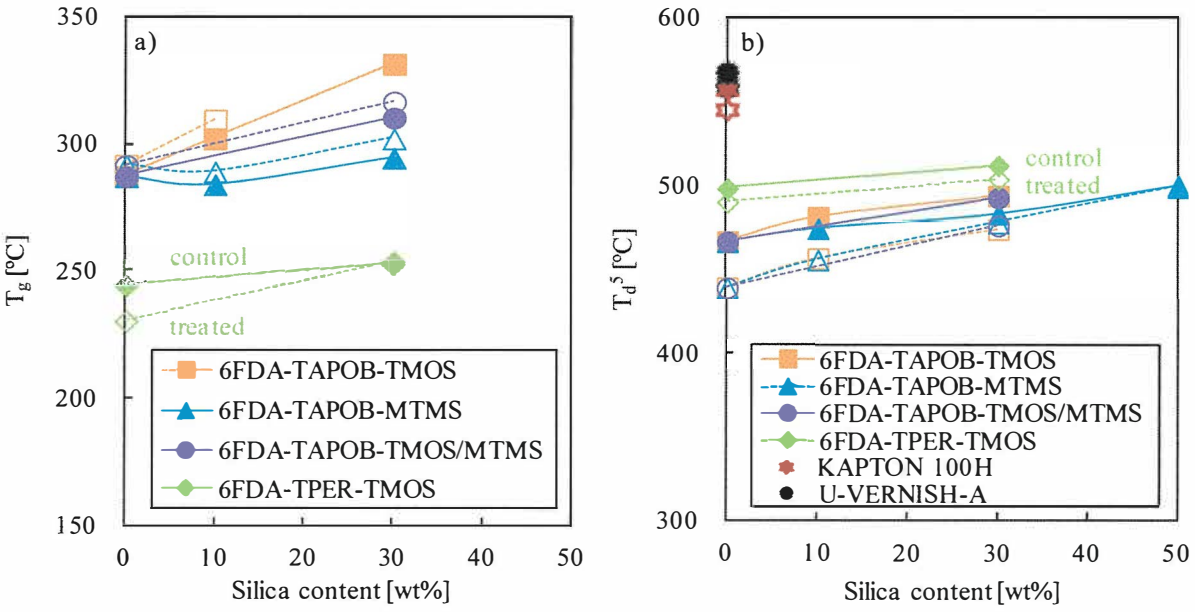

Figure 8-4 a) Glass transition temperatures (T_gs) and b) 5% weight-loss temperatures (T_d^5s) of the polyimide-silica hybrids before and after CO_2 treatment. (Filled symbols : before treatment, Open symbols : after treatment)

terminal of the polyimide molecular chains were decomposed during CO_2 treatment and the molecular weight decreased. There are many molecular terminals in the HBPI, so the T_d^5 value change of the HBPI is larger than that of the linear-type polyimide. In the silica hybrid system, the change of T_d^5 decreased with increased silica content, indicating that the three-dimensional Si-O-Si network inhibits the decomposition of polyimide molecular chains caused by CO_2 treatment.

Figures 8-5 a) and b) show the effect of CO_2 treatment on the Young's moduli (Es) and the tensile strengths (σs) of the 6FDA based polyimide films. For all films except the MTMS system 6FDA-TAPOB HBPI-silica hybrid (SiO_2=50wt%) and the 6FDA-TPER, E and σ increased after CO_2 treatment. These results indicate that the restraints of the micro-Brownian motion or the densification of polyimide molecular chains and the stiffening of the three-dimensional Si-O-Si networks were caused by CO_2 treatment, in agreement with the results of the thermal property investigation. Meanwhile, for the MTMS system, the change of the E and σ decreased with increasing silica content. This

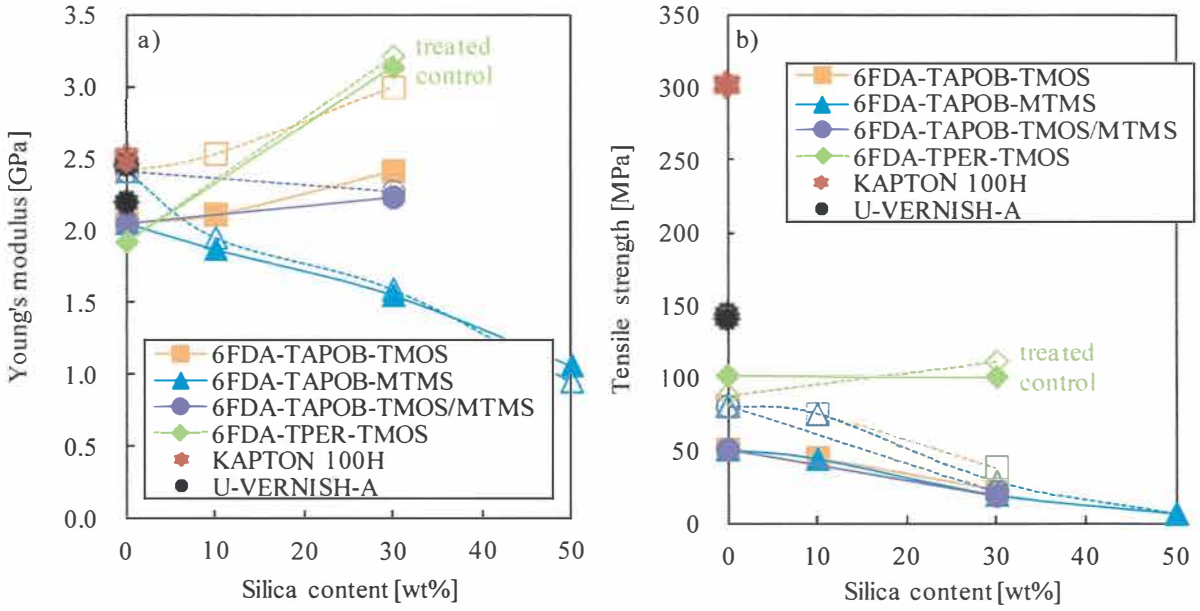

Figure 8-5 a) Young's modulus and (b) Tensile strength of the polyimide-silica hybrid membranes before and after CO_2 treatment. (Filled symbols : before treatment, Open symbols : after treatment)

suggests that the methyl groups may suppress the stiffening of the three-dimensional Si-O-Si networks due to CO_2 treatment.In the 6FDA-TPER film, after CO_2 treatment, the Young's modulus did not increase, and, in contrast, tensile strength slightly decreased. These results indicate that the plasticization may be caused in the 6FDA-TPER film by CO_2 treatment.

3.2 Gas transport properties

Gas permeability, diffusion, and solubility coefficients of the 6FDA based polyimide membranes before and after CO_2 treatment are summarized in Table 8-2 with those of typical liner-type polyimide membranes. And CO_2 permeability, diffusion, and solubility coefficients were plotted against the silica content in Figure 8-6 (a-c). Gas permeability of all 6FDA-TAPOB HBPI membranes except MTMS system HBPI-silica hybrid (SiO_2=50wt%) decreased after CO_2 treatment. The decreases of diffusion coefficients were more remarkable than those of solubility coefficients. This is because by CO_2 treatment, the restraint of the micro-Brownian motion or the densification of

Table 8-2 Gas transport properties of the polyimide-silica hybrid membranes at 76 cmHg and 25°C before and after CO_2 treatment

Sample		$P\times10^{10}$ [cm^3(STP)cm / cm^2 s cmHg]		$D\times10^8$ [cm^2 / s]		$S\times10^2$ [cm^3(STP) / cm^3 polym cmHg]	
		CO_2	CH_4	CO_2	CH_4	CO_2	CH_4
Control							
6FDA-TAPOB		7.3	0.11	0.31	0.028	23	3.7
TMOS	10wt% SiO_2	7.5	0.15	0.34	0.053	22	2.8
	30wt% SiO_2	10	0.17	0.32	0.051	32	3.3
MTMS	10wt% SiO_2	20	0.42	0.90	0.13	22	3.2
	30wt% SiO_2	84	4.4	5.0	1.5	17	3.0
	50wt% SiO_2	236	18	15	5.7	16	3.2
TMOS/MTMS	30wt% SiO_2	40	0.94	1.7	0.29	24	3.2
6FDA-TPER		5.6	0.095	0.30	0.033	19	2.9
TMOS	30wt% SiO_2	9.6	0.14	0.25	0.032	39	4.2
KAPTON 100H®		0.46	0.0087	0.026	0.0024	17	3.6
U-VERNISH-A®		0.10	0.0056	0.0087	0.0019	12	3.0
CO_2 treated							
6FDA-TAPOB		7.0	0.10	0.31	0.036	23	2.8
TMOS	10wt% SiO_2	7.2	0.11	0.28	0.034	26	3.1
	30wt% SiO_2	7.9	0.11	0.22	0.027	37	4.0
MTMS	10wt% SiO_2	18	0.37	0.83	0.13	21	2.8
	30wt% SiO_2	73	3.2	4.0	0.99	19	3.2
	50wt% SiO_2	266	20	19	6.9	14	2.9
TMOS/MTMS	30wt% SiO_2	21	0.37	0.90	0.14	23	2.6
6FDA-TPER		5.9	0.099	0.30	0.044	20	2.3
TMOS	30wt% SiO_2	7.3	0.11	0.21	0.024	34	4.5
KAPTON 100H®		0.40	0.012	0.030	0.0018	13	6.8
U-VERNISH-A®		0.091	0.01	0.0081	0.0027	11	3.7

polyimide molecular chains and the stiffening of the three-dimensional Si-O-Si networks. Consequently, diffusions of the gases through the membranes became slower. Plasticization is a phenomenon in which a polymer is swollen by a penetrant such as CO_2. In general, this swelling causes an increase of free volume and a flexible of a polymer, resulting in the decrease of Tg and mechanical strength, and the increase of gas permeability. In this study, for all of 6FDA-TAPOB HBPI membranes except the 6FDA-TAPOB-MTMS (SiO_2=50%), Tg and mechanical strength increased and gas permeability decreased after CO_2 treatment. These results indicate that plasticization seems not to be caused in the 6FDA-TAPOB HBPI membranes. For the TMOS system, because the robust three-dimensional Si-O-Si network is formed, gas permeability of

the CO_2 treated membrane decreases with increasing the silica content. In contrast, for the MTMS system, insufficient and loose three-dimensional Si-O-Si network is formed due to the methyl group. For this reason, it is thought that the CO_2 plasticization resistance of TMOS system membrane is superior to that of MTMS system membrane.

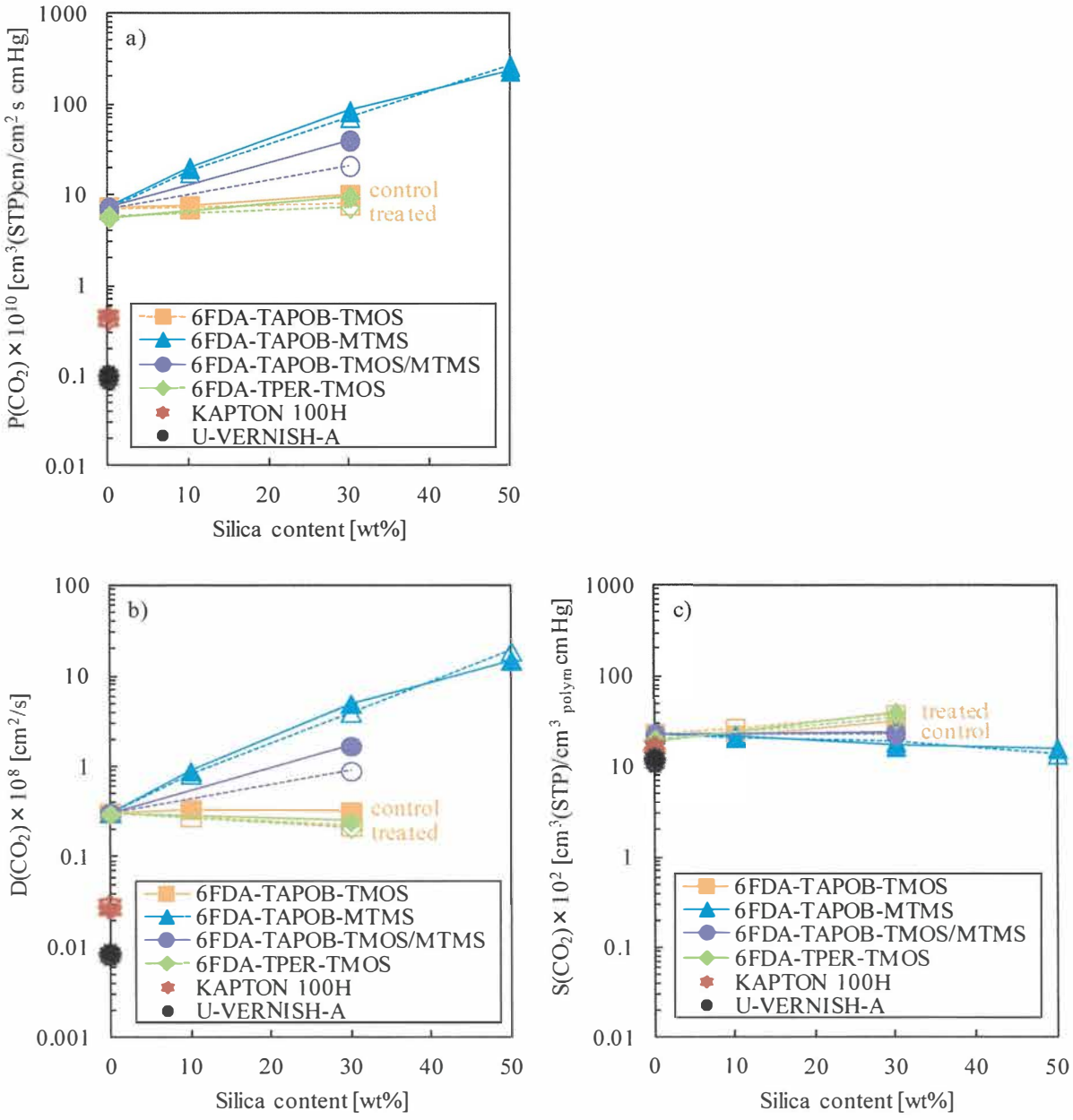

Figure 8-6 CO_2 a) permeability, b)diffusion and c) solubility coefficient of the polyimide-silica hybrid membranes before and after CO_2 treatment. (Filled symbols : before treatment, Open symbols : after treatment)

After CO_2 treatment, the gas permeability coefficient of the 6FDA-TPER membrane increased a little, suggesting that the plasticization was caused by CO_2 treatment slightly. On the other hand, because the gas permeability coefficient of the TMOS system 6FDA-TPER hybrid membrane (30 wt%) decreased, the plasticization seems to be inhibited by hybridization.

3.3 CO_2/CH_4 selectivity

The ideal permselectivity for the combination of gases A and B [α(A/B)] is defined by the following equation (4) [16]:

Table 8-3 CO_2/CH_4 selectivites of the polyimide-silica hybrid membranes at 76 cmHg and 25°C before and after CO_2 treatment

Sample		CO_2/CH_4 selectivity		
		$\alpha(CO_2/CH_4)$	$\alpha^D(CO_2/CH_4)$	$\alpha^S(CO_2/CH_4)$
Control				
6FDA-TAPOB		66	11	6.2
TMOS	10wt% SiO_2	50	6.4	7.9
	30wt% SiO_2	59	6.3	9.7
MTMS	10wt% SiO_2	48	6.9	6.9
	30wt% SiO_2	19	3.3	5.7
	50wt% SiO_2	13	2.6	5.0
TMOS/MTMS	30wt% SiO_2	43	5.9	7.5
6FDA-TPER		59	9.1	6.6
TMOS	30wt% SiO_2	69	7.8	9.3
KAPTON 100H®		53	11	4.7
U-Vernish-A®		18	4.6	4.0
CO_2 treated				
6FDA-TAPOB		70	8.6	8.2
TMOS	10wt% SiO_2	65	8.2	8.4
	30wt% SiO_2	72	8.1	9.3
MTMS	10wt% SiO_2	49	6.4	7.5
	30wt% SiO_2	23	4.0	5.9
	50wt% SiO_2	13	2.8	4.8
TMOS/MTMS	30wt% SiO_2	57	6.4	8.8
6FDA-TPER		60	6.8	8.7
TMOS	30wt% SiO_2	66	8.8	7.6
KAPTON 100H®		33	17	1.9
U-Vernish-A®		9.1	3.0	3.0

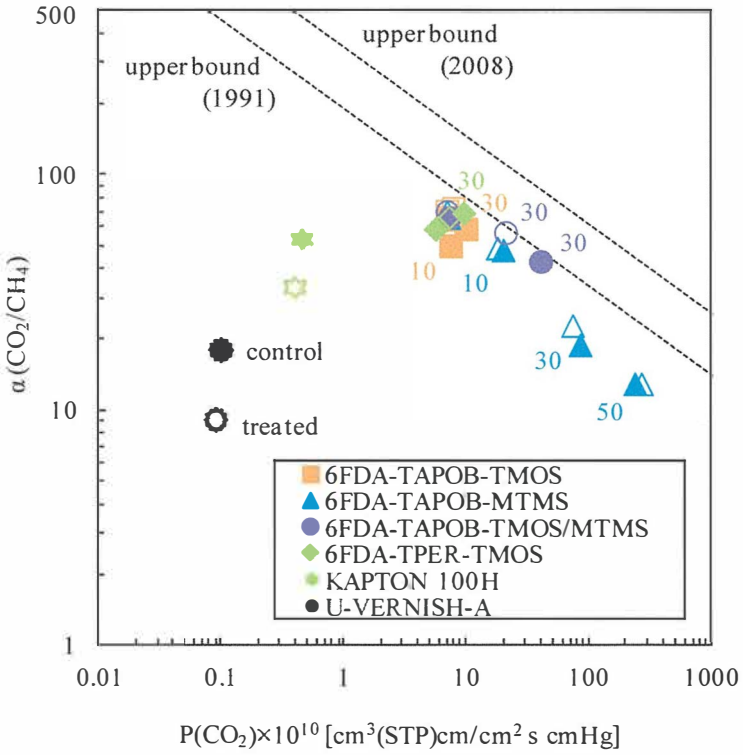

Figure 8-7 Ideal CO_2/CH_4 permselectivity [$\alpha^D(CO_2/CH_4)$] of the polyimide-silica hybrid membranes before and after CO_2 treatment plotted against CO_2 permeability coefficient. The numbers beside the plots represent the SiO_2 content. (Filled symbols : before treatment, Open symbols : after treatment)

$$\alpha(A/B)=\frac{P(A)}{P(B)}=\frac{D(A)}{D(B)}\times\frac{S(A)}{S(B)}=\alpha^D(A/B)\times\alpha^S(A/B) \qquad (4)$$

where $\alpha^D(A/B)$ is the diffusivity selectivity, and $\alpha^S(A/B)$ is the solubility selectivity. The CO_2/CH_4 selectivities of the 6FDA based polyimide membranes before and after CO_2 treatment are listed in Table 8-3, and CO_2/CH_4 permselectivity is plotted against the CO_2 permeability coefficient in Figure8-7. In Figure 8-7, it is recognized that the $\alpha(CO_2/CH_4)$ values of the 6FDA based polyimide membranes change slightly after CO_2 treatment along with the upper bound trade-off line for CO_2/CH_4 separation demonstrated by Robeson [17,18]. On the other hand, both the permeability and the permselectivity of KAPTON® and U-VARNISH-A®, which are non-6FDA based polyimides, decreased after CO_2 treatment. These results suggest that the stability of gas

transport property of the 6FDA based polyimide membrane was superior to that of non-6FDA based polyimide membrane. Trifluoromethyl group having a low surface energy in 6FDA may inhibit the penetration of CO_2.

4. Conclusions

Physical and gas transport properties of the polyimide-silica hybrid membranes treated with carbon dioxide (CO_2) gas were investigated. Comparison of ATR FT-IR spectra shows no marked change before and after CO_2 treatment, suggesting that there was no influence on the polyimide molecular chain and three-dimensional Si-O-Si network themselves by CO_2 treatment. For the 6FDA-TAPOB HBPI, T_g, Young's modulus, and tensile strength increased, whereas the gas permeability coefficient decreased. By contrast, for the 6FDA-TPER linear-type polyimide, T_g, Young's modulus, and tensile strength decreased, whereas the gas permeability coefficient increased slightly. These experimental results indicate that the restraints of the micro-Brownian motion or densification of polyimide molecular chains in the 6FDA-TAPOB HBPI membrane are caused by CO_2 treatment. For the polyimide-silica hybrids, CO_2 treatment stiffened the three-dimensional Si-O-Si network and improved the thermal stability of polyimide-silica hybrids. Further, although both the gas permeability and the permselectivity decreased in the non-6FDA based polyimide membranes, CO_2 treatment increased the selectivity of the 6FDA based polyimide membranes. For this reason, it is suggested that the 6FDA based polyimides have relatively high stability of gas transport property even after CO_2 treatment.

.

References

[1] J.D. Wind, C. Staudt-Bickel, D.R. Paul, W.J. Koros, Solid-state covalent cross-

linling of polyimide membranes dor corbon dioxide plasticization reduction, Macromolecules, 36 (2003) 1882-1888.

[2] J.D. Wind, C. Staudt-Bickel, D.R. Paul, W.J. Koros, The effects of crosslinking chemistry on CO_2 plasticization of polyimide gas separation membranes, Ind. Eng. Chem. Res., 41 (2002) 6139-6148.

[3] J.D. Wind, D.R. Paul, W.J. Koros, Natural gas permeation in polyimide membranes, J. Membr. Sci., 228 (2004) 227-236.

[4] A. Shimazu, T. Miyazaki, T. Matsushita, M. Maeda, K. Ikeda, Relationships Between Chemical Structures and Solubility, Diffusivity, and Permselectivity of 1,3-Butadiene and n-Butane in 6FDA-Based Polyimides, J. Polym. Sci. Part B: Polym. Phys., 37 (1999) 2941-2949.

[5] A. Shimazu, T. Miyazaki, M. Maeda, K. Ikeda, Relationships between the Chemical Structures and the Solubility, Diffusivity, and Permselectivity of Propylene and Propane in 6FDA-Based Polyimides, J. Polym. Sci. Part B: Polym. Phys., 38 (2000) 2525–2536.

[6] T. Takeichi, J. K. Stille, Star and Liner Imide Oligomers Containing Reactive End Caps: Preparation and Thermal Properties, Macromolecules, 19 (1986) 2093-2102.

[7] R.S. Prabhakar, B.D. Freeman, I. Roman, Gas and Vapor Sorption and Permeation in Poly(2,2,4-trifluoro-5-trifluoromethoxy-1,3-dioxole-co-tetrafluoro-ethylene), Macromolecules, 37 (2004) 7688-7697.

[8] N. Muruganandam, W.J. Koros, D.R. Paul, Gas Sorption and Transport in Substituted Polycarbonates, J. Polym. Sci. Part B: Polym. Phys., 25 (1987) 1999-2026.

[9] A. Morisato, H.C. Shen, S.S. Sankar, B.D.Freeman, I. Pinnau, C.G. Casillas, Polymer Characterization and Gas Permeability of Poly(1-trimethylsilyl-1-propyne) [PTMST], Poly(1-phenyl-1-propyne) [PPP], and PTMSP/PPP Blends, J. Polym. Sci.

Part B: Polym. Phys., 34 (1996) 2209-2222.

[10] D.H. Weinkauf, H.D. Kim, D.R. Paul, Gas Transport Properties of Liquid Crystalline Poly(p-phenyleneterephthalamide), Macromolecules, 25 (1992) 788-796.

[11] T. Suzuki, Y. Yamada, Y. Tsujita, Gas Transport Properties of 6FDA-TAPOB Hyperbranched Polyimide Membrane, Polymer, 45 (2004) 7167-7171.

[12] J. Fang, H. Kita, K. Okamoto, Gas Permeation Properties oh Hyperbranched Polyimide Membranes, J. Membr. Sci., 182 (2001) 245-256.

[13] H. Chen, J. Yin, Synthesis and Characterization of Hyperbranched Polyimides with Good Organosolubility and Thermal Properties Based on New Triamine and Conventional Dianhydrides, J. Polym. Sci. Part A: Polym. Chem., 40 (2002) 3804-3814.

[14] C. Hibshman, C.J. Cornelius, E. Marand, The Gas Separation Effects on Annealing Polyimide-Organosilicate Hybrid Membranes, J. Membr. Sci., 211 (2003) 25-40.

[15] N. Tomokiyo, Y. Yamada, T. Suzuki, J. Oku, Preparation and Characterization of Hyperbranched Polyimide - Colloidal Silica Hybrids, Polym. Prep. Japan., 55 (2006) 5175-5176.

[16] B.D. Freeman, Basis of Permeability/Selectivity Tradeoff Relations in Polymeric Gas Separation Membranes, Macromolecules, 32 (1992) 375-380.

[17] L.M. Robeson, Correlation of Separation Factor versus Permeability for Polymeric Membranes, J. Membr. Sci., 62 (1991) 165-185.

[18] L.M. Robeson, The Upper Bound Revisited, J. Membr. Sci., 320 (2008) 390-400.

Chapter 9

Conclusions

In recent years, a large number of researches on polymeric membranes have been conducted because membrane is a key technology for gas separation with high performance and low cost. Especially CO_2 separation membrane is expected to develop the alternative energy source of fossil fuel and to solve global warming through Carbon dioxide Capture and Storage (CCS). The hyperbranched polyimide (HBPI)-silica hybrid membranes have been received much attention because the newly combined materials offer the advantages of both properties of a polymer (e.g., flexibility, dielectric, ductility, and processability) and an inorganic material (e.g., rigidity and thermal stability).

The main objective of this thesis was to synthesize the HBPI-silica hybrid / composite membranes with various structures and to investigate their physical and gas transport properties in order to clarify the structure-property relationship and gas transport mechanism.

In Chapter 2, the HBPI membranes with various basic structures were prepared using four kinds of dianhydride monomers; pyromellitic dianhydride (*PMDA*), 3,3',4,4'-biphenyltetracarboxylic dianhydride (*BPDA*), 4,4'-(hexafluoroisopropylidene) diphthalic anhydride (*6FDA*), and 4,4'-oxidiphthalic anhydride (*ODPA*), and triamine, 1,3,5-tris(4-aminophenoxy)benzene (*TAPOB*), by polycondensation reaction of $A_2 + B_3$ monomer system. The 6FDA based HBPI membranes demonstrated the highest gas permeability and relatively high CO_2/CH_4 permselectivity due to the high FFV and the appropriate pore size.

In Chapter 3, the effect of the degree of terminal modification was investigated. A part of molecular terminals of HBPIs were modified with a silane coupling agent to enhance the compatibility between HBPI and silica, and thereby to improve the dispersibility of silica element. The mobility of HBPI molecular chains decreased in the rubbery region and that the free volume holes of HBPIs increased in the glassy region with increasing the degree of modification. Consequently, the gas permeability coefficients of the HBPI-silica hybrid membranes increased with increasing the degree of terminal modification.

In Chapter 4, the dianhydride-terminated (DA-) and amine-terminated (AM-) HBPI-silica hybrid membranes were prepared and their physical and gas transport properties were investigated to clarify the influence of molecular terminal groups. The gas permeability coefficient of the pristine AM-HBPI membrane without silica was higher than that of the pristine DA-HBPI membrane. In addition, the gas permeability and CO_2/CH_4 permselectivity of the DA- and AM-HBPI-silica hybrid membranes increased with increasing silica content. Especially, the CO_2/CH_4 permselectivity of AM-HBPI-silica hybrid membranes remarkably increased with increasing silica content. This behavior was probably due to the characteristic distribution and interconnectivity of free volume holes created by the incorporation of silica and the high affinity of hydroxyl groups remaining in the silica domain to CO_2.

In Chapter 5, the asymmetric HBPI-silica hybrid membranes were prepared and their physical and gas transport properties were investigated, comparing with those of symmetric HBPI-silica hybrid membranes. The asymmetric HBPI was more linear than the symmetric HBPI because the degree of branching was low. The dispersibility of silica components in the asymmetric HBPI-silica hybrids was not as fine as in the symmetric HBPI-silica hybrids. As a result, the long and tortuous diffusion path formed

by hybridization with silica caused decreasing of gas permeability.

In Chapter 6, the gas transport mechanism in the HBPI-silica hybrid and composite membranes was discussed. The structures of HBPI-silica hybrid membranes are different depending on the preparation method (hybrid or composite) and the silica source (sol-gel reaction or colloidal silica). The gas transport could occur through the porous silica network having a molecular sieving effect derived from sol-gel reaction and/or through the narrow interfacial region between silica components and organic matrix. Therefore, it is concluded that the high permeability and CO_2/CH_4 permselectivity in the HBPI-silica hybrid membranes were controlled by the narrow interfacial region and the pore size of silica network.

In Chapter 7, the nanostructures of HBPI-silica hybrids were examined by several methods to clarify the gas transport mechanism. From the relationship between FFV and gas diffusivity, it was confirmed that the larger the FFV was, the larger diffusion coefficient was. The diffusion path was found to be formed inside silica domain of the HBPI-silica hybrid membranes from the measurements of nitrogen adsorption isotherms, wide angle X-ray diffractometry (WAXD), and positron annihilation lifetime spectroscopy (PALS). The results of WAXD and PALS measurement also revealed that the HBPI-silica hybrid membranes possessed the CO_2/CH_4 separation ability attributed to a size-selective molecular sieving effect brought by the incorporation of silica. The linear correlation was found between the *d*-spacing determined from WAXD and the average diameter of free volume holes estimated from PALS.

Finally, in Chapter 8, the influence of the molecular structure on the stability of gas transport property of the polyimide-silica hybrid membranes treated with CO_2 gas was investigated. The 6FDA based polyimides have relatively high stability of gas transport property even after CO_2 treatment. Hybridization with silica was also effective to

stabilize against CO_2 treatment.

In this thesis, several types of HBPI-silica hybrid membranes were prepared and their physical and gas transport properties were investigated, and the structure-property relationship of HBPI-silica hybrid membranes was elucidated. The high permeability and CO_2/CH_4 permselectivity in HBPI-silica hybrid membranes resulted from the high FFV and the characteristic hyperbranched and hybrid structures. In addition, the HBPI-silica hybrid membranes possessed the CO_2/CH_4 separation ability attributed to a size-selective molecular sieving effect brought by the incorporation of silica.

Chapter 10

Acknowledgement

This research was accomplished at Prof. Yamada's laboratory of Graduate School of Science and Technology, Department of Biomolecular Engineering, Kyoto Institute of Technology.

I would like to express my sincere gratitude to my supervisor, Prof. Yasuharu Yamada, for providing me this precious study opportunity as a project researcher in his laboratory. I am also very grateful to Dr. Tomoyuki Suzuki, Mr. Jun Sakai, Mr. Hideki Horiuchi, Mr. Yasuyuki Ishikawa, Mr. Masaya Haraguchi, and all other members of Prof. Yamada's laboratory for their valuable cooperation in my experiments. I especially want to thank Dr. Saburo Hosokawa of Kyoto Univ. for the nitrogen adsorption/desorption measurements.

In addition, I owe a very important debt of gratitude to Prof. Yoshiyuki Ohishi of Iwate Univ. who offered continuing support and constant encouragement.

I would also like to express my gratitude to my darling husband, Keiji, my dear children, Rio, Sotaro, and Harunosuke, and my parents for their moral support and warm encouragements.

Finally, a part of this research was supported by Regional Innovation Strategy Support Program "Kyoto Environmental Nanotechnology Cluster" and JST-project to develop "innovative seeds".